Statistical descriptions of stochastic quantum dynamics

Tara Kalsi, MPhys (Hons)

Physics Department

Lancaster University

A thesis submitted for the degree of

Doctor of Philosophy

2025

Statistical descriptions of stochastic quantum dynamics

Tara Kalsi, MPhys (Hons).
Physics Department, Lancaster University

A thesis submitted for the degree of *Doctor of Philosophy*. 2025.

Abstract

Random-matrix theory provides a versatile framework for describing complex quantum systems, focusing on universal features only constrained by dimensionality and symmetry properties. In particular, the spectral fluctuations of random matrices provide a highly applicable benchmark for quantum chaos and ergodic phases.

This thesis focuses on the spectral properties of complex many-body quantum systems as they dynamically approach a chaotic, ergodic phase, where initially localised information becomes dispersed and scrambled over the system degrees of freedom. Measures of scrambling and chaos bounds are typically formulated in terms of dynamical correlations, such as those characterised by out-of-time-ordered correlators. We instead utilise spectral statistics, particularly the spectral form factor, which analyses correlations between the eigenvalues of a system, as a sensitive diagnostic tool to provide insights into the temporal evolution towards chaotic behaviour. We explore these features in three steps. First, we investigate this theme in the context of random quantum circuits, contrasting entanglement dynamics when unitary gates are drawn from each of the circular ensembles of Dyson's Threefold Way. By combining exact analytical results for the minimal case of two qubits and numerical results for the full circuit dynamics, we find that the imposition of time-reversal symmetric gates reduces entanglement generation in the circuits. Next, we introduce a scaling theory for maximally efficient quantum-dynamical scrambling and formulate chaos bounds that we show to be saturated by Dyson's Brownian motion. Finally, we show how exact analytical and asymptotic results can be obtained for a wide class of systems, for which the Brownian Sachdev-Ye-Kitaev model serves as a template. The results of this thesis lay the foundations for a deeper understanding of complex many-body quantum dynamics from a unified statistical perspective.

Acknowledgements

Henning and Alessandro — thank you for your excellent guidance. I am so very grateful to you both for the generosity of your time and expertise. I have learnt so much.

Thanks to Licia and Sarah for honouring Lancaster's open-door policy, especially towards the end, and a big thank you to David for his (long-distance) support over these past many years.

I would also like to extend my thanks to the rest of the theory group and, of course, to everyone in the office for providing such a warm and supportive environment.

I must also express my gratitude to Irina Grigorieva and Samantha Hickson at the Graphene NOWNANO CDT for ensuring that my PhD experience was a seamless one, and to EPSRC funding, particularly Grant No. EP/T518037/1.

Declaration

I declare that the work presented in this thesis is, to the best of my knowledge and belief, original and my own work. The material has not been submitted, either in whole or in part, for a degree at this or any other university.

Chapters 3, 4, and 5 are based on and appear as the following respective works [1–3]

T. Kalsi, A. Romito, and H. Schomerus
'Three-fold way of entanglement dynamics in monitored quantum circuits'
Journal of Physics A: Mathematical and Theoretical **55**, 264009 (2022).

T. Kalsi, A. Romito, and H. Schomerus
'Spectral chaos bounds from scaling theory of maximally efficient quantum-dynamical scrambling'
arXiv:2310.11355 [quant-ph] (2024).

T. Kalsi, A. Romito, and H. Schomerus
'Hierarchical analytical approach to universal spectral correlations in Brownian Quantum Chaos'
arXiv:2410.15872 [cond-mat.mes-hall] (2024).

Contents

Chapter 1

Introduction

A central objective in physics is to establish universal characteristics that transfer between systems and application domains. In particular, the principles of universality and symmetry are integral to our understanding of the behaviour of complex systems, whereby we can categorise different physical phenomena based on their underlying mechanisms. A primary motivation for this thesis is the study of these universal properties in the context of complex many-body systems. This theme spans from its historic origins in nuclear physics [4–12] to disordered and wave-chaotic electronic and photonic systems [13–17], over to isolated interacting models that display many-body eigenstate thermalisation [18–23]. Notions of universality in these settings have been developed in analogy to related concepts in statistics mechanics [24–27], where the microscopic (fine-grained) details of a system (e.g., microscopic lattice structure, disorder, and defects) may not matter in the study of its macroscopic (large-scale) properties. Broadly speaking, systems can then be grouped into *universality classes* that only depend on very general system characteristics, such as dimensionality and symmetries. The latter typically constrain the dynamics of a system and play a crucial role in determining the possible phases and transitions that a system can undergo.

In this thesis, we explore the interplay of symmetry constraints and structure in complex many-body dynamics, particularly the dynamical and spectral signatures of the scrambling process. Scrambling is the mechanism by which local information is dispersed into many-body correlations that extend over the whole system, manifesting highly entangled many-body states. What universal characteristics govern the approach

to ergodicity? When is this process maximally efficient? How does the presence of further structure and symmetries influence scrambling dynamics? What additional universal features emerge in this case? These are some of the questions that guide our investigation. To explore them, we choose a specific yet broad setting. In physics, many processes are *stochastic*, that is, subject to some randomness or external level of noise, characterised by random probability distributions that may be analysed statistically but not precisely predictable [28–30]. Addressing these questions in the context of stochastic dynamics therefore describes a wide range of physical systems and dynamical processes.

Throughout this thesis, we will make use of the fact that, from a more general perspective, much of our understanding of complex quantum dynamics can be built on the identification of universality classes based on symmetries of the system [17]. This is firmly embedded in random-matrix theory (RMT), where Dyson's Threefold Way categorising systems based on time-reversal symmetry [8, 9] has led to a comprehensive classification—the Tenfold Way—that now also includes topological aspects [31–33] and has started to reach beyond the case of unitary dynamics [34]. The success of RMT in describing complex quantum systems stems from the key insight of Wigner and Dyson's statistical theory of energy levels that essentially replaces *complexity* with *randomness* [4, 8]. Specifically, one can renounce exact knowledge of the nature of the complex system in order to gain insight into its spectra by assuming that the local statistical behaviour of energy levels of a sufficiently complicated system is captured by that of the eigenvalues of a random matrix, constrained only to share the same symmetry as the physical system. The RMT description then anticipates generically complex systems to exhibit universality in their spectral statistics based on the symmetries and dimensionality of the system, with the most notable effect given in the form of energy-level repulsion [11, 14, 16, 17, 35]. A body of supporting literature has since been produced, with the first notable numerical observations carried out on complex atomic spectra by Porter and Rosenzweig [36]. On the other hand, particularly in statistical physics, random-matrix ensembles are well-studied thanks to their analytic tractability and the fact that their associated spectra can closely approximate those of systems with many degrees of freedom, with applications reaching beyond the field of physics, to finance [37] and biology [38, 39], for instance.

Specifically, we will make contact with one of the key observations of *quantum chaos*,

namely that the spectral statistics of non-disordered low-dimensional systems can also exhibit these surprisingly universal characteristics, which furthermore reflect the chaotic or regular dynamics of the underlying classical limit where it exists. This link between chaos and the universal statistical properties of spectra (in the single-particle setting) was formalised by the Bohigas-Giannoni-Schmit (BGS) conjecture [35], which posits that the statistical properties of the energy levels of quantum systems whose classical counterparts are fully chaotic follow the predictions of RMT (e.g., exhibiting level repulsion [11, 14, 16, 17, 35]) and can be modelled by appropriate random-matrix ensembles. Specifically, when studied at a sufficiently fine energy resolution, the Hamiltonian of a chaotic system generally takes the form of an appropriate random matrix chosen from one of the standard Dyson ensembles according to the symmetries of the system [8, 9, 11, 12, 16, 17, 35, 40]. By contrast, generically regular (integrable) dynamics are characterised by energy spectra whose levels are uncorrelated, such that the spacings between consecutive levels behave like a sequence of independent random variables that follow a Poisson distribution [41]. Consequently, the study of spectral statistics is one of the main diagnostics of quantum chaos [16, 17, 35]. Typical spectral quantities are the nearest-neighbour level statistics and subsequent spacing distribution. Unlike these quantities, the spectral form factor—defined as the Fourier transform of the two-level density correlation function—probes correlations over *all* (energy, or its inverse, time) scales [16, 17, 42–61] and is therefore the central diagnostic tool to study quantum-chaotic dynamics employed in this thesis.

The same questions can be formed for many-body systems. In these, universal features become further linked to the notion of *ergodicity*. Ergodicity is central to the discussion of classical chaos in which chaotic trajectories fully explore the entire phase space, whereby two initially infinitesimally close phase-space paths diverge exponentially in time with a positive Lyapunov exponent [62, 63]. Since the uncertainty principle in quantum mechanics precludes the definition of a trajectory in phase space, the wave function contains all information about the state of a quantum system at a given time. In *many-body* quantum systems evolving under unitary dynamics, repeated interactions between the system degrees of freedom create correlations, termed *entanglement*. The dynamical process by which information that was once initially localised spreads over the system degrees of freedom and is no longer accessible to local

measurements is known as *scrambling* [50, 64–71]. Formally, a universal endpoint of the scrambling dynamics can be defined in terms of RMT, and systems that approach this endpoint are described as being *ergodic* [50]. The fact that both complex (strongly) interacting many-body systems and simpler quantum-chaotic single-particle systems typically share statistical spectral properties is a significant example of universality. Universal random-matrix behaviour also sets benchmarks for systematic deviations reflecting the specific structure of a system, such as those observed in the interplay of short-range interactions, disorder, and conservation laws [16, 17, 35, 43].

Interestingly, these questions also emerge in high-energy physics, where the concepts of scrambling and chaos shed light on some of the most fundamental questions about the nature of information, quantum mechanics, and spacetime. The conjectured state outside the horizon of a black hole is an important motivation [47, 48, 51, 64, 65, 67–69, 72–79], particularly for maximal chaos and in the resolution of the black hole information paradox. First articulated by Hawking in 1974 [80], the paradox asks what happens to the information contained in matter that falls into a black hole. Because a black hole is so dense— infinitely so at its singularity—that not even light can escape its gravitational pull, classical general relativity suggests that there is an irretrievable loss of information, which contradicts the principle of unitarity in quantum mechanics. The proposed resolution is that rather than be lost, information is rapidly *scrambled* and dispersed across the black hole's surface (event horizon) so that it seems inaccessible to any local observer, yet is preserved in some form [81]. The rate at which black holes scramble information is believed to be the fastest in nature [65, 67].

This scrambling behaviour has since been transferred to the context of quantum information theory, where it is studied using concepts like out-of-time-order correlators. These have been used to formulate scrambling bounds, the most famous being the Maldacena-Shenker-Stanford bound [72] that provides a quantum analogue of the Lyapunov exponent in classical chaos. We will study a variant of the Sachdev-Ye-Kitaev (SYK) model, which in its original form is an all-to-all interacting model of M Majorana fermions with random couplings [73–79]. The SYK model has emerged in the high-energy physics setting as a toy model for studying the chaotic properties of black holes in $0+1$d since, at strong coupling, it saturates the Maldacena-Shenker-Stanford chaos bound on scrambling dynamics [72–76], which is a characteristic of black holes in

Einstein gravity [68, 72, 82]. While the SYK model is a fully soluble model for AdS/CFT holographic duality, whose dual theory includes a sector of Jackiw-Teitelboim gravity [79, 83–85], in condensed matter, it is a simple model for the study of many-body quantum chaos and thermalisation that is analytically soluble in the large-M limit [73–78]. The quantum-chaotic nature of the SYK model was first established following the study of the nearest-neighbour level spacing distribution [86], which adheres to the RMT predictions of the symmetry class determined by M. Subsequently, RMT statistics have also been observed in the spectral form factor [48, 50, 51, 87]. These characteristics render the SYK model particularly desirable for the study of quantum chaos and scrambling.

Such stochastic models are our main vehicle to establish the universal aspect of scrambling dynamics, where, more generally, randomness is a critical ingredient in the construction of generic non-integrable models that remain soluble. In this thesis, we will encounter these in the form of random quantum circuits which have materialised as a popular setting to study the scrambling and thermalisation dynamics of local information (see Ref. [70] for a recent review). One common circuit architecture acts on nearby degrees of freedom with random unitary operations over discrete time steps in a bricklayer geometry, which may be interleaved with local measurements (so-called hybrid unitary-projective circuits) [88–91]. Since there is no Hamiltonian operator, there exists neither the notion of energy conservation nor temperature so that the dynamics can be interpreted as occurring at infinite temperature and are therefore anticipated to reproduce certain features of the high-energy physics generated by Hamiltonians. Moreover, randomness in the circuit elements promotes analytical tractability: a common approach involves leveraging randomness to map the circuit dynamics onto effective statistical mechanical models or processes (e.g., [54, 70, 88, 92]) or to obtain exact results for ensemble averages in the general spirit of RMT. For instance, one can explicitly calculate the spectral form factor both in the thermodynamic limit [53, 55, 93] and limit of large local Hilbert space dimension [52, 54, 94]. In all circuit variations, a multitude of theoretical control enables one to manipulate dynamics and observe a rich variety of out-of-equilibrium phenomena. For instance, sufficiently strong and frequent measurements in hybrid unitary-projective circuits can induce a dynamical phase transition by driving the system from an ergodic,

non-localised, highly entangled phase to a non-ergodic, localised phase characterised by states with low entanglement. We will find that constraining unitary operations to be time-reversal symmetric reduces entanglement generation, shifting this transition.

Secondly, we will study stochastic models that do not have a built-in notion of distance or locality (since interactions are all-to-all) and therefore effectively model scrambling in black holes [48, 51], particularly in the limit of continuous time, for which operations are implemented over time steps of duration $dt \to 0$, i.e., described by continuous-time stochastic processes or *Brownian circuits*. This Brownian circuit setting lends itself well to the investigation of universality in stochastic models, where we will make use of the symmetry classes that appear naturally in the context of the SYK model as a consequence of the number of Majorana fermions therein. A key approach taken in this thesis is to investigate the universal features that emerge in the spectral correlations of these stochastic models and to use this Brownian circuit setting as a foothold for understanding and describing universal correlations in complex quantum many-body evolution. In this spirit, we will identify spectral signatures of maximal chaos and establish that these are exhibited by another continuous-time stochastic process with origins in RMT: Dyson's Brownian motion.

1.1 Outline

This thesis is organised as follows.

In Chapter 2, we outline the useful background theory. In Section 2.1, we begin by reviewing time evolution in quantum systems and the basic principles of quantum mechanical measurement. It transpires that these fundamentals are all that is required to formulate the current programme. We then give a synopsis of RMT in Section 2.2. In Section 2.3, we detail how the study of the spectral statistics of random matrices is a powerful tool for probing the correlations inherent to quantum-chaotic systems [16, 17]. We review typical signatures of many-body quantum chaos using RMT predictions for spectral statistics and information-theoretic measures, such as the entanglement entropy and out-of-time-ordered correlators that are commonly used to formulate chaos bounds. In Section 2.4, we introduce random quantum circuits as minimal models to study many-body dynamics and information scrambling. Here, we review the two

broad classes of circuits and outline some basic physical properties and phenomena, in particular, the measurement-induced entanglement transition in the structure of quantum trajectories. We also define Dyson's Brownian motion, originally conceived as a technical tool in the RMT context [7], as a dynamical stochastic process of interest. We then introduce the Brownian SYK model that exhibits maximally chaotic dynamics reflecting the symmetry classes defined by the number of Majorana fermions in the model [48, 50, 51, 86, 87].

The following three chapters report the main findings of this thesis.

In Chapter 3, we investigate the interplay between local entanglement generation by gates and its reduction by measurements in random quantum circuits built from gates sampled from Dyson's Threefold Way, which categorises systems based on time-reversal symmetry. We find that imposing time-reversal symmetry on the level of individual gates reduces entanglement generation and, for the system sizes that we study, shifts the measurement-induced entanglement transition towards smaller critical measurement rates since fewer measurements are required to sufficiently disentangle the system degrees of freedom.

In Chapter 4, we investigate the scrambling mechanism and develop a single-parameter scaling theory for the maximally efficient scrambling scenario. We identify spectral signatures of maximal chaos and use these to formulate chaos bounds, enabling us to distinguish between inefficient and efficient yet incomplete scrambling. We find that Dyson's Brownian motion is an example of a maximally efficient process that meets these chaos bounds in its approach to the ergodic dynamical endpoint.

In Chapter 5, we further study Dyson's Brownian motion and investigate spectral statistics in zero-dimensional Brownian models of quantum chaos. We demonstrate how our approach can be formulated for all system sizes, in each of the three standard symmetry classes (unitary, orthogonal, and symplectic, as determined by the presence and nature of time-reversal symmetry), and applies exactly to all systems with stochastically emerging basis invariance, including the Brownian SYK model. We show how this manifests a complete analytical description of the spectral correlations and allows us to identify which are universal in a large class of models.

Finally, we collect our conclusions in Chapter 6.

Chapter 2

Background theory

2.1 Time evolution of quantum systems

We start by very briefly recapping the fundamental framework of quantum theory required for this work [95, 96].

A description of the condition of a quantum system at any given time is termed a state. A pure physical state of a quantum system at time t can be represented by a state vector $|\psi(t)\rangle$ that is an element of a Hilbert space $\mathcal{H} \equiv \mathbb{C}^N$ on which a scalar product $\langle\cdot|\cdot\rangle : \mathcal{H} \times \mathcal{H} \to \mathbb{C}$ is defined. We will largely focus on the quantum mechanics of physical systems whose Hilbert space dimensions $\dim \mathcal{H} = N$ are finite (e.g., multi-qubit systems), although the limit $N \to \infty$ is often studied for a variety of systems and theories, including the random-matrix theory context (Section 2.2).

The state vector is often referred to as the wave function and is a complete description of the system from which one may compute physical observables. Unlike a pure state, which is entirely known and may be represented by a state vector $|\psi\rangle$ with unit norm, a mixed state is given by a statistical ensemble of pure states $|\psi_i\rangle$, each of which is associated to a probability p_i, where $\sum_i p_i = 1$. In general, a mixed quantum state is described by the Hermitian density operator $\hat{\rho} = \sum_i p_i |\psi_i\rangle \langle\psi_i|$, whose operator status is denoted by the hat. For a pure state, $\hat{\rho} = |\psi\rangle \langle\psi|$. We will soon drop these hats from all operators.

2.1.1 The time-evolution operator

The time evolution of the state of a quantum system is determined by the Hamiltonian operator $\hat{H}(t)$ via the time-dependent Schrödinger equation,

$$i\hbar\frac{\partial}{\partial t}\left|\psi(t)\right\rangle = \hat{H}(t)\left|\psi(t)\right\rangle, \tag{2.1}$$

where $\hbar$ is the reduced Planck's constant. The Hamiltonian is a Hermitian linear operator that is the generator of translations in time and is the observable corresponding to the total system energy E. The general solution of Eq. (2.1) for a time-independent Hamiltonian $\hat{H}(t) = \hat{H}$ and initial state $|\psi(0)\rangle$ can be compactly expressed as

$$\left|\psi(t)\right\rangle = e^{-i\hat{H}t/\hbar}\left|\psi(0)\right\rangle, \tag{2.2}$$

where the time-evolution operator

$$\hat{U}(t) = e^{-i\hat{H}t/\hbar} \tag{2.3}$$

is unitary and therefore preserves the inner product between vectors in the Hilbert space $\mathcal{H}$, $\langle\psi'|\hat{U}^\dagger(t)\hat{U}(t)|\psi\rangle = \langle\psi'|\psi\rangle$. This has important consequences when defining chaos in quantum systems (see Section 2.3). For instance, one cannot naively generalise the so-called butterfly effect in classical chaos (which diagnoses chaotic dynamics via sensitivity to initial conditions) to quantum states and propose that the inner product between some initial state $|\psi\rangle$ and some perturbed state $|\psi'\rangle$ diminishes quickly with time since it remains constant under unitary time evolutions.

For completeness, we can express the time evolution of an initial state $|\psi(0)\rangle$ by expanding in the energy eigenfunctions $\hat{H}\left|n\right\rangle = E_n\left|n\right\rangle$,

$$\left|\psi(0)\right\rangle = \sum_n \left|n\right\rangle\left\langle n|\psi(0)\right\rangle = \sum_n c_n(0)\left|n\right\rangle. \tag{2.4}$$

Substituting the time-dependent state

$$\left|\psi(t)\right\rangle = \sum_n \left|n\right\rangle\left\langle n|\psi(t)\right\rangle = \sum_n c_n(t)\left|n\right\rangle \tag{2.5}$$

into the time-dependent Schrödinger equation (2.1) gives

$$i\hbar \sum_n \frac{dc_n(t)}{dt} |n\rangle = \hat{H} \sum_n c_n(t) |n\rangle = \sum_n E_n c_n(t) |n\rangle . \tag{2.6}$$

Projecting out the mth component gives

$$i\hbar \frac{dc_m(t)}{dt} = E_m c_m(t), \tag{2.7}$$

which is solved by

$$c_m(t) = c_m(0) e^{-iE_m t/\hbar} \tag{2.8}$$

so that the time-evolved state can be expressed as

$$|\psi(t)\rangle = \sum_n c_n(t) |n\rangle = \sum_n c_n(0) e^{-iE_n t/\hbar} |n\rangle . \tag{2.9}$$

From hereon, we drop the hat notation for operators, whose status is obvious from the context, and set $\hbar$ to unity.

2.1.2 Stochastic time evolution

We will be interested in Brownian processes in which the state of a system evolves stochastically in time. In this setting, the unitary time-evolution operator at finite times is obtained from the prescription

$$U(t) \to U(t + dt) = u(t; dt) U(t) \tag{2.10}$$

in which the unitary time-evolution operator $U(t)$ implementing the dynamics is initialised to the identity, $U(0) = \mathbb{1}$, and updated incrementally by randomly generated unitary matrices $u(t; dt) \simeq \mathbb{1}$ over a small time step dt.

One can express the unitary operator implementing dynamics over an incremental time step dt at time t in terms of an instantaneous Hamiltonian $h(t)$ as

$$u(t; dt) = \exp\left(-ih(t)\, dt\right), \quad 0 < dt \ll 1. \tag{2.11}$$

In the stochastic setting (2.10), it is convenient to rescale the instantaneous Hamiltonian in such a way that $H(t) = h(t)/\sqrt{dt}$ to give

$$u(t; dt) = \exp\left(-iH(t)\sqrt{dt}\right), \quad 0 < dt \ll 1, \tag{2.12}$$

or equivalently (to order dt) as a manifestly unitary form that is suitable for numerical implementation,

$$u(t; dt) = \left(\mathbb{1} - \frac{iH(t)}{2}\sqrt{dt}\right)\left(\mathbb{1} + \frac{iH(t)}{2}\sqrt{dt}\right)^{-1}. \tag{2.13}$$

This delivers a well-defined stochastic process in the limit $dt \to 0$ that is of Brownian nature if the instantaneous Hamiltonians $H(t)$ at different time steps are independent of each other. In Section 2.4.2, we specify this incremental time evolution in detail for the models of interest, where Dyson's Brownian motion (Section 2.4.2.1) and the Brownian Sachdev-Ye-Kitaev model (Section 2.4.2.2) are central to our considerations.

2.1.3 Measurement backaction

An isolated (closed) quantum system evolves under unitary evolution as described by the time-dependent Schrödinger equation (2.1) with constant Hamiltonian $H(t) = H$ and its solution (2.2). Measurement of the system extracts information about the state of the system through an interaction with the environment (i.e., with the observer and their measuring apparatus). Consequently, during the measurement procedure, the system is no longer isolated and its evolution is no longer unitary. In classical physics, the full state of a physical system can be determined by performing appropriate measurements on a single copy of the system that do not affect the state of the system. In contrast, measurements in quantum physics are probabilistic and inevitably disturb the system state, as we now outline.

Conventional (standard) projective measurements in quantum mechanics were introduced by von Neumann [97, 98] and are defined using a set of projection operators, hence the nomenclature [99, 100]. The measurement postulates for quantum mechanical measurement of a pure state $|\psi\rangle$ read as follows.

i There exists a Hermitian operator $O = \sum_{i,n} \lambda_i |i,n\rangle \langle i,n| = \sum_i \lambda_i P_i$ associated to every quantum mechanical physical observable, where $P_i = \sum_n |i,n\rangle \langle i,n|$ is a projector[1] onto the associated subspace of eigenstates $|i,n\rangle$. The index i labels the eigenvalues λ_i of O, which correspond to the measurement outcomes that may occur, while the index n labels any degeneracies of the eigenvalue λ_i. The hermiticity of O ensures that the eigenvalues λ_i are real and that the respective eigenvectors $\{|i,n\rangle\}$ form a complete orthonormal basis for the Hilbert space. The measurement outcome λ_i corresponds to the eigenspace $\{|i,n\rangle\}_n$.

ii Measurement of O on state $|\psi\rangle$ gives the eigenvalue result λ_i with probability p_i.

iii The probability of measuring the result λ_i is $p_i = |P_i |\psi\rangle|^2 = \langle\psi| P_i^2 |\psi\rangle = \langle\psi| P_i |\psi\rangle$.

iv The post-measurement state of the system following result λ_i is

$$|\varphi_i\rangle = \frac{P_i |\psi\rangle}{\sqrt{\langle\psi| P_i |\psi\rangle}} = \frac{P_i |\psi\rangle}{\sqrt{p_i}}, \tag{2.14}$$

where $|\varphi_i\rangle$ is a normalised eigenstate of O. An immediate second measurement of O gives the same result λ_i with certainty. This and the previous postulate constitute the Born rule [101].

v If the measurement result is *not* recorded, the post-measurement state of the system is described by the density operator (or density matrix)

$$\rho = |\psi\rangle \langle\psi| \to \tilde{\rho} = \sum_i p_i |\varphi_i\rangle \langle\varphi_i| = \sum_i P_i |\psi\rangle \langle\psi| P_i, \tag{2.15}$$

which represents the mixed state resulting from the measurement.

The above postulates are applicable for a pure initial state.[2] If the measurement

[1] State orthogonality requires $P_i P_j = P_i \delta_{ij}$ so that $P_i^2 = P_i$, ensuring eigenvalues of P_i are 0 and 1.

[2] If the initial state is mixed, the postulates iii, iv, and v are adapted. For the outcome λ_i, the post-measurement state is

$$\rho \to \tilde{\rho} = \frac{P_i \rho P_i}{\mathrm{tr}\,[P_i \rho P_i]} = \frac{P_i \rho P_i}{\mathrm{tr}\,[P_i \rho]}. \tag{2.16}$$

This outcome has probability $p_i = \mathrm{tr}\,[P_i \rho P_i] = \mathrm{tr}\,[P_i^2 \rho] = \mathrm{tr}\,[P_i \rho]$. Not recording the measurement result yields the post-measurement state $\tilde{\rho} = \sum_i P_i \rho P_i$. These reduce to iii, iv, and v in the case of a pure state density matrix $\rho = |\psi\rangle \langle\psi|$, with post-measurement state $\tilde{\rho} = |\varphi_i\rangle \langle\varphi_i|$.

outcome is recorded, there is conservation of purity in a sense: a pure pre-measurement state results in a pure post-measurement state. One says that measurement induces backaction by projecting the state onto the eigenspace associated with the measurement outcome. In particular, if A and B are non-commuting observables, then a first measurement of A will affect the outcome of a subsequent measurement of B.

The measurement process is random; although we can predict the spectrum of possible results and the probability at which these occur, we cannot predict the measurement outcome itself. The ensemble interpretation of quantum mechanics follows from this, in which the general state ρ describes an ensemble of identically prepared systems on which we can perform the same measurement and calculate the moments of the measurement-generated probability distribution $\{p_i\}$. The first moment is the expectation value of the observable O, denoted by $\langle O\rangle = \sum_i \lambda_i \operatorname{tr}[P_i\rho] = \operatorname{tr}[\rho O]$. This cannot be determined by a single measurement and is experimentally found via repeated measurement of O on the prepared state ρ, generating N results. The statistical average converges to $\langle O\rangle$ in the limit $N \to \infty$. An ideal measurement is one with negligible noise and measurement error so that an eigenvalue λ_i of O is measured. Real measurements are typically not ideal, partially due to the finite temporal resolution of macroscopic devices coupled to the quantum system via finite-energy interactions.

The above projective formalism is limiting and not an exhaustive description of all possible measurements that can be performed on quantum systems, particularly open quantum systems [99–101]. This is achieved by generalised measurements, namely Positive Operator-Values Measures (POVMs),[3] which account for the specifics of the measurement method and apparatus, and can furthermore distinguish measurement from other interactions. However, we mention this for completeness since this thesis is concerned with conventionally projective quantum mechanical measurement.

[3]POVMs are described by a set of Hermitian positive semi-definite operators $\{E_i\}$ satisfying $\sum_i E_i = \mathbb{1}$, where each E_i is associated with a measurement outcome. In a standard measurement implementation via the Kraus representation, there exist Kraus operators M_i satisfying $E_i = M_i^\dagger M_i$. For any state ρ, the probability of measuring an outcome indexed by i is $p_i = \operatorname{tr}[E_i\rho]$. The respective post-measurement state is

$$\rho \to \tilde{\rho} = \frac{M_i\rho M_i^\dagger}{\operatorname{tr}[E_i\rho]} = \frac{M_i\rho M_i^\dagger}{p_i}. \tag{2.17}$$

Comparison with Eq. (2.16) implies that projective measurements are a particular case in which $M_i = M_i^\dagger = P_i$ and $E_i = P_i$ since $P_i^\dagger P_i = P_i$. In general, the POVM elements do not obey the orthogonality relation applicable to the projectors in conventional quantum mechanical measurement.

2.2 Random-matrix theory

A random matrix is a matrix whose entries are random variables. Random-matrix theory (RMT) is the study of the properties of such matrices and has origins in Wishart's statistical study of populations [102]. Famously used to explain the spectrum of nuclei of heavy atoms [4, 5], the study of properties of typically large random matrices has since emerged as a framework for the statistical description of spectra and physical phenomena, for instance, explaining the behaviour of large disordered Hamiltonians [103] and quantum transport, including universal conductance fluctuations in disordered conductors [13, 104–106]. The key insight of RMT is that rather than studying the exact energy levels of a complex (complicated) physical system, one can study the statistics of random matrices that share the same symmetries of the system [8–11].

In this section, we first give a brief overview of random-matrix theory (2.2.1) and introduce the random-matrix ensembles of interest that follow the symmetry classification of Dyson's Threefold Way (Section 2.2.2). This leads to a clarification on the conceptual interplay between *universality* and *symmetry classes* (Section 2.2.3) in the setting of this thesis. Finally, we report on other measures of spectral statistics (Section 2.2.4), in particular, the spectral form factor that probes correlations on all scales (Section 2.2.4.3).

2.2.1 Wigner's surmise

In the 1950's, Eugene Wigner first introduced the concept of random matrices to the nuclear physics setting when trying to understand the statistics of compound nuclei resonances [4–6, 10]. Due to the complicated interactions between the many protons and neutrons that constitute a heavy nucleus, Wigner postulated that the spacings between energy levels in the spectrum at a sufficient distance above the ground state are more or less akin to the spacings between the eigenvalues of a random matrix and should depend only on the symmetry class of the Hamiltonian describing the nucleus. Beyond this symmetry consideration and the constraint that the Hamiltonian be Hermitian (and if real, symmetric), no other information is contained in the random-matrix ensemble to which the random matrix belongs.

An ensemble of random matrices is completely specified by a set of matrices and

the probability density defined on this set. Wigner [4–6, 10], and later Dyson [8, 9], considered random-matrix ensembles of $N \times N$ Hermitian matrices $H = (H_{ij})_{i,j=1}^{n}$ defined by the probability distribution

$$P(H) = \mathcal{N} \exp\left(-\frac{1}{2\sigma^2} \operatorname{tr} H^2\right), \tag{2.18}$$

where $\mathcal{N}$ is some normalisation constant dependent on the set of matrices that is chosen such that the integral against the measure $d\mu(H)$ is equal to one. The scale parameter σ can be any positive number and is related to the variance of the distribution from which the matrix elements H_{ij} are sampled, which themselves fluctuate independently about zero. These random-matrix ensembles are known as the Gaussian ensembles since the individual matrix elements obey Gaussian distributions. The trace operation in the exponent ensures that this probability density describes random-matrix ensembles that are invariant under action by the unitary group $\mathrm{U}(N)$,

$$H \to UHU^\dagger, \quad U \in \mathrm{U}(N). \tag{2.19}$$

Geometrically, this can be interpreted so that no direction of the Hilbert space is preferred. The space-time symmetries of the system restrict the allowed set of matrices. In the absence of additional symmetries, H is a random Hermitian matrix whose elements are random complex numbers. The symmetry group that acts by conjugation on the ensemble of Hermitian matrices is the unitary group $\mathrm{U}(N)$, as given by Eq. (2.19). In the presence of a time-reversal symmetry T,[4] $\mathrm{U}(N)$ is reduced to the subgroup that commutes with T. If $T^2 = 1$, $\mathrm{U}(N)$ reduces to $\mathrm{O}(N)$, and the Hermitian matrices H are real and symmetric $H_{ij} = H_{ji}$. In contrast, if $T^2 = -1$, $\mathrm{U}(N)$ reduces to $\mathrm{Sp}(N)$, and the antisymmetric matrix elements $H_{kj} = -H_{jk}^R$ can be specified using real quaternions. A real quaternion q is a linear combination of the identity and Pauli matrices, $q = a\mathbb{1} + ib\sigma_x + ic\sigma_y + id\sigma_z$ with real coefficients $a, b, c, d \in \Re$, whose

[4] Any time-reversal operator T can be expressed as the product of some appropriately chosen unitary operator U and the antiunitary operator K that implements complex conjugation (with respect to a standard representation, typically that of position), in the form $T = UK$ [17]. The anti-unitarity of T, $\langle T\psi | T\phi\rangle = \langle \phi | \psi \rangle$, follows from the explicit factor of i in the Schrödinger equation (2.1) and the fact that action by T ought to leave the modulus of the scalar product unchanged. Moreover, action by T twice should reproduce a given wave function within a phase factor, which when combined with $T = UK$ gives $T^2 = \pm 1$.

conjugate is given by $q^R = a\mathbb{1} - ib\sigma_x - ic\sigma_y - id\sigma_z$. The dual Q^R of a matrix Q with quaternion elements $Q_{nm} = a_{nm}\mathbb{1} + ib_{nm}\sigma_x + ic_{nm}\sigma_y + id_{nm}\sigma_z$ has elements $Q^R_{nm} = a_{mn}\mathbb{1} - ib_{mn}\sigma_x - ic_{mn}\sigma_y - id_{mn}\sigma_z$. In other words, the Hermitian matrices H are invariant under the basis change $H \to MHM^{-1}$, where M is a unitary, orthogonal, or symplectic matrix, such that there is no preferred direction in the Hilbert space. The associated ensembles are called the Gaussian Unitary Ensemble, Gaussian Orthogonal Ensemble, or Gaussian Symplectic Ensemble (abbreviated hereafter as GUE, GOE, or GSE), respectively. These Gaussian ensembles are indexed by the random-matrix theory symmetry index β, which takes the values of $1, 2$ and 4 in the GOE, GUE, and GSE so that β counts the number of real parameters required to describe one matrix element.

Hamiltonians whose statistics are of the GUE type correspond to physical situations in which time-reversal symmetry is broken, for instance, by a magnetic field or magnetic impurities. Statistics of the GOE and GSE types correspond to time-reversal invariant situations, with $T^2 = 1$ for systems with integer total spins and $T^2 = -1$ for systems with half-odd integer total spins. The latter may apply to systems with spin-orbit interactions. In Wigner's original context of nuclear physics, $T^2 = 1$ or -1 for nuclei with an even or odd number of nucleons, respectively.

For invariant ensembles, such as the Gaussian ensembles, the probability distribution can be expressed in terms of the eigenvalues E_n of H and is independent of the eigenvector variables, such that

$$P(H) \propto \exp\left[-\frac{1}{2\sigma^2}\sum_n E_n^2\right]. \tag{2.20}$$

To see this, note that for any rotation of basis by the unitary matrix A, $H' = AHA^\dagger$, the measure (volume element) remains unchanged $d\mu(H') = d\mu(H)$. The cyclicity of the trace implies that $P(H) = P(H')$. In particular, $P(H) = P(\Lambda)$, where the diagonal matrix $\Lambda = \mathrm{diag}\{E_n\}$[5] is constructed from the eigenvalues E_n since H admits the eigendecomposition

$$H = U\Lambda U^\dagger. \tag{2.21}$$

[5]For $\beta = 4$, there exists a twofold degeneracy for each of the N distinct eigenvalues (known as *Kramers' degeneracy*) and $\Lambda = \mathrm{diag}\{E_n\mathbb{1}_2\}$.

The unitary matrix U,[6] whose columns (equivalently rows) are normalised eigenvectors of H, satisfies $UU^\dagger = U^\dagger U = \mathbb{1}$. To fully recast the probability distribution (2.18) instead in terms of E_n, one must perform a change of variables. The measure (volume element) transforms as [11, 107]

$$d\mu(H) = \prod_{i<j} |E_i - E_j|^\beta \, dE \, d\mu(U), \tag{2.22}$$

where the constant β is defined above as the random-matrix index and $dE = \prod_i dE_i$. It is instructive to introduce the Vandermonde determinant [11, 17]

$$\det(V) = \Delta(\{E_n\}) = \begin{vmatrix} 1 & 1 & \cdots & 1 \\ E_1 & E_2 & \cdots & E_N \\ E_1^2 & E_2^2 & \cdots & E_N^2 \\ \vdots & \vdots & \ddots & \vdots \\ E_1^N & E_2^N & \cdots & E_N^N \end{vmatrix} = \prod_{i<j} (E_j - E_i), \tag{2.23}$$

which is non-zero if and only if all eigenvalues E_i are distinct since the determinant is vanishing if any two columns are equal. The Jacobian for the transformation (2.21) is simply given by $|\Delta(\{E_n\})|^\beta$ [107]. Integrating over the variables U, we are left with the joint probability distribution of eigenvalues[7] [40, 108, 109]

$$P(E_i, ..., E_N) = \mathcal{N} \exp\left(-\frac{1}{2\sigma^2} \sum_k E_k^2\right) \prod_{i<j} |E_i - E_j|^\beta \tag{2.24}$$

$$= \mathcal{N} \exp\left(-\frac{1}{2\sigma^2} \sum_k E_k^2\right) |\Delta(\{E_n\})|^\beta. \tag{2.25}$$

Consequently, finding pairs of energy levels nearby in the spectrum is statistically improbable. This repulsion between energy levels at short distances is termed *level repulsion* and is characteristic of random matrices [11]. The strength of this repulsion increases with β, so it is largest for the GSE and smallest for the GOE. It has been

[6] U is uniformly distributed in the orthogonal, unitary, and symplectic (sub)groups, respectively.

[7] Although the convention is to denote both quantities using P, one can differentiate between the quantities by the argument of the probability distribution.

experimentally shown that 'repulsion of energy levels' of the same symmetry type occurs in complex atomic spectra, e.g., [36]. By contrast, Poisson-distributed energy levels have a vanishing degree of level repulsion, $\beta = 0$ [17].

One can then ask what the spacing statistics are between neighbouring energy levels[8] on a scale small compared to the overall energy scale, where the latter is defined by the details of the problem, for instance, by the specific nucleus in Wigner's original context. Independent random energy levels are uncorrelated such that the spacing s between neighbouring levels[9] is described by a Poisson distribution

$$p_{\text{Poisson}}(s) = \exp(-as), \tag{2.26}$$

where a is a constant. In contrast, the probability distribution function for the spacing between adjacent energy levels for the Gaussian ensembles (indexed by β) is approximated[10] by the Wigner surmise [10, 11, 40]

$$p_{\text{Wigner}}(s) = c_\beta s^\beta \exp\left(-a_\beta s^2\right), \tag{2.27}$$

where the parameters a_β and c_β are fixed by normalisation. There is a strong β-dependent level repulsion at small spacings (see Figure 2.1). This is consistent with the joint eigenvalue probability distribution (2.24) since there is a vanishing probability for eigenvalues to coincide so that the spacing s is zero, in contrast to the Poisson distribution for which there is a finite probability. In the limit of large s, both distributions decay exponentially, with Wigner's decaying faster with a Gaussian falloff.[11] Porter and Rosenzweig [36] performed the first numerical investigation into the distribution of successive eigenvalues associated with random matrices, specifically in the context of complex quantum spectra, suggesting that the Wigner surmise and associated level statistics hold in general for sufficiently complex quantum systems.

[8] Or, synonymously between adjacent characteristic values of a random matrix [10].

[9] Convention is to rescale the spectra such that the mean level spacing is equal to unity for meaningful comparison between different systems (see Section 2.2.4.1).

[10] The Wigner surmise is exact for the case of 2×2 Gaussian ensembles and is a good approximation for the actual distribution of general $N \times N$ Gaussian ensembles, whose level statistics do not have a closed analytical form.

[11] This is unrelated to the Gaussian distribution of the ensembles and is a direct manifestation of the measure (volume element) [14].

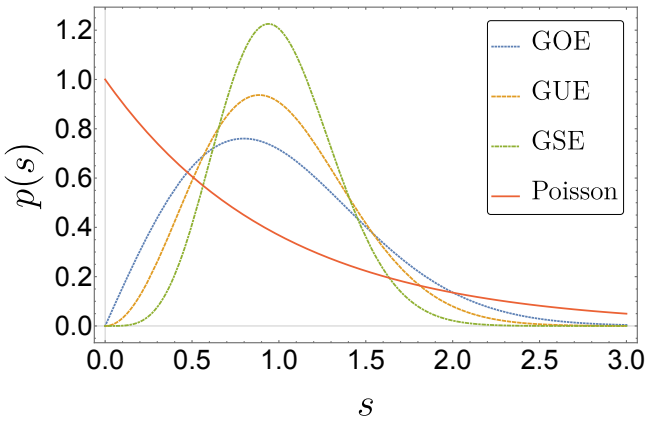

Figure 2.1: The Wigner surmise (2.27) is a universal scaling form of the nearest-neighbouring energy level spacing distribution $p(s)$ for spectra of uniform mean level spacing that correspond to GOE, GUE, and GSE statistics, here plotted for the 2×2 case and contrasted with that for a spectrum of Poisson-distributed energy levels given by Eq. (2.26).

2.2.2 Dyson's Threefold Way of random unitary matrices

In the original application of RMT to nuclear physics, the random Hermitian matrices were interpreted as Hamiltonians governing the system dynamics. Dyson's Threefold Way [8, 9] introduces the circular ensembles of random matrices as unitary analogues to the Gaussian Hermitian matrices, whose names arise due to the confinement of their eigenvalues to the unit circle in the complex plane. The Circular Orthogonal Ensemble, Circular Unitary Ensemble, and Circular Symplectic Ensemble, (COE, CUE, and CSE), respectively, are invariant under the corresponding symmetry transformations of their Gaussian analogues and indexed by the same values of β. Moreover, the circular ensembles are characterised by a flat density of states and share the same local fluctuations as their Gaussian counterparts (that instead have a semicircular density of states as described by the Wigner semicircle distribution [4, 6, 10]). We later report on the spectral statistics of the circular ensembles in Section 2.2.4.3.

Matrices of the circular ensembles are uniformly distributed in the unitary group, subject only to the constraints imposed by time-reversal and spin-rotation symmetry. Specifically, the distribution of the CUE is the Haar (invariant) measure[12] on the unitary

[12]For the unitary matrices U, V, the Haar measure $d\mu(M)$ is invariant under multiplication $d\mu(M) =$

group U(N) of $N \times N$ unitary matrices [110–112]. Analogous statements apply to the COE and CSE, and their respective cosets defined by time-reversal and spin-rotation symmetry. A simple method to generate a random COE or CUE matrix starts with an $N \times N$ matrix whose elements are independently and identically distributed real or complex Gaussian random variables (i.e., from the Ginibre ensemble [112, 113]) and whose columns can be orthonormalised via the Gram-Schmidt process that constructs an orthonormal basis from a set of vectors in an inner product space. Alternatively, one can efficiently generate random matrices from the circular ensembles by performing a QR decomposition on the Ginibre ensemble to obtain CUE matrices, which can then be used to generate matrices of the COE and CSE [112]. If $W \in$ CUE, then

$$W^T W \in \text{COE}, \quad \text{and} \tag{2.28}$$

$$-JW^T JW \in \text{CSE}, \quad \text{where } J = i\sigma_y \otimes \mathbb{1}_2, \tag{2.29}$$

such that $-JW^T J \equiv W^R$. It follows that since W is Haar-distributed by definition, so are $W^T W$ and $-JW^T JW$, noting that J is a constant matrix.

Dyson's Threefold Way gives the classification of random-matrix ensembles based on the general Hilbert space setting with symmetries and describes how [9]

> 'the most general kind of matrix ensemble, defined with a symmetry group which may be completely arbitrary, reduces to a direct product of independent irreducible ensembles each of which belongs to one of the three known types.'[13]

Dyson's Threefold Way is cardinal to many areas in physics, including the statistical theory of complex many-body systems, mesoscopic physics, disordered electron systems, and the field of quantum chaos (e.g., see Refs. [13, 17, 103]). In Chapter 3, we explore Dyson's Threefold Way in the context of information scrambling and entanglement spreading, specifically investigating the imposition of local time-reversal symmetry on entanglement generation.

$d\mu(UMV)$, such that the product UMV satisfies the symmetries obeyed by matrix M (i.e., $V = U^T$ for $\beta = 1$ and $V = U^R$ for $\beta = 4$ [13].)

[13] There exists a natural extension of Dyson's Threefold Way describing three symmetry classes to ten symmetry classes upon the introduction of particle-hole symmetry to time-reversal symmetry, as demonstrated by Altland and Zirnbauer [31] and elaborated on by Ryu, Schnyder, Furusaki, and Ludwig [33].

2.2.3 Universality and symmetry classes

In the context of complex systems and stochastic settings, one is typically interested in properties that do not depend on the details of the specific physical system since these change in time and are not reproducible in different experiments. The features of interest are instead those that do not depend on such details and are hence *universal*. While the concept of *universality* may vary in different settings, in the case of RMT, it is connected to that of *symmetry* since, as we have seen, symmetries are the defining features of the different ensembles. In this section, we introduce and discuss the interplay between the notions of universality and symmetry in the context of this thesis. In particular, we aim to clarify how symmetry classification is a weaker concept when compared to universality within a symmetry class.

The statistics of energy levels distinguished by time-reversal symmetry in RMT are known as Wigner-Dyson statistics. The corresponding systems are said to belong to the so-called Wigner-Dyson symmetry classes [9, 11, 17]. Symmetry classes categorise systems based on the symmetries of their governing Hamiltonians, focusing on invariance under specific transformations, and are distinct from the notion of universality within each class. One can see that in specific settings, different physical behaviours may fall within the same symmetry class. Zirnbauer [114] gives the example of the Wigner-Dyson symmetry class of real symmetric matrices. While weakly disordered time-reversal-invariant metals exhibit the universal energy level statistics of the GOE type, Anderson tight-binding models with real hopping and strong disorder have localised eigenfunctions and Poisson statistics in the limit of large system size. As soon as the universality of a group of systems within a symmetry class is established, we can use the notion of a universality class. These classes may involve further constraints, such as dimensionality and the nature of disordered interactions.

Universality is the concept that systems with suitable constraints on their underlying physics are described by the same laws and is one of the fundamental principles in RMT. In a more general context, this mechanism describes the observation that if many sources of randomness contribute to some outcome, then the specifics of the underlying mechanisms and dynamical details are not pertinent to the observed result. Universality often emerges when one considers the limit of large system sizes. While the microscopic details of a physical problem may differ (dramatically) at finite scales,

on larger scales, different physical systems can sometimes be described by the same mathematical model and are said to fall into the same universality class in a scaling limit. Statistical mechanics formally defines a universality class to be comprised of mathematical models whose behaviour is characterised under renormalisation group flow by the same scale-invariant limit [25]. Models within the same universality class share the same critical exponent values and behaviour for other asymptotic phenomena [26, 27].

In probability theory, this notion is at the heart of the central limit theorem (CLT), which describes how the outcome resulting from the combination of many random quantities follows the normal distribution whose shape is the bell curve [115, 116]. The CLT is universal: a sufficiently large set of averages of samples of the measured quantity will be normally distributed, even if the distribution of the measured quantity itself is not. Regardless of the specifics (shape, skew, or other characteristics) of the underlying distributions of random variables, the aggregated behaviour (sum or average) of a large number of such variables will converge to the normal distribution. This emergent behaviour is often the crux of universality: diverse systems across a wide range of different situations exhibit the same patterns at large scales.

A related mathematical theorem is the law of large numbers (LLN) [115], which states that as the sample number of independent and identically distributed random variables increases, the sample average converges to the expected value (mean) of the underlying distribution. Regardless of the specifics of the underlying distribution, the average outcome of random processes will converge to a predictable value. The CLT and LLN will be useful in the discussion context of stochastic processes (2.10) in Chapter 5.

Universality motivates and justifies the use of simpler 'toy' models in the study of more complicated systems. Indeed, Wigner assumed that one can take the system Hamiltonian H to be a random matrix with elements restricted only by the symmetry properties of the problem. The idea is that in many physical settings, in the limit of large system size N, the statistical properties of the eigenvalues of H become mostly independent of the probability density of H_{ij} and depend only on the symmetry class of the random matrix. It can be established that the local statistical properties of a large random matrix are independent of the distribution of the individual elements, in the same spirit as the CLT. More formally, the spectral correlations become largely

independent of the trace argument in the probability distribution (e.g., Eq. (2.18)) as $N \to \infty$, provided that one is sufficiently far from the edge of the spectrum. This is termed the *universality of spectral correlations* [13]. While rigorous proofs of universality are known for invariant matrix ensembles [117, 118] and Wigner matrices [119, 120], the fact that one observes the same spectral correlations in the circular and Gaussian ensembles for $N \to \infty$ can be understood intuitively by the fact that these ensembles describe the thermal equilibrium distribution of particles that experience the same repulsive interaction at small distances [17].

2.2.4 Probes of spectral statistics

The joint eigenvalue probability distribution determines the full spectral statistics of a system. In this section, we introduce quantities that further probe these.

Consider a quantum system whose dynamics are governed by its Hamiltonian H, which is typically a complex Hermitian matrix of dimension N. One may calculate the energy levels to obtain its energy spectra $E_0, E_1, E_2, \cdots, E_N$ and define the density of states as $\rho(E) = \sum_{n=1}^{N} \delta(E - E_n)$.

As the energy E increases, the spacing between consecutive energies in the spectra typically decreases, so the energy level density $\rho(E)$ is an increasing function. To study the spectral statistics, one typically focuses on an energy interval ΔE centred at E, where the interval is sufficiently narrow to be much smaller than E but sufficiently larger than the mean distance between neighbouring levels $\langle d \rangle$ in order to contain many energy levels and allow for a statistical approach,

$$\langle d \rangle \ll \Delta E \ll E. \tag{2.30}$$

Since these scales vary significantly between physical systems, it is conventional to normalise the energy level spacings by their average in the interval of interest via a process called *unfolding* the spectrum [14, 17] that removes the system-specific mean level density to analyse fluctuation properties.

2.2.4.1 Unfolding the spectrum

In order to isolate the spectral fluctuations from the local level density, one unfolds the spectra by mapping the energy level sequence $E_0 \leq E_1 \leq E_2 \cdots$ onto the new sequence $x_0 \leq x_1 \leq x_2 \cdots$ with the same fluctuation properties but characterised by a unit mean energy level density. Introducing the counting function $N(E) = \int_{-\infty}^{E} \rho(E')dE' = \sum_{n=1}^{N} \Theta(E - E_n)$ (i.e., a cumulative density function that counts the number of levels with energy equal to or less than E) and its average value $\langle N(E) \rangle$, the transformation

$$x_n = \langle N(E_n) \rangle \tag{2.31}$$

defines the new sequence with unit mean level spacing whilst maintaining system-specific spectral fluctuations. Henceforth, we will consider the unfolded sequence $x_0, x_1, x_2, \cdots, x_N$ that is ranked in increasing order by construction, with corresponding unfolded density of states $\varrho(y) = \sum_{n=1}^{N} \delta(y - x_n)$.

2.2.4.2 Spectral correlation functions

Having unfolded the spectra, we can now make meaningful comparisons between different systems and calculate statistical measures.

Nearest-neighbour spacing distribution—Let $s_n = x_{n+1} - x_n$ be the spacing between the nth and $(n+1)$th energy levels so that the nearest-neighbour spacing distribution is the distribution of spacings between adjacent energy levels, given by

$$P_{\mathrm{NN}}(s) = \left\langle \frac{1}{N} \sum_{j=1}^{N} \delta\left(s - s_j\right) \right\rangle. \tag{2.32}$$

$P_{\mathrm{NN}}(s)$ probes the short-range correlations (where $s \lesssim 1$ corresponds to level spacings smaller than the mean level spacing before unfolding) and reveals the level repulsion characteristic of the Wigner-Dyson ensembles, which, albeit cannot be expressed as closed form solutions, are well approximated by the Wigner surmise (2.27). For uncorrelated levels, the result reduces to the Poisson distribution (2.26). Probing the scale of the mean level spacing corresponds to probing statistics over an exponentially long time in the case of a many-body system, since the spacing is exponentially small in

the system size. This motivates the discussion of probes capable of extracting spectral information on different (time) scales.

Correlation functions—The simplest spectral statistics are the n-point correlation functions

$$R_n(y_1, y_2, \dots y_n) = \langle \varrho(y_1)\varrho(y_2)\dots\varrho(y_n)\rangle. \tag{2.33}$$

$R_1(y)$ is the mean density of the unfolded level $\langle\varrho(y)\rangle$, which is equal to one by construction. If the energy levels are uncorrelated, the n-point correlation function reduces to $R_n(y_1, y_2, \dots, y_n) = R_1(y_1)R_1(y_2)\dots R_1(y_n)$ ($= 1$ in this case).

The two-point spectral correlation function

$$R_2(y_1, y_2) = \langle \varrho(y_1)\varrho(y_2)\rangle \tag{2.34}$$

$$R(E, \omega) = \langle \rho(E)\rho(E+\omega)\rangle \tag{2.35}$$

gives the probability of finding two energy levels at E and $E + \omega$.

2.2.4.3 The spectral form factor (SFF)

For autonomous systems with an effectively finite-dimensional Hilbert space, the spectral form factor (SFF) is defined by the temporal Fourier transform of the two-point spectral correlation function and can be expressed as

$$K(t) = \overline{\operatorname{tr} U(t) \operatorname{tr} U^\dagger(t)} = \overline{\sum_{nm} e^{-i(E_n - E_m)t}}, \tag{2.36}$$

where the unitary time-evolution operator $U(t) = e^{-iHt}$ generates the dynamics governed by the Hamiltonian H over time t and $\{E_i\}$ are the eigenenergies of the Hamiltonian [16, 17, 42–61, 121, 122]. The SFF is analytically tractable and a relatively simple quantity to calculate (summing over two sets of eigenvalues) when compared to other measures (such as the entanglement entropy and out-of-time-order correlator introduced in Section 2.3.3). While the SFF is sometimes normalised such that $K(0) = 1$, we adopt the common convention for finite-dimensional systems in which $K(t)$ is such that $K(0) = N^2$, where N is the Hilbert space dimension. The SFF is not self-averaging [42] and thus requires the additional average over an ensemble of statistically similar

systems or multiple time intervals, denoted by the overline. In high-energy physics, calculation of the SFF involves the analytical continuation of the partition function of the system at inverse temperature $\beta \to \beta + it$, i.e., from $Z(\beta) \equiv \operatorname{tr} e^{-\beta H}$ to $Z(\beta, t) \equiv \operatorname{tr} e^{-\beta H - iHt}$. The SFF is then defined as $g(\beta, t) = \overline{Z^*(\beta, t) Z(\beta, t)} / \overline{Z(\beta)^2}$, where the overline again denotes averaging over disorder realisations [48].

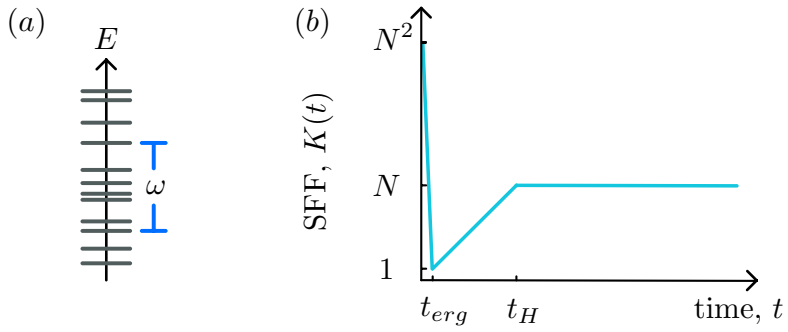

Figure 2.2: (*a*) The (two-point) correlation function (2.35) gives the probability that two energy levels are located within the energy range ω, whose Fourier transform is the SFF $K(t)$ (2.36). (*b*) RMT predicts that $K(t)$ assumes a dip-ramp-plateau structure [17, 123], here shown schematically for a fixed matrix dimension N of the GUE symmetry class. $K(t)$ dips from N^2 to 1 over the ergodic time t_{erg}, before linearly ramping up to plateau at the Heisenberg time t_H, where it takes the value N.

Unlike the nearest-neighbour level spacing distribution (2.32), the SFF measures the correlations between eigenvalues over time and probes (time) scales beyond the (inverse) mean level spacing. In Section 2.3, we detail how the precise form of the SFF directly gives information about basic properties of the system. Loosely speaking, for non-integrable systems, the SFF is typically associated with a *dip-ramp-plateau* behaviour that is modified in the presence of symmetry. For the GUE symmetry class describing Hamiltonians with no additional symmetries, the fingerprint of the level repulsion discussed in Section 2.2.1 is the ramping up of the SFF as $K(t) \propto t$ until the Heisenberg time $t_H = N$, at which the discreteness of the spectrum is resolved and $K(t)$ plateaus. The quantity $\overline{\sum_n e^{-iE_n t}}$ can be interpreted as a random walk of N steps in the complex plane by unit steps in the directions given by the phases $E_n t$. For $t \geq N$, these phases are random, $\overline{|\sum_n e^{-iE_n t}|} = \sqrt{N}$, so that $K(t) \to N$. This ramping is preceded by an initial dip from $K(0) = N^2$ to $K(t_{\text{erg}}) = 1$, which describes the onset of RMT behaviour over the *ergodic time* t_{erg}, hence the paradigmatic *dip-ramp-plateau*

structure schematically detailed in Figure 2.2. The details of this specific form contain information about the symmetry class, while systematic deviations can be used, for instance, to analyse the onset of thermalisation in structured systems [52, 124]. For Poissonian level statistics, the SFF is flat for all times $t > 0$, $K(t) = N$.

These features take a particularly simple form in a stroboscopic setting, such as those realised by quantum maps or in periodically driven dynamics with period T [17]. Using the Floquet operator $U(T)$ such that $U(nT) = U^n(T)$, the natural extension of Eq. (2.36) gives the stroboscopic SFF

$$K_n \equiv \overline{|\operatorname{tr} U^n(T)|^2}. \tag{2.37}$$

This probes the full range of correlations in the spectrum of $U(T)$. The theory can then be formulated directly in terms of the unitary operators $U(T)$, which in RMT are drawn from a corresponding circular ensemble. The CUE result,

$$K_n = N^2\delta_{n0} + \min(n, N), \tag{2.38}$$

replicates the dip-ramp-plateau behaviour with $t_{\text{erg}} = 1$ and $t_H = N$. For intermediate times, one expects $K_n = n$ and this linear ramp to abruptly plateau. This behaviour is depicted in Figure 2.3 along with the corresponding results for the other two ensembles, which implement constraints arising from time-reversal symmetry and modify the specific shape of the SFF [16, 17, 123]. The presence of time-reversal invariance recasts the linear ramp and plateau as a curve that plateaus gradually for COE dynamics, or as the joining of two regimes by a sharp kink in the case of the CSE. In contrast, Poissonian statistics translate to a flat SFF that takes the value of N for all stroboscopic times $n \geq 1$ and hence is devoid of the dip-ramp-plateau behaviour.

In this thesis, we will study the dynamics in systems with an explicit non-periodic time dependence. The concept of the SFF can then be applied to analyse the spectral features of the time-evolution operator $U(t)$ at any instance of time. This leads to the notion of the instantaneous SFF, which is given by [2, 3, 125, 126]

$$K_n(t) \equiv \overline{|\operatorname{tr} U^n(t)|^2}. \tag{2.39}$$

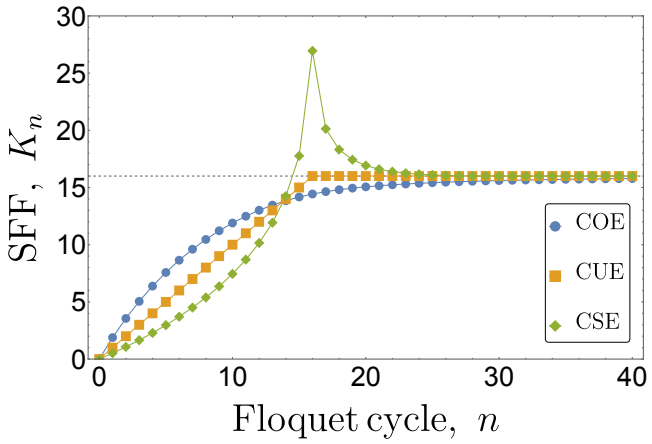

Figure 2.3: RMT predicts that the stroboscopic SFF K_n (2.37) assumes a paradigmatic (dip-)ramp-plateau structure that takes different forms in different symmetry classes [17, 123]. Here, this is illustrated for a fixed matrix dimension $N = 16$ for the three standard classes (unitary, orthogonal, and symplectic, as based on their corresponding circular ensembles). The dashed line indicates the level of the plateau attained at large n, which coincides with the n-independent Poissonian level statistics.

Here, the continuous time t follows the dynamical evolution of the system, where, in particular, $K_1(t) = K(t)$ in Eq. (2.36). Furthermore, the discrete time n systematically resolves the spectral information in $U(t)$ by probing a wider range of correlations in its spectrum. Physically, this can also be interpreted as analysing the stroboscopic dynamics obtained for a freely imposed period $T = t$, according to Eq. (2.37).

The instantaneous SFF is particularly useful to study how quantum systems establish ergodic characteristics over time. For instance, when they are driven into an infinite-temperature state, the endpoint of the dynamics would be expected to conform to the RMT predictions for the stroboscopic SFF shown in Figure 2.3. Detailed insights into the ergodisation dynamics are then obtained by studying the instantaneous SFF for earlier times t, where the index n resolves the spectral features on different scales, fully probing the dynamics on all energy and time scales [125, 126].

In the following section, we describe how the SFF is an important tool in distinguishing between quantum-chaotic and integrable systems, whereby we compare its behaviour with RMT predictions to infer the underlying nature of the system.

2.3 Chaos

In classical mechanics, the state of a system is defined in $2N$-dimensional phase space using particles' positions and momenta. A $2N$-dimensional Hamiltonian system is integrable if there exist N functionally independent constants of the motion that are *in involution* with the Hamiltonian, that is, with vanishing Poisson brackets [62]. This means that integrable dynamical systems are defined by the existence of sufficiently many constants of motion in addition to the energy, whose dynamics are given by non-linear differential equations that can *in principle* be solved analytically. By contrast, energy is the only constant of motion in a non-integrable—*chaotic*—system [62, 63]. In this section, we briefly describe how classical chaos (Section 2.3.1) translates to the quantum regime, firstly in the single-particle (Section 2.3.2) and then in the many-body (Section 2.3.3) setting, by highlighting the connection to RMT via the BGS conjecture. This posits that the statistical properties of the energy levels of quantum systems whose classical counterparts are chaotic follow the predictions of random-matrix theory (e.g., exhibiting level repulsion) and can be modelled by appropriate random-matrix ensembles. This section culminates by discussing how one typically diagnoses chaotic dynamics in many-body quantum systems, whose signatures can be observed in entanglement properties and operator spreading, in addition to the spectral statistics of the generating Hamiltonian (Section 2.2.4).

2.3.1 Chaos *vs.* integrability

The definition of integrable systems places stringent constraints on the dynamics, resulting in regular and predictable motion, which is typically confined to well-defined, stable orbits in a submanifold of much smaller dimensionality than that of the system's phase space. A simple example is the N-dimensional harmonic oscillator.

On the other end of the spectrum, chaotic systems exhibit aperiodic[14] long-term behaviour in a deterministic[15] way and are characterised by phase-space trajectories that are highly sensitive to their initial conditions [63]. Two identical copies of the system whose initial states start close to one another in phase space are characterised

[14] There exist trajectories which do not tend to fixed points, periodic orbits, or quasiperiodic orbits as $t \to \infty$.

[15] There exist no random or noisy parameters responsible for the system's irregular behaviour.

by trajectories that diverge (exponentially in the fully chaotic limit), manifesting unpredictable and complex dynamics. The (exponential) divergence of initially close trajectories is popularly termed *the butterfly effect* and is characterised by the derivative of the system's trajectory $x(t)$ with respect to its initial condition x_0,

$$\left|\frac{\partial x(t)}{\partial x_0}\right| \sim e^{\lambda t}, \tag{2.40}$$

where $\lambda > 0$ is the Lyapunov exponent. For fully chaotic systems, there is non-integrable motion in the entire phase space (termed 'hard' or 'global' chaos, to be contrasted with 'soft' chaos for which the phase space is generically comprised of regions of both chaotic and integrable motion). Chaotic trajectories fully explore the phase space on a scale set by the ergodic time t_{erg}, with neighbouring trajectories diverging exponentially in time $\propto \exp(t/t_{\text{erg}})$.

While classical chaos is well-understood and typically characterised by this sensitive dependence on initial conditions, the classical concept of a phase-space trajectory does not have a straightforward analogue in quantum mechanics due to the uncertainty principle and wave-particle duality. Rather, the wave function describes the state of the quantum system, whose evolution is governed by the linear and deterministic Schrödinger equation (2.1). Although quantum systems lack the notion of a classical trajectory, they ought to still exhibit signatures of chaos, particularly when the classical counterpart is chaotic. The question is then how classical chaos, typically characterised in the language of phase-space trajectories, manifests in such systems. To answer this, we next introduce Berry and Tabor's conjecture that is applicable to quantum integrable systems, along with its quantum-chaotic counterpart, the BGS conjecture.

2.3.2 Single-particle quantum chaos

Single-particle quantum chaos focuses on the quantum behaviour of systems comprised of only one particle (or very few degrees of freedom). Typical examples of such *simple*[16] systems include quantum billiards describing particles restricted to two-dimensional motion within specific geometric boundaries, whose motion can be chaotic or regular.

[16] *Simple* is used as opposed to *complex*, where the latter is associated with the existence of many degrees of freedom and with interactions taking place at different scales.

For instance, the circular billiard is an integrable system, while the Sinai billiard is strongly chaotic [35, 127].

In the late 1970s, much work was carried out with the aim of describing simple quantum mechanical systems for which one can define a classical limit. Berry and Tabor's 1977 conjecture [41] describes quantum systems with *integrable* classical analogues, stating that the energy levels of these systems exhibit no level repulsion, with statistics that coincide with the Poissonian statistics of a random process.

Simultaneously, investigation of quantum conservative billiard systems with *chaotic* classical limits, such as the Bunimovich stadium [128, 129] and the Sinai billiard [127], found energy spectra to be consistent with the Wigner surmise (2.27). In 1984, Bohigas, Giannoni, and Schmit produced a significant dataset for a single particle in an infinite two-dimensional potential well in the setting of the Sinai billiard [35]. In a sufficiently narrow window of energy at sufficiently high energy (2.30), the spectral fluctuation properties were found to correspond to the Wigner-Dyson distribution of the GOE. Generalising this, the resulting BGS conjecture asserts that the spectral statistics of quantum systems whose classical counterparts exhibit chaotic behaviour are described by RMT, specifically that [35]

> 'spectra of time-reversal-invariant systems whose classical analogues are K systems show the same fluctuation properties as predicted by GOE (alternative stronger conjectures that cannot be excluded would apply to less chaotic systems, provided that they are ergodic).'

While the conjecture refers to K systems which are the most strongly mixing classical systems, that is, fully (maximally) chaotic, the authors emphasise that one can replace K systems with less chaotic systems, subject only to the constraint that they are ergodic. The significance of the conjecture is the connection it makes between quantum chaos and random-matrix theory, relating the physical properties of quantum-chaotic systems to the spectral statistics of random matrices and formalising Wigner's insight that the Hamiltonian of a complex (complicated) system resembles a random matrix. For (chaotic) systems without time–reversal invariance, the GUE replaces the GOE in the conjecture, as demonstrated by billiards whose time-reversal symmetry is broken by an Aharonov-Bohm flux [130, 131]. The usual formulation of the conjecture is that quantum-chaotic systems typically have level statistics which, locally, coincide

with those of random matrices. Numerically, Wigner-Dyson level statistics have been observed for a range of non-integrable systems both in the presence of disorder [103] and lack thereof, including the original BGS context of billiard systems [16, 35], hydrogen in a magnetic field [132], and strongly interacting electron models [133]. As of now, no mathematically rigorous proofs exist for the two conjectures, albeit a semiclassical approach using periodic orbit theory based on the saddle–point approximation to Feynman's path integral for $\hbar \to 0$ [44, 134, 135] (and the Gutzwiller trace formula [62]) provides a heuristic reasoning for the BGS conjecture.

2.3.3 Many-body quantum chaos

Although the BGS conjecture was initially formulated in the context of single-particle systems, it is also applicable to Wigner's original setting of complex nuclei and many-body quantum systems, where chaotic behaviour is associated with RMT-like spectral statistics with energy level spacings that exhibit level repulsion. In comparison to single-particle systems, many-body quantum chaos involves systems with a large number of interacting particles, thus with much greater dimensionality and complexity.

In many-body classical systems, one typically characterises chaos via trajectories in a high-dimensional phase space. Chaotic behaviour in many-body classical systems can lead to phenomena like thermalisation and ergodicity, describing how the system explores its phase space over time in a way that resembles statistical ensembles.[17] This notion of ergodicity and thermalisation also appears for chaotic quantum many-body systems, where it can be formulated via the eigenstate thermalisation hypothesis (ETH). The ETH posits that, even in isolated quantum systems, thermalisation occurs at the level of individual eigenstates of the system's Hamiltonian so that long-time observables behave as if the system were in thermal equilibrium,[18] despite the system being in a pure quantum state and evolving under unitary dynamics (which preserves the information of the initial state) [18–22, 136]. A system obeying the ETH is indicative that the system

[17] Specifically, ergodicity as posited by the ergodic hypothesis implies that the long-time average of an observable for a single system is equal to the average of the observable over an ensemble of identically prepared systems. This means that one can replace time averages with ensemble averages when calculating macroscopic properties of systems in equilibrium.

[18] If the ETH holds, it implies that almost all individual eigenstates within a small energy window yield expectation values of observables that match those predicted by statistical mechanics, such that the outcome depends on the energy alone (and is therefore independent of the initial conditions).

is ergodic, which is a hallmark of chaotic behaviour, and typically leads to strong correlations (entanglement) between distant parts of the system. More specifically, any small part of the larger system will be entangled with the rest of the system, leading to a mixed state for the subsystem that mimics thermal equilibrium and results in the thermalisation of local observables.

Consequently, many-body quantum chaos can also be viewed from a quantum information perspective that quantifies the speed at which information spreads (*scrambles*) across a system [50, 64–69, 71], as further discussed in the following subsection. Information that was initially local becomes delocalised across the system, whose degrees of freedom are said to be *entangled*. The extent of this can be quantified using information-theoretic quantities, such as the entanglement entropy that can be calculated using the system wave function (which is non-localised in the ergodic limit). Interacting spin systems, such as the Ising or Heisenberg models, can demonstrate chaotic behaviour when the interactions and system parameters lead to entangled states [27, 137, 138], while cold atom experiments with optical lattices contribute a platform to study many-body quantum chaos in a controlled environment [139–141].

2.3.4 Other signatures of many-body quantum chaos

In Section 2.3.2, we introduced the BGS conjecture that makes a connection between the spectral fluctuations of quantum-chaotic systems and appropriately chosen random-matrix ensembles. Since the SFF (discussed in Section 2.2.4.3 in the RMT context) probes correlations over all scales, it is the main quantity that we will study in the setting of quantum-chaotic dynamics. In this context, the SFF can provide insights into how quickly a system thermalises and how information is scrambled within it.

In addition to RMT-like spectral statistics (Section 2.2), there exist other signatures of chaotic behaviour in many-body systems. Here, we introduce the von Neumann bipartite entanglement entropy and out-of-time-ordered correlators, which diagnose chaotic behaviour from state and operator perspectives, respectively.

2.3.4.1 Entanglement properties

By virtue of the correlations created by interactions between system degrees of freedom in generic many-body quantum settings, the information encoded by systems quickly becomes inaccessible if the associated degrees of freedom couple with the environment. This effective information loss can be captured by quantum statistical methods, such as the von Neumann bipartite entanglement entropy [142], whose scaling properties with system size can be used to characterise ergodic thermal-like or non-ergodic localised phases [90, 137, 143–148] and is defined as follows. For a system with density matrix ρ, the von Neumann bipartite entanglement entropy is given by

$$S_A = -\mathrm{tr}\,(\rho_A \ln \rho_A), \tag{2.41}$$

where ρ_A is the reduced density matrix of subsystem A, calculated by bipartioning the system and tracing out the subsystem complementary to A.[19] The quantity S_A is a measure of the entanglement between the two subsystems,[20] where $S_A = 0$ for separable states and $S_A > 0$ for entangled states. In chaotic systems, $S_A(t)$ typically grows linearly[21] with time after a quench to a low-entanglement initial state [92, 150, 151],

[19]Entropy is complementary when the total state is pure, so $S_A = S_B$ where subsystem B is complementary to A. This can be seen by expressing the state of the system in terms of the singular values of the Schmidt decomposition. Denote components of the system wave function as $\psi_{a,b}$, where indices a and b detail contributions from subsystems A and B. The density matrix of the whole system is $\rho = \psi\psi^\dagger$, with components $\rho_{a,b;a',b'} = \psi_{a,b}\psi^*_{a',b'}$, such that ρ_A has components

$$(\rho_A)_{a;a'} = (\mathrm{tr_B}(\rho))_{a;a'} = \sum_b \psi_{a,b}\psi^*_{a',b}. \tag{2.42}$$

This resembles the matrix multiplication $\rho_A = \Psi\Psi^\dagger$, where Ψ has coefficients $\Psi_{a;a'} = \psi_{a;a'}$ and its Hermitian conjugate has entries $\Psi^\dagger_{a;a'} = \psi^*_{a';a}$. The entanglement entropy follows from the diagonalisation of ρ_A to get its eigenvalues λ_i, $S_A = -\sum_i \lambda_i \ln \lambda_i$. Alternatively, we can exploit the fact that ρ_A is positive semi-definite and that Ψ may be seen as its 'square root'. More precisely, the singular values of Ψ are square roots of singular values (and due to hermiticity, eigenvalues) of ρ_A. Singular Value Decomposition (SVD) entails reshaping ψ to form Ψ, calculating its singular values s_i and then the entropy,

$$S_A = -\sum_i s_i^2 \ln s_i^2 = S_B. \tag{2.43}$$

[20]It is also typical to consider the nth Rényi entropy, $S_A^{(n)} = (1-n)^{-1}\ln(\mathrm{tr}\,\rho_A^n)$, $n \geq 0$, where the limit $n \to 1$ recovers the von Neumann entropy [149].

[21]By contrast, in many-body localised systems, a quantum-chaotic system prepared in an initial state with low-entanglement entropy typically evolves with $S_A(t) \propto \ln t$ [23].

before eventually saturating to a value $S_A(\infty)$ consistent with thermal equilibrium, which is then maximised for a random pure state (sometimes called a Page state) as dictated by the Page result [152]. For a one-dimensional system of size L whose partitioned subsystems are of size $L/2$, the Page result maximises the quasistationary bipartite entanglement entropy,

$$\text{Page result:} \quad S_A(\infty) = \frac{L}{2}\ln 2 - \frac{1}{2}. \tag{2.44}$$

This extensive scaling of entanglement entropy between the system and its environment that is proportional to the volume[22] of the subsystem, which is often referred to as a *volume law* $S_A(\infty) \propto L^d$, is a signature of maximally ergodic (chaotic) systems. These include open quantum systems in thermal equilibrium, where the state of the system is completely random in the Hilbert space. Thermalisation erases local memory of the initial system conditions and configuration, due to the coupling of the quantum system to an external environment ('reservoir') with which the system can exchange energy. As discussed in Section 2.3.3, an extensive scaling of entanglement entropy can also occur in a certain class of closed systems, as detailed by the ETH [18–23], which results in the attainment of an effective thermal equilibrium in a finite time, manifesting ergodic dynamics and internally highly entangled states.

In contrast, for integrable systems and when the interactions are constrained to be local, the associated entanglement entropy may be restricted to a sub-extensive *area law* $S_A(\infty) \propto L^{d-1}$, scaling with the boundary of the subsystem, thus violating the ETH if applicable. This is typical of eigenstates of disordered systems in the many-body localised phase, which arises in locally interacting isolated systems that are furthermore strongly disordered [20, 137, 143–145, 153–157]. The saturation of $S_A(t)$ in late time can be used to quantify the complexity of a given quantum state and suggests a *volume-to-area-law* entanglement transition as a function of system parameters, e.g., disorder. This is further detailed in Section 2.4.1 and investigated in Chapter 3 where quantum mechanical measurement controls the transition.

[22] The volume in 1-dimension ($d = 1$) is the length L.

The von Neumann entanglement entropy is the quantum 'equivalent' of the classical Shannon entropy [158], despite being introduced 20 years earlier. The entanglement entropy can also be used to define a basis-independent measure of correlations between subsystems A and B whose union is not necessarily the entire system, i.e., the quantum counterpart to the classical (bipartite) mutual information. This quantity, the (bipartite) mutual information, is defined as

$$\mathcal{I}_2 = \mathcal{I}_{A:B} = S_A + S_B - S_{A\cup B}. \tag{2.45}$$

For pure quantum states $S_{A\cup B} = 0$, so this is twice the bipartite entanglement entropy between two halves of a many-body system. Since quantum fields (on many-body systems in the thermodynamic limit) have infinitely many degrees of freedom, the entanglement entropy is divergent [159] and it is desirable to define a quantity such as the mutual information that is an appropriate linear combination of various entanglement entropies to mitigate against this, particularly in this context. Note that the sub-additivity property of the entanglement entropy guarantees that mutual information is always non-negative and zero only for a product state $\rho = \rho_A \otimes \rho_B$. While the bipartite mutual information quantifies the correlations between subsystems A and B (i.e., how much information they share), the tripartite mutual information

$$\mathcal{I}_3 = \mathcal{I}_{A:B:C} = S_A + S_B + S_C + S_{A\cup B\cup C} - S_{A\cup B} - S_{A\cup C} - S_{B\cup C}, \tag{2.46}$$

measures the correlations between three subsystems, A, B, and C, as schematically detailed in Figure 2.4 (a). This quantity can be used to measure the extensivity of the mutual information and is therefore often used to diagnose the extent of correlations [69]. For instance, to study the measurement-induced entanglement transition that is introduced in Section 2.4.1 and further investigated in Chapter 3, one typically calculates the tripartite mutual information $\mathcal{I}_3$ between three of four adjacent subsystems of equal size for which $S_{A\cup B\cup C} = S_D$, as sketched in Figure 2.4 (b).

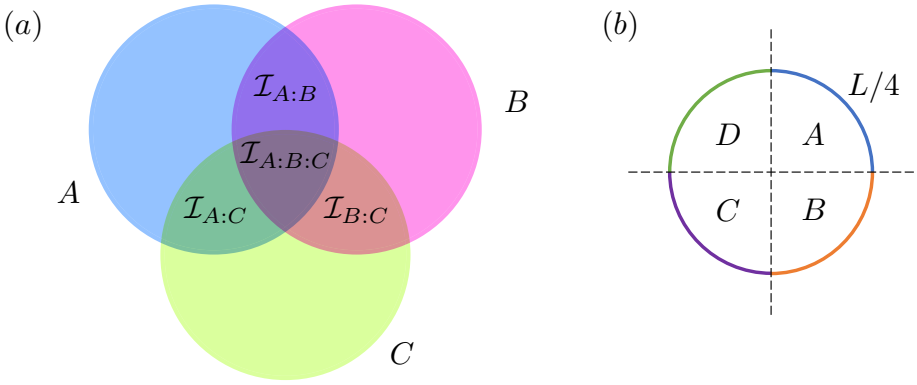

Figure 2.4: (a) Venn diagram representation of the mutual information. The three circles represent the individual entanglement entropies of subsystems A, B, and C, whose overlapping regions correspond to the respective mutual information. Pairwise overlaps correspond to the bipartite mutual information $\mathcal{I}_2$ (2.45), while the overlap of all three circles represents the tripartite mutual information $\mathcal{I}_3 = \mathcal{I}_{A:B:C}$ (2.46). (b) For the measurement-induced entanglement transition, $\mathcal{I}_3$ is typically computed for three adjacent subsystems, with the total system of size L divided into four equal parts.

2.3.4.2 The out-of-time-ordered correlator (OTOC)

In chaotic many-body quantum systems, local operators typically evolve in time to be highly non-trivial, complex objects. As such, information that is initially localised becomes quickly inaccessible and delocalised (scrambled) throughout the system [65, 68, 72]. The Lieb-Robinson bound [160, 161] is a rigorous mathematical result that places an upper limit on the (finite) speed at which information can propagate in physical systems with local interactions. Since it is independent of the system's chaotic status, is not a diagnostic tool for quantum chaos or scrambling but rather a constraint on how fast information can propagate. Instead, one may diagnose the chaotic behaviour of a system by probing the support of an operator[23] as it evolves in time via the out-of-time-ordered correlator (OTOC). These correlators originated in the semiclassical description of superconductivity [162] but also appear as measures of operator growth and information scrambling in quantum many-body systems, including random circuit models, black hole physics, and the SYK model [49, 52, 68, 69, 71–73, 75, 78, 82, 150, 151, 161, 163–171] motivated by possible relations between black hole

[23] That is, the region over which the operator acts non-trivially.

systems and quantum mechanical systems through the AdS/CFT correspondence [172].

Per its definition, an OTOC probes the correlation of a time-evolved Heisenberg operator $W(t)$ with a fixed operator $V(0)$ at a fixed earlier time, which is quantified using the thermal expectation value $\langle\cdot\rangle$ at inverse temperature β of their squared commutator

$$\mathcal{O}(t) = \langle [W(t), V(0)]^\dagger [W(t), V(0)] \rangle. \tag{2.47}$$

(For fermionic operators in fermionic systems, one should consider the squared anticommutator instead of the squared commutator.) In this thesis, we assume that V and W are observables and hence Hermitian. For initially commuting observables, $\mathcal{O}(0) = 0$, the OTOC will evolve in time to be significantly different from zero once $W(t)$ has spread to the location of V. The name of this correlator arises from the fact that when expanded, it then contains contributions of the form

$$F(t) = \langle V(0)W(t)V(0)W(t) \rangle, \tag{2.48}$$

which is of an uncommon structure in terms of the order of time arguments. In Chapter 5, we develop an analytical approach to the spectral form factor and out-of-time ordered correlators in zero-dimensional Brownian models of quantum chaos.

OTOCs are used to quantify the sensitivity of a quantum system to small perturbations, analogous to the classical concept of the butterfly effect (2.40) [168]. In the setting of quantum-chaotic dynamics, the ballistic behaviour at early times allows for the extraction of the quantum analogue of the Lyapunov exponent, which facilitates the formulation of chaos bounds. The famous Maldacena-Shenker-Stanford bound on chaos is found to be saturated both in black holes and in the SYK model [72–75] (whose stochastic time-dependent variant, the Brownian SYK model, is introduced in Section 2.4.2.2). However, this exponential behaviour has been shown not to be universal in quantum-chaotic systems, where some non-integrable systems with RMT-like spectral statistics are characterised instead by OTOCs with a power-law growth [173–176]. Consequently, one may look to benchmark chaotic behaviour with other indicators of quantum chaos based on the spectra and the eigenstates of the systems considered, such as the inverse participation ratio that measures how localised (or delocalised) a wave function is in a given basis [137, 177].

2.4 Random quantum circuits as minimal models for information scrambling

Quantum circuits describe the time evolution of lattice models comprised of spins (with local Hilbert space dimension q) as they evolve under local unitary operations (gates) and local measurements. When these local unitary gates are drawn from a random-matrix ensemble or implement dynamics generated by a random Hamiltonian, the resulting random quantum circuit introduces the notion of locality to the analytical tractability of RMT. The considerable interest (see Ref. [70] for a recent review of the area) in these simple models (so-called minimal models of spatially-extended many-body quantum systems) stems from this tractability for the study of many-body dynamics and universal collective phenomena far from equilibrium. Here, we introduce two classes of random quantum circuits that interpolate between discretised- and continuous-time dynamics, and detail how randomness is a critical ingredient in enabling quantum-classical mappings, including mappings to classical geometric and statistical models.

2.4.1 Discretised circuits: (monitored) random unitary circuits

Random unitary circuits describe discrete time evolution in lattice models and are composed of local unitary operations drawn from a suitable ensemble of unitary gates. The dynamics may be subject to monitoring by an external observer who performs (repeated) local measurements with a tuneable probability. The discretisation of time is similar to the 'trotterisation' of continuous-time Hamiltonian dynamics [178]. However, unlike trotterisation, each local operation is not always close to the identity and the time step is not necessarily infinitesimally small. Consequently, energy is not typically conserved in these circuits.

Random unitary circuits are an example of closed quantum systems that can achieve a local thermal equilibrium through purely unitary evolution (i.e., thermalisation). Without special properties or symmetry constraints, a minimally structured quantum random unitary circuit quickly reaches a steady state that is locally fully disordered,

where local observables match those of a statistical ensemble at infinite temperature. Key universal properties of the evolving state can be captured by information-theoretic measures, such as the entanglement entropy and quantum mutual information (Section 2.3.4.1). These measures reflect correlations that depend non-linearly on the reduced density matrix of a subsystem and are especially relevant in the context of minimal circuits because they do not depend on the specific choice of local basis but are still sensitive to core features of the dynamics, like locality and unitarity.

In the original design of these circuits [88–91], the evolution of a chain of spins is implemented via two-site unitary matrices drawn from the CUE in the brick-layer structure depicted in Figure 2.5 (*a*). The unitary time-evolution operator is

$$U(t) = \mathcal{U}(t)\mathcal{U}(t-1)\mathcal{U}(t-2)\ldots\mathcal{U}(2)\mathcal{U}(1), \tag{2.49}$$

where

$$\mathcal{U}(t) = \begin{cases} \bigotimes_{i\in 2\mathbb{Z}} \mathcal{U}_{i+1,i}(t) & \text{for odd } t \\ \bigotimes_{i\in 2\mathbb{Z}} \mathcal{U}_{i,i+1}(t) & \text{for even } t. \end{cases} \tag{2.50}$$

For a spin chain of qubits with local Hilbert space dimension $q = 2$, $\mathcal{U}_{i,j}(t)$ is a 4×4 Haar-random unitary (CUE) matrix acting on the ith and jth neighbouring sites and so acts on even or odd bonds exclusively in alternating layers. These circuits can be further subject to monitoring by their environment that fully records measurements[24] performed at a tuneable probability or rate p (see Figure 2.5 (*b*)).

2.4.1.1 Measurement-induced entanglement transitions (MIET)

Consider the entanglement dynamics of a system of length L whose initial state is separable, thus characterised by zero average entanglement entropy $\overline{S_A(0)} = 0$ (Section 2.3.4.1). In the limit of purely random unitary evolution ($p = 0$), the unobserved circuit is characterised by an entanglement entropy that grows ballistically $S_A(t) \propto t$ [88, 92, 150, 151] until saturation in a quasistationary regime, where it obeys a volume law (hence, a linear scaling of the quasistationary entropy with system

[24] Each circuit realisation is characterised by a pure-state trajectory corresponding to a particular sequence of measurement outcomes, where the inherently probabilistic nature of quantum mechanical measurement means that the same circuit configuration can yield other trajectories.

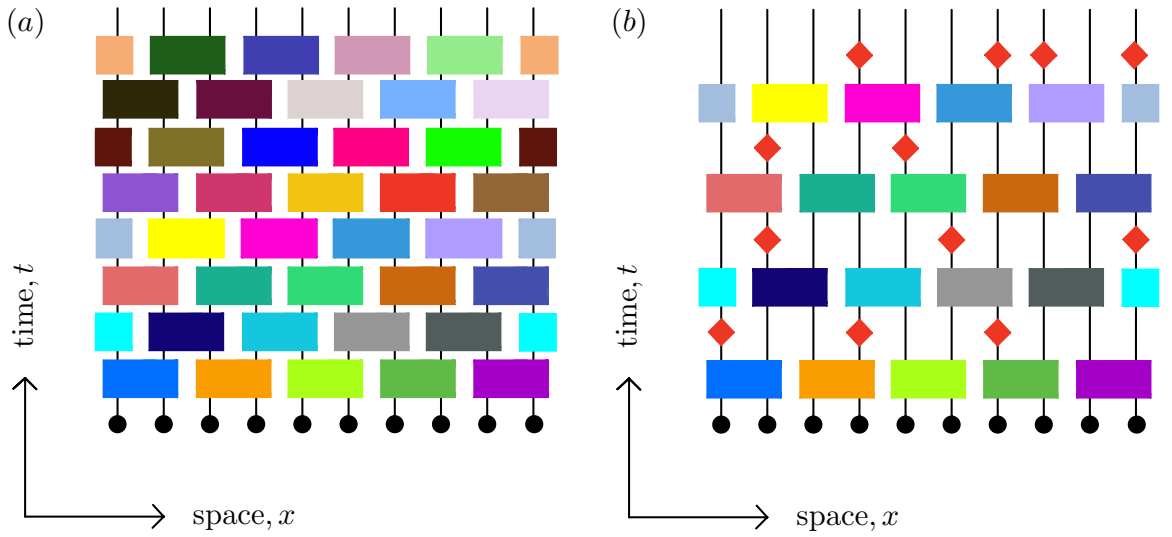

Figure 2.5: Schematic space–time diagram of random unitary circuits with a brick-wall geometry. Each site (black dot) has a q-dimensional Hilbert space and is evolved in time under two-site unitary gates (a) exclusively, or (b) which furthermore may be subject to monitoring via local projective measurements (red diamonds) performed with some tuneable measurement rate p (here, $p = 0.3$). Each rectangle represents an independently-drawn two-site $q^2 \times q^2$ random unitary matrix.

size). Specifically, the realisation-averaged entanglement entropy is anticipated to recover the Page result (2.44). The act of performing local measurements (typically single-site Pauli measurements) with recorded outcomes at rate p keeps the system in a pure state but induces stochastic non-unitary backaction counteracting this entanglement entropy growth (Figure 2.6). The monitored circuit dynamics are non-linear and non-unitary since the quantum trajectory of a state evolving under a specific circuit realisation has Born probabilities that depend on the state. These hybrid unitary-projective circuits have been used to establish that sufficiently frequent local projective measurements drive a transition to a sub-extensive area-law scaling of the quasistationary entanglement entropy, which in this one-dimensional setting hence becomes independent of the system size. Indeed, local measurements performed with sufficient frequency and strength manifest the quantum Zeno effect [91, 179, 180], in which dynamics are frozen and entropy does not grow at all.

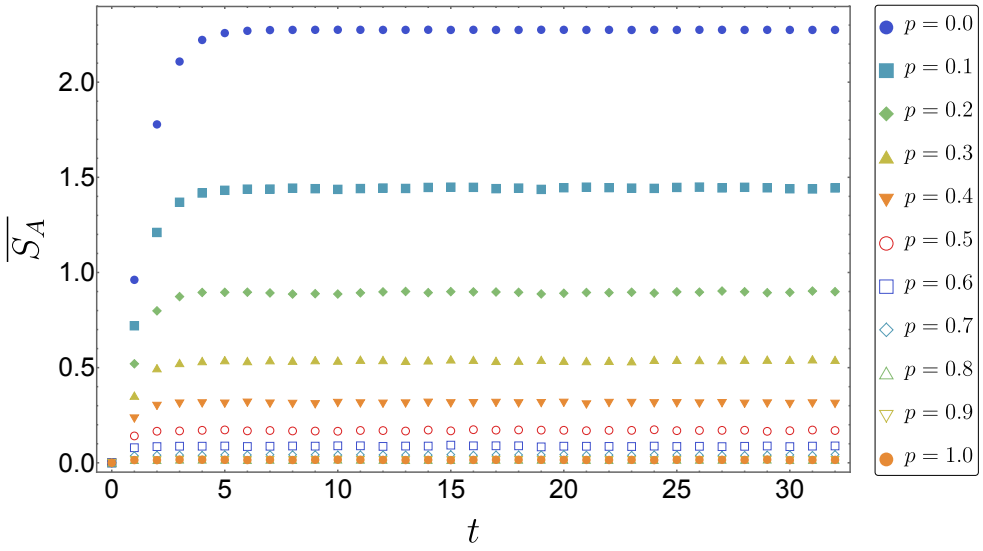

Figure 2.6: Time evolution of the averaged steady-state entanglement entropy $\overline{S_A(t)}$ (2.41). Data is generated over 10^4 realisations for a hybrid random unitary-projective circuit of size $L = 8$ built from Haar-random (CUE) gates for varying measurement rates p modelling the detection of the z-component of spin. For the separable initial state, $\psi(0) = |00..0\rangle$ characterised by vanishing entanglement entropy $\overline{S_A(0)} = 0$, free unitary evolution $p = 0.0$ manifests the Page result (2.44), while measuring with certainty $p = 1.0$ manifests the quantum Zeno effect in which the state is continually reset to a product state and entanglement entropy does not grow, $\overline{S_A(t)} = 0$.

This so-called *measurement-induced entanglement transition* (MIET) has been investigated extensively numerically (see Ref. [70] and references contained therein) and, to some extent, experimentally (e.g., [181–183]). From an analytical perspective, randomness in the circuit elements is crucial since it can enable mappings between real-time quantum dynamics and effective classical statistical mechanics models or dynamical processes. In simple limits (e.g., large local Hilbert space dimension q), some observables reduce to classical geometrical properties of the circuit. For instance, the MIET can be understood via a mapping to a classical geometrical problem, namely the minimal cut through a percolation configuration in which the circuit realisation is interpreted as a tensor network where a projection operator breaks a bond. For sufficiently small p, the majority of bonds are unbroken such that the circuit is connected on large scales [88, 92]. Circuits in which the gates are sampled from the Clifford

group render numerics computationally tractable for large system sizes [89, 184–190] and identify a finite critical measurement rate $p_c \approx 0.17$ separating the volume- and area-law entangled phases in $1+1$-dimensions, which furthermore exhibits a conformal symmetry [190, 191]. A dynamical exponent $z = 1$ characterises this critical point, consistent with Haar-random simulations that are typically restricted to much smaller system sizes [184, 190] and characterised by a critical measurement rate $p_c \approx 0.27$ [88]. The MIET can also be viewed as a dynamical purification transition in which sufficiently frequent measurements performed at a rate $p > p_c$ can purify a maximally mixed initial density matrix $\rho(0) = \mathbb{1}/2^L$ at a system-size-independent rate [188, 192, 193]. In Chapter 3, we ask whether the MIET persists for monitored random quantum circuits whose unitary gates are sampled from Dyson's other two circular ensembles, contrasting the entanglement dynamics in the Threefold Way.

2.4.1.2 Circuit variations

One can further restrict dynamics and remove randomness in time to obtain Floquet (time-periodic) random unitary circuits, which have a well-defined spectrum (unlike random unitary circuits) and remain analytically tractable [52, 54, 56, 90]. Other circuit variations capture special dynamical cases, for instance, deterministic unitary evolution preserving Gaussian states [194–202] and dual-unitary circuits in which unitary transfer matrices describe evolution both in time and space, protecting the ballistic spread of entanglement [203–205]. This dual-unitary class of circuits includes instances of both integrable (i.e., with local conservation laws) and chaotic unitary dynamics. Furthermore, quantum circuits based on an array of qudits (of local Hilbert space dimension q) are generic models of chaotic quantum dynamics [52, 92, 150, 164, 165, 206]. The circuits can also be adapted to display quasi-continuous stochastic dynamics, in which the entanglement transition can be induced via continuous [147] or variable-strength measurements [207].

2.4.2 Continuous circuits: Brownian circuits and zero-dimensional models

Random dynamics can also be formulated in the continuous-time limit for quantum circuits, in which the unitary evolution of the quantum state is modelled as a continuous-time stochastic process that is mathematically analogous to Brownian motion (a Wiener process) [208, 209]. These circuits are inspired by the concept of Brownian motion in classical physics, where a particle follows a random continuous path due to collisions with other particles. In so-called Brownian circuit models, Hamiltonians are chosen randomly (from certain ensembles or models) and independently at each small time step dt [50, 67, 69, 210–213]. The quantum state evolves according to a time-dependent unitary operator, which is a product of infinitesimal random unitaries applied over time t. After $M = t/dt$ time steps, the unitary evolution is given by

$$U(t) = u(t_M; dt)\, u(t_{M-1}; dt) \cdots u(t_1; dt), \tag{2.51}$$

where the general form for the time-evolution operator implementing dynamics generated by some random instantaneous Hamiltonian h_i over time step dt is given by Eq. (2.11) (equivalently, Eq. (2.12)) in Section 2.1.2. The random quantum circuits discussed in Section 2.4.1 are a discretised version in which the dynamics generated by each operator $e^{-ih_i dt}$ is instead implemented by some unitary gate $\mathcal{U}_i$ drawn from an appropriate ensemble. For randomly chosen *chaotic* Hamiltonians h_i, the evolution of the quantum state is governed by a random walk in the space of unitary operators (the unitary group $\mathrm{U}(N)$), converging to the Haar-random ensemble (CUE). The onset of random-matrix behaviour corresponds to how quickly the spectrum of $U(t)$ starts displaying CUE statistics. As the circuit evolves under the random unitary operations, the system tends to reach a thermal equilibrium where local observables behave as though they are in a high-temperature ensemble as detailed by the ETH (Section 2.3.3). The growth of entanglement entropy in these circuits can provide insights into how information scrambles and how systems thermalise, where one expects that the scrambling time scales in these circuit models to be a lower bound for those in the corresponding Hamiltonian systems [50]. In Chapter 4, we develop a

single-parameter scaling theory in terms of spectral statistics (specifically, the SFF introduced in Section 2.2.4.3) for the scenario of maximally efficient scrambling, whose predictions are matched by Dyson's Brownian motion, which we next introduce, and otherwise serve as bounds for other dynamical scrambling scenarios. We will see that this allows one to quantify inefficient or incomplete scrambling on all time scales.

2.4.2.1 Dyson's Brownian motion (DBM)

Dyson's Brownian motion (DBM) [7] is a prominent example of continuous-time random circuits in RMT. Historically, this process was introduced to facilitate RMT calculations [7] and has since served as a central tool in celebrated proofs of universality over a broad class of RMT models [116, 214]. In its original formulation, DBM describes a Brownian motion of the $N \times N$ elements of a Hermitian matrix, specifically how [7]

> 'the elements of the matrix execute independent Brownian motions without mutual interaction. By a suitable choice of initial conditions, the Brownian motion leads to an ensemble of random matrices which is a good statistical model for the Hamiltonian of a complex system possessing approximate conservation laws.'

Another equivalent definition describes a Brownian motion of the eigenvalues of a random Hermitian matrix that is mathematically modelled using the machinery of the Wiener process [116, 126, 215, 216], for which, despite this underlying disorder, an ordered distribution of energy levels manifests [217]. This process is generated by stochastic unitary matrices that update the Hamiltonian and hence can be defined as a dynamical process in its own right, which then takes the form of a Brownian motion on the group $\mathrm{U}(N)$ of $N \times N$ complex unitary matrices that is initialised by the identity matrix [2, 126, 218–225]. In the stochastic description (2.10) outlined in Section 2.1.2, this dynamical version of DBM is formally implemented by generating the incremental unitary time steps (2.12) from instantaneous Hamiltonians $H(t)$ that are drawn from one of the standard Gaussian random-matrix ensembles [16, 17].

In the GUE, the normally distributed matrix elements satisfy

$$\overline{H(t)_{lm}} = 0 \quad \text{and} \quad \overline{H(t)_{kl} H(t)_{mn}} = N^{-1} \kappa \, \delta_{kn} \delta_{lm}, \tag{2.52}$$

which are scaled such that

$$\overline{H(t)} = 0 \quad \text{and} \quad \overline{H^2(t)} = \kappa \mathbb{1}. \tag{2.53}$$

Here, κ is a real positive constant that sets the time and energy scales of the dynamics. Indeed, in Chapter 5, we will see that κ defines an effective rate for the dynamics, enabling the comparison of DBM with other stochastic processes. Since the instantaneous Hamiltonians $H(t)$ generating dynamics are sampled from the GUE, $U(t)$ performs a random walk in the unitary group, sampling it uniformly according to the Haar measure. In Chapter 4, we study universality in the approach to ergodicity in the DBM setting for instantaneous Hamiltonians $H(t)$ sampled from the GUE. In Chapter 5, we build on this and explore universal features for all three standard symmetry classes (unitary, orthogonal, and symplectic), therefore for dynamics generated by Hamiltonians sampled from the GOE and GSE, too, which are distributed analogously subject to constraints from time-reversal symmetry.

In the GOE, $H = H^T$ so that all matrix elements obey $H_{lm} = H_{ml}$ and are real. This modifies their two-point correlations to read

$$\overline{H(t)_{kl} H(t)_{mn}} = (N+1)^{-1} \kappa \left(\delta_{kn}\delta_{lm} + \delta_{km}\delta_{ln}\right). \tag{2.54}$$

In the GSE, the matrices are self-dual,

$$H = (\sigma_y \otimes \mathbb{1}_{N/2}) H^T (\sigma_y \otimes \mathbb{1}_{N/2}) \equiv H^R, \tag{2.55}$$

where σ_r with $r = x, y, z$ denotes the Pauli matrices, and the matrix dimension N is necessarily even. Such matrices are formed out of 2×2-dimensional quaternion blocks

$$H_{lm} = H^{(0)}_{lm} \mathbb{1} + i \sum_r H^{(r)}_{lm} \sigma_r \quad (l, m = 1, 2, \ldots N/2), \tag{2.56}$$

where Hermiticity imposes that all parameters are real. With this constraint, these parameters are independently normally distributed such that

$$\overline{H(t)_{kl} H(t)_{mn}} = (N-1)^{-1} \kappa \left(\delta_{kn}\delta_{lm} - \delta_{km}\delta_{ln}\right) \mathbb{1}_2. \tag{2.57}$$

Both here and in Eq. (2.54) we introduced the scale κ so that Eq. (2.53) still holds.

These features are all that we need to formulate our analytical approach in Chapter 5 to the instantaneous SFF in DBM.

2.4.2.2 Brownian Sachdev-Ye-Kitaev (BSYK)

The Brownian Sachdev-Ye-Kitaev (BSYK) model [51, 73, 74, 226–228] is a quantum mechanical model of M Majorana fermions ψ_a with random q-local, all-to-all interactions that depend stochastically on time. The Majorana fermions obey the algebra $\{\psi_a, \psi_b\} = \delta_{ab}$ and are defined in a Hilbert space of dimension $\dim \mathcal{H} = 2^{M/2}$. Specialising to $q = 4$, the BSYK Hamiltonian [51] is given by

$$\begin{aligned} H(t) &= \frac{1}{4!} \sum_{a,b,c,d} J_{abcd}(t) \psi_a \psi_b \psi_c \psi_d \\ &= \sum_{a<b<c<d} J_{abcd}(t) \psi_a \psi_b \psi_c \psi_d, \end{aligned} \tag{2.58}$$

where the completely antisymmetric coupling tensor $J_{abcd}(t)$ is drawn independently at each instance of time t. Each independent element of the instantaneous coupling tensor is a random real number sampled from a Gaussian distribution with vanishing mean and variance

$$\overline{J_{abcd}(t) J_{a'b'c'd'}(t')} = \delta_{aa'}\delta_{bb'}\delta_{cc'}\delta_{dd'}\delta(t-t')\frac{J^2(q-1)!}{M^{q-1}}, \tag{2.59}$$

where $q = 4$ and the overline $\overline{[...]}$ denotes an average over realisations. Here, J sets an overall energy scale of the system, which we henceforth set to unity.

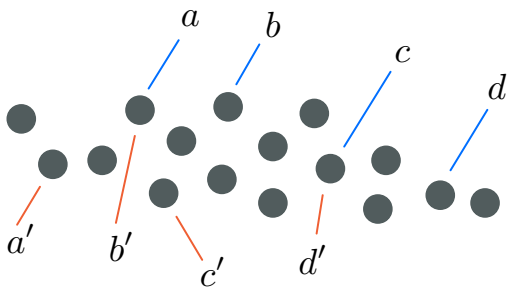

Figure 2.7: Schematic of BSYK interactions at different instances of time, t and t'. At each instant, the M Majorana fermions are coupled within clusters of size q.

The BSYK Hamiltonian (2.58) reduces to that of the conventional SYK model when the couplings are taken to be independent of time. This autonomous SYK model is argued to exhibit strongly chaotic dynamics for sufficiently dense systems and hence closely obeys RMT predictions [229–232]. The fact that the couplings are correlated only at the same instance of time in the BSYK model makes this model simpler than the regular SYK model, where, in particular, the system is expected to relax into an infinite-temperature quasistationary steady state at long times [51], whose instantaneous statistics then should match the description by a random state vector in a suitable RMT ensemble. In Chapter 5, we will examine to what extent RMT universality already holds even before the steady state is reached, where we will relate this to the fast emergence of unitary invariance in the time evolution.

In particular, these features should be manifest in the spectral statistics and dynamical correlations of the system. As described in Section 2.2.4.3, the structure of the SFF for a given dynamical evolution is expected to be sensitive to the symmetry class of a model. The autonomous SYK model is no exception [48]. While in all three scenarios, the SFF exhibits ramp and plateau regions, the detailed structure differs, with a sharp corner in the unitary class, a smooth curve in the orthogonal class, and a kink in the symplectic class. This replicates the key features of the circular ensembles depicted in Figure 2.3. Analogously, in Chapter 5, we will establish a very direct correspondence of the instantaneous spectral statistics and dynamical correlations between the BSYK model and the DBM model generated by the different Gaussian ensembles.

The specifics of this correspondence will therefore depend on the symmetry class of the model, which here is dictated by the number of Majorana fermions M. To describe these we utilise the fact that, for even M, the model may be recast in terms of $M_d = M/2$ Dirac fermions c_i, which we also exploit for the numerical implementation of the model. The Dirac fermions satisfy the usual algebra

$$\{c_i, c_j^\dagger\} = \delta_{ij}, \quad \{c_i, c_j\} = 0, \quad \{c_i^\dagger, c_j^\dagger\} = 0, \tag{2.60}$$

from which one can define Majorana fermions as

$$\psi_{2i} = \frac{c_i + c_i^\dagger}{\sqrt{2}}, \quad \psi_{2i-1} = \frac{i(c_i - c_i^\dagger)}{\sqrt{2}}. \tag{2.61}$$

The Hamiltonian (2.58) preserves the total fermion parity $Q = \prod_{i=1}^{M_d} i^{M_d}\psi_i$ so that it can be decomposed into blocks corresponding to even and odd values of Q. Furthermore, the SYK model obeys a particle-hole symmetry [86, 233, 234], described by the operator

$$P = K \prod_{i=1}^{M_d} \left(c_i^\dagger + c_i\right), \tag{2.62}$$

where K implements complex conjugation. The properties of P impose symmetry constraints on the charge parity sectors of the Hamiltonian, where all three Wigner-Dyson symmetry classes are encountered [47, 86, 235]. The particular symmetry class is determined by the value of $M \bmod 8$, where the eightfold periodicity in M conforms with the Atland-Zirnbauer symmetry classification [31, 236]. When $M_d = M/2$ is odd, i.e., for $M \bmod 8 = 2\,\text{or}\,6$, P maps the even and odd charge parity sectors onto each other. The two sectors are then degenerate and do not have any anti-linear symmetry, so the model falls into the unitary symmetry class. For even $M_d = M/2$, P maps each sector to itself and can square to ± 1. If $M \bmod 8 = 4$, $P^2 = -1$, which when combined with the anti-linearity of P means that P cannot map eigenstates to themselves. There is Kramers' double degeneracy of all levels within each sector, and the corresponding symmetry class is symplectic. On the other hand, when $M \bmod 8 = 0$, $P^2 = +1$ and there is no protected degeneracy; the corresponding symmetry class is orthogonal. This is summarised as

M	8	10	12	14	16	18
symmetry class	O	U	S	U	O	U

and so forth.

Our numerical implementation of the BSYK model exploits this block structure, in which a unitary transformation permutes the Hamiltonian (2.58) to assume block form,

$$\begin{pmatrix} \cdot & 0 \\ 0 & \cdot \end{pmatrix}, \tag{2.63}$$

where each block corresponds to even or odd values of the charge Q and the specific RMT statistics of the blocks are dependent on the action of the particle-hole symmetry

operator (2.62) [47, 86]. Once the Hamiltonian of dimension $2N$ has been reduced to block form, we need only evolve the system in the symmetry-reduced space of the smaller dimension $N = 2^{(M/2)}/2 = 2^{(M/2)-1}$. This is then further simplified by constraints and correlations observed for these blocks in the different symmetry classes. In the unitary symmetry class, the blocks are formed by a matrix A and its transpose A^T,

$$\begin{pmatrix} A & 0 \\ 0 & A^T \end{pmatrix}. \tag{2.64}$$

The dynamics obtained from both blocks are spectrally degenerate, so we need only to generate dynamics for one of them. This degeneracy does not occur in the orthogonal and symplectic symmetry classes, where one instead obtains two independent blocks

$$\begin{pmatrix} A & 0 \\ 0 & B \end{pmatrix}. \tag{2.65}$$

In the orthogonal symmetry class, both matrices can be brought into symmetric form, $A = A^T$ and $B = B^T$, while in the symplectic symmetry class they can be brought into self-dual form, $A = A^R$ and $B = B^R$ so that in the latter case they display Kramers' degeneracy.

Chapter 3

Threefold Way of entanglement dynamics in monitored random quantum circuits

3.1 Overview

Random quantum circuits (Section 2.4) have emerged as a tuneable setting that provides insights into quantum-chaotic dynamics by reproducing many generic features of quantum-chaotic systems, including the scrambling of quantum information and ballistic entanglement spreading. Interleaving measurement into the random unitary circuits manifests a complex interplay between the local entanglement generation by gates and the entanglement reduction by measurements, leading to distinct entanglement phases of the system that are distinguished by whether repeated measurements are performed at a sufficient frequency throughout the bulk of the system to prevent the build-up of long-range quantum entanglement.

In this chapter, we aim to obtain further insights into the entanglement dynamics in quantum circuits built upon Dyson's circular ensembles introduced in Section 2.2.2. Besides the CUE implemented in the original circuit architecture [88–91], this also encompasses the COE for systems obeying a conventional time-reversal symmetry and the CSE representing systems with spin-rotation symmetry [8, 9, 17, 112]. Since the variation of measurements and operations manifests stochastic evolution that typically

renders an analytic approach to the full circuit dynamics intractable, we combine exact analytical random-matrix results for the entanglement generated by the individual gates in the different ensembles and numerical results for the complete quantum circuit.

To analytically quantify the difference between these circuits on the local level, we utilise a statistical measure of entangling power, which we formulate via a characteristic entanglement matrix that captures the essence of the Cartan KAK decomposition of a two-qubit gate [237]. The statistical entangling power is largest in the CUE, followed by the COE, and finally the CSE. It therefore displays a non-monotonous dependence on the standard RMT symmetry index $\beta = 2, 1, 4$ [13, 17]. On the level of the complete circuit, we then show by extensive numerical results that this leads to an entanglement transition also in the COE and CSE, which is shifted towards smaller values of the tuneable measurement rate for the system sizes that we study. This is consistent with interpreting the CUE as providing an upper bound for the entanglement production in the other two cases.

This chapter is organised as follows. In Section 3.2, we introduce the characteristic entanglement matrix and relate its statistical properties to the different ensembles. This is supplemented by Appendix A, where we derive the eigenvalue statistics of antisymmetric matrices associated with the CSE. In Section 3.3, we describe the quantum circuit model and its numerical implementation, and we present the results of the entanglement transition in the full circuit. We summarise our results in Section 3.4.

3.2 Local entanglement generation

Quantum circuits consist of many degrees of freedom evolving in discrete time steps under local gate operations, manifesting complex dynamics in which entanglement builds up over time. To capture the essence of these dynamics in the different symmetry classes, we first obtain analytical results for the statistics of the local entanglement generation, which is the focus of this section. This involves gates acting on pairs of qubits, corresponding to 4×4-dimensional unitary matrices. We proceed in two steps. First, we describe the statistics of entanglement generated by a given unitary matrix when acting on separable states. This can be quantified by a suitable entangling power [238–241], which we here formulate efficiently by introducing a characteristic

entanglement matrix that we then evaluate with a focus on the average entanglement generated by the gate. In the second step, we analyse the complete statistics of this entangling power when the gates are drawn randomly from the appropriate circular ensembles.

3.2.1 Statistics of entanglement generated by a fixed gate

All transformations $U \in \mathrm{SU}(4)$ on the two-qubit Hilbert space of states

$$|\psi\rangle = \alpha\,|00\rangle + \beta\,|01\rangle + \gamma\,|10\rangle + \delta\,|11\rangle \tag{3.1}$$

are either local or non-local, categorised by how they act on the components of the bipartite system. Local operations act on one component of the bipartite system and thus can be expressed as a tensor product of single-qubit operations $A_i \in \mathrm{SU}(2)$,

$$U_{\mathrm{local}} = A_1 \otimes A_2 \in \mathrm{SU}(2) \otimes \mathrm{SU}(2). \tag{3.2}$$

As such, local operations cannot change the entanglement properties of the bipartite system. This is different for non-local two-qubit gates, which cannot be written in this form and do change the entanglement properties of the state. The capacity of these gates to produce entanglement in a bipartite system can be quantified via a suitably defined *entangling power*, typically utilising the entanglement entropy post-operation maximised or averaged over all separable states [238–241]. Here, we implement this notion via a characteristic entanglement matrix, to which we are guided by studying the average of the squared concurrence

$$\mathcal{C}^2 = 4|\alpha\delta - \beta\gamma|^2 \tag{3.3}$$

in the normalised post-operational state $|\psi\rangle$.

Let us therefore consider the effect of acting by an arbitrary but fixed two-qubit gate U on a random initial separable state $|\phi\rangle = |\chi_1\rangle \otimes |\chi_2\rangle$. In the computational

basis, this state can be written as

$$\begin{aligned} |\phi\rangle &= (a\,|0\rangle + b\,|1\rangle) \otimes (c\,|0\rangle + d\,|1\rangle) \\ &= ac\,|00\rangle + ad\,|01\rangle + bc\,|10\rangle + bd\,|11\rangle \end{aligned} \tag{3.4}$$

so that the squared concurrence vanishes. For the post-operation state $|\psi\rangle = U\,|\phi\rangle$, however, we obtain a finite result, which we average by assuming independent uniform distributions of the two input states $|\chi_i\rangle$ over their respective Bloch spheres. This result can be written compactly as

$$\overline{\mathcal{C}^2} = \frac{4}{9} - \frac{1}{36}|\mathrm{tr}\,V|^2, \tag{3.5}$$

where

$$V = YU^TYU, \quad Y = \sigma_y \otimes \sigma_y \tag{3.6}$$

is a characteristic matrix that efficiently captures the essence of the intrinsic entanglement characteristics.

To demonstrate this, we make use of Cartan's KAK decomposition [237], which allows us to explicitly re-express any two-qubit operation via unitary single-qubit operations and 3 entanglement parameters. Explicitly, the decomposition asserts that for any $U \in \mathrm{SU}(4)$, there exist single-qubit gates $A_i, B_i \in \mathrm{SU}(2)$ and parameters $a, b, c \in \mathbb{R}$ such that

$$U = (A_1 \otimes A_2)\exp[i(a,b,c)\cdot(X,Y,Z)](B_1 \otimes B_2), \tag{3.7}$$

where (X, Y, Z) is the vector of the tensor products of the single-qubit Pauli matrices, $X = \sigma_x \otimes \sigma_x$ and $Z = \sigma_z \otimes \sigma_z$, analogous to the definition of Y above. Hence, KAK parameterises the 15-parameter Lie Group SU(4) such that 12 parameters (those associated with SU(2)) characterise local operations and 3 parameters (a, b, and c) characterise non-local operations, and does this for all $U \in \mathrm{SU}(4)$ (including all matrices in the three circular ensembles). Noting that $v_n^* = \sigma_y v_n \sigma_y$ for any SU(2) matrix v_n then

enables us to re-express the characteristic matrix V as

$$V = (B_1 \otimes B_2)^\dagger \exp[2i(a,b,c)\cdot(X,Y,Z)](B_1 \otimes B_2). \tag{3.8}$$

That is, the characteristic matrix V and the matrix exponential $\exp[2i(a,b,c)\cdot(X,Y,Z)]$ are related by a basis change such that their eigenvalues coincide,

$$\lambda_1 \equiv \exp(i\varphi_1) = \exp(-2i(a+b+c)), \tag{3.9}$$
$$\lambda_2 \equiv \exp(i\varphi_2) = \exp(2i(-a+b+c)), \tag{3.10}$$
$$\lambda_3 \equiv \exp(i\varphi_3) = \exp(2i(a-b+c)), \tag{3.11}$$
$$\lambda_4 \equiv \exp(i\varphi_4) = \exp(2i(a+b-c)), \tag{3.12}$$

depending only on the parameters a, b, and c,

$$a = (\varphi_3 + \varphi_4 - \varphi_1 - \varphi_2)/8, \tag{3.13}$$
$$b = (\varphi_2 + \varphi_4 - \varphi_1 - \varphi_3)/8, \tag{3.14}$$
$$c = (\varphi_2 + \varphi_3 - \varphi_1 - \varphi_4)/8. \tag{3.15}$$

Different permutations of the eigenvalues φ_i deliver combinations of a, b, and c that differ only by the single-qubit operations. The parameters a, b, and c are furthermore independent of an overall U(1) phase in the matrix V. While analogous relations have been derived before [240], they usually rely on the isomorphism from $\mathrm{SU}(2)\times\mathrm{SU}(2)$ to $\mathrm{SO}(4)$. With the characteristic matrix V, the parameters a, b, and c can be obtained directly from the standard definition of the gate.

Based on these observations, we can then derive explicit expressions for the entanglement characteristics using the data from V. This is already manifest in Eq. (3.5) for the averaged square of the concurrence that can be further expressed as

$$\overline{\mathcal{C}^2} = \frac{1}{3} - \frac{1}{9}(\cos 4a \cos 4b + \cos 4a \cos 4c + \cos 4b \cos 4c), \tag{3.16}$$

which is completely symmetric in the real parameters a, b, and c. The corresponding

averaged purity of the reduced density matrix of each qubit then follows from

$$\overline{\mathcal{P}} = 1 - \overline{\mathcal{C}^2}/2. \tag{3.17}$$

From here on, it is useful to capture this data in the quantity

$$t = \frac{1}{16}|\mathrm{tr}\, V|^2, \quad 0 \leq t \leq 1. \tag{3.18}$$

The different circular ensembles impose different constraints on the structure of U and hence the parameters a, b, and c, which translates into distinct statistics of the entanglement characteristic t, to which we turn next.

3.2.2 Statistics of entanglement generated by random gates

Rather than only averaging over all possible initial separable states, we can consider the gate U itself being randomly taken from one of the standard circular ensembles. This translates into the statistics of the characteristic matrix V, particularly its eigenvalues, which then determine the statistics of the quantity t.

To do this, we exploit the fact that matrices of the CUE can be used to generate matrices from the other circular ensembles [112] (Section 2.2.2). The ensembles of characteristic matrices to consider are therefore

$$V = \begin{cases} YW^TYW, & (U \text{ in CUE}) \\ YW^TWYW^TW, & (U \text{ in COE}) \\ -YW^TJWYW^TJW, & (U \text{ in CSE}) \end{cases} \tag{3.19}$$

with W from the CUE. It proves helpful to introduce the matrix $y = (\mathbb{1}+iY)/\sqrt{2i} = y^T$, which satisfies $y^2 = Y$ and $y^{-1} = Yy$. Using the measure-preserving substitutions $W \to yWy$ for the CUE, $W \to Wy$ in the COE and CSE, and the eigenvalue-preserving similarity transformation $V \to yVYy$, we can then eliminate the Y matrices without

affecting the statistics. This gives the equivalent ensembles

$$V = \begin{cases} W^T W, & (U \text{ in CUE}) \quad \to V \text{ in COE} \\ (W^T W)^2, & (U \text{ in COE}) \quad \to V \text{ in COE}^2 \\ -(W^T J W)^2, & (U \text{ in CSE}) \quad \to V \text{ in A}^2 \end{cases} \tag{3.20}$$

where A is the ensemble of antisymmetric matrices $A = iW^T JW$ associated with the CSE [242]. For U in the CUE or COE, the eigenvalue statistics of V can be read off directly from the known statistics of the COE, obeyed by the eigenvalues φ_i or $\varphi_i/2$. For U in the CSE, we derive the joint eigenvalue distribution for the ensemble A^2 with arbitrary matrix dimension in Appendix A. This takes the form of a CUE eigenvalue distribution with 2 two-fold degenerate eigenvalues. Applied to the two-qubit gates, this exact eigenvalue degeneracy implies that only one of the three KAK parameters a, b, or c is ever finite. We then only need the distribution of the one finite parameter, which we identify with the parameter a.

The joint probability distributions of eigenvalues $\{\lambda_n\}$ for the COE, CUE, and CSE (indexed respectively by the standard RMT symmetry index $\beta = 1, 2$, and 4) are

$$P(\{\lambda_n\}) \propto \prod_{n<m} |\lambda_n - \lambda_m|^\beta , \tag{3.21}$$

such that the joint distributions of eigenphases $\{\varphi_n\}$ read

$$P(\{\varphi_n\}) \propto \prod_{n<m} \left|e^{-i\varphi_n} - e^{-i\varphi_m}\right|^\beta = \prod_{n<m} \left|\sin \frac{\varphi_n - \varphi_m}{2}\right|^\beta . \tag{3.22}$$

We need only the statistics of the COE (for U in the CUE or COE) and the CUE (for U in the CSE). In terms of the parameters a, b, and c, we then obtain the joint

distributions

$$P(a,b,c) \propto \begin{cases} |\sin(2b+2c)\sin(2a+2c)\sin(2a+2b)\sin(2a-2b) & \\ \qquad \sin(2a-2c)\sin(2b-2c)|\,, & (U \text{ in CUE}) \\ |\sin(b+c)\sin(a+c)\sin(a+b)\sin(a-b)\sin(a-c) & \\ \qquad \sin(b-c)|\,, & (U \text{ in COE}) \\ \sin^2(2a). & (U \text{ in CSE}) \end{cases} \tag{3.23}$$

These joint distributions capture the complete statistics of the entanglement characteristics in each ensemble. For instance, they imply the respective ensemble averages of t

$$\bar{t} = \begin{cases} 1/10, & (U \text{ in CUE}) \\ 23/140, & (U \text{ in COE}) \\ 1/4. & (U \text{ in CSE}) \end{cases} \tag{3.24}$$

In the CSE, where $t = \cos^2(2a)$, we can furthermore obtain the complete probability distribution

$$P_{\text{CSE}}(t) = \frac{2}{\pi}\sqrt{t^{-1}-1}. \tag{3.25}$$

In the entangling power (3.5), the quantity t appears with a minus sign so that the averaged squared concurrence $\overline{\mathcal{C}^2}$ is largest for the CUE and smallest for the CSE. Notably, this means that the entangling power follows an unconventional ordering in the standard RMT symmetry index β, given by $\beta = 1$ for the COE, $\beta = 2$ for the CUE, and $\beta = 4$ for the CSE, separating this characteristic from the behaviour of other observables [13, 17].

We now turn to question how this affects the entanglement transition in the full monitored circuit dynamics, where these processes compete with measurements.

3.3 Entanglement transition

3.3.1 Model

The numerical model implemented is based on the universal quantum-circuit architecture [90, 92, 147, 150, 151] introduced in Section 2.4 and diagrammatically shown in Figure 3.1. The quantum circuit is a spatially periodic one-dimensional chain of L spins (where L is even), whose quantum state is evolved in discrete time steps, each of which consists of four layers of operations. The first layer applies unitary two-spin operators U to consecutive pairs of spins, namely, the spins labelled by indices $2l-1$ and their next-neighbouring site $2l$ ($l = 1, \ldots, L/2$). The second layer implements projective measurements M of the z-component of each spin, which for each spin are carried out independently with probability p. The third operation applies unitary two-spin operators U to each even and next-neighbouring site, labelled by indices $2l$ and $2l+1 \mod L$. The fourth and final layer again implements independent projective measurements M on each spin, with the same probability p as in the second layer.

The variation of unitary operations and measurements throughout space and time manifests a stochastic time evolution. Local measurements are implemented by the standard von Neumann protocol [99, 100, 142] (Section 2.1.3) and induce stochastic non-unitary backaction, reducing quantum correlations—projecting the system onto an eigenstate of a local operator completely disentangles the corresponding local degree of freedom from the rest of the system. Importantly, it is assumed that all measurement results are recorded so that the system remains in a pure state.

As described in Section 2.4.1, these measurements are combined with unitary two-spin operators drawn independently from the CUE in the original circuit design [88–91], each generating entanglement locally as considered in the previous section. In the dynamics of the quantum circuit, the entanglement then spreads out over the system, until the system settles into a quasistationary state whose entanglement characteristics depend on the measurement rate p. It was found that the system displays a transition in the von Neumann bipartite entanglement entropy S_A (2.41) (Section 2.4.1.1). In this transition, S_A scales linearly with system size L below a critical measurement rate p_c, manifesting a volume law, but becomes independent of system size for $p > p_c$, manifesting an area law.

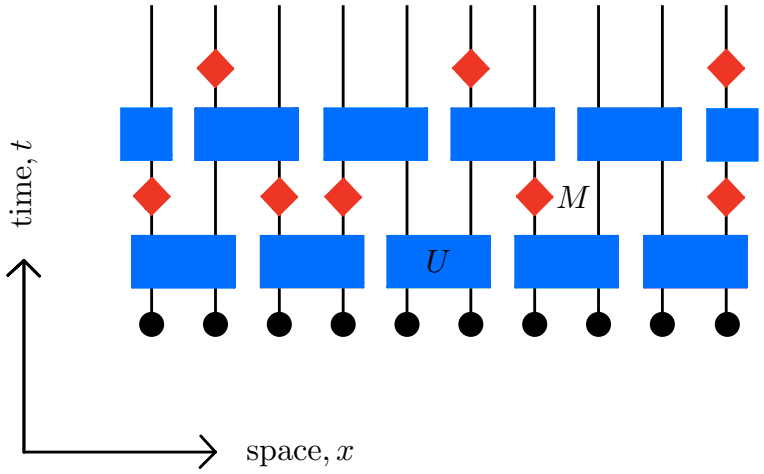

Figure 3.1: Schematic illustration of the unitary-projective time evolution of a one-dimensional quantum circuit during a single time step. Each of the L spin locations is denoted by a solid black dot. Alternating unitary operations U on pairwise spins are represented by blue rectangular blocks and generate entanglement between adjacent degrees of freedom, while red diamond shapes represent local projective measurements M implemented with probability p, which remove entanglement. The illustration depicts one possible random realisation of the measurements.

3.3.2 Numerical results

Our goal is to establish the persistence of a measurement-induced entanglement transition in the model in which entanglement dynamics are now generated by either the COE or CSE. In each case, the unitary two-spin operators U are generated randomly and independently with probability given by the corresponding Haar measure [112, 243], while the measurement protocol is kept as before. We consider the dynamics of a system of length L whose initial state is separable, thus characterised by a vanishing entanglement entropy. We then obtain the numerically averaged bipartite von Neumann entropy $\overline{S_A(t)}$ (2.41) as a function of the discrete iteration time t, where the average is carried out over different realisations of the unitary gates and randomly applied measurements and outcomes, as well as the two inequivalent choices of bipartition (cutting through a pair of spins entangled in the last layer, or between such pairs). In the quasistationary regime, here always fully attained after $4L$ time steps, the steady-state entropy $\overline{S_A(\infty)}$ is consistently observed to be independent of the initial state so that

we can set it to $|\psi(t=0)\rangle = |000...0\rangle$.

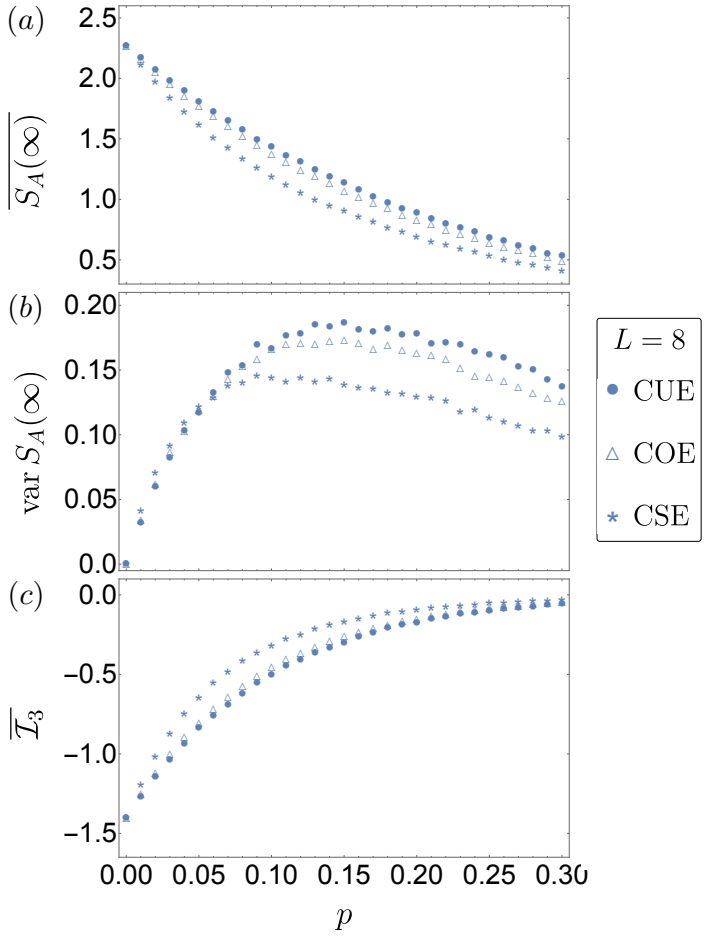

Figure 3.2: Comparison of the quasistationary entanglement statistics in quantum circuits of size $L = 8$, whose unitary dynamics are generated from the three different symmetry classes, CUE (filled circles), COE (open triangles), and CSE (stars). (a) Ensemble-averaged quasistationary entanglement entropy $\overline{S_A(\infty)}$, (b) corresponding fluctuations $\mathrm{var}\, S_A(\infty)$, and (c) tripartite mutual information $\overline{\mathcal{I}_3}$, all plotted as a function of the measurement rate p. Each data point is obtained from 10^4 realisations.

Figure 3.2 depicts the resulting entanglement statistics generated by the three circular ensembles for quantum circuits of fixed size $L = 8$, as a function of the projective measurement rate p. Panel (a) shows the steady-state entanglement entropy $\overline{S_A(\infty)}$. In the limit of purely random unitary evolution (i.e., in the absence of measurement, $p = 0$), $\overline{S_A(\infty)}$ consistently recovers the Page result [152] given by Eq. (2.44). As the

projective measurement rate p increases, the quasistationary entanglement entropy is suppressed, which is a consequence of the measurement backaction. When comparing the results for the different ensembles within panel (a) for $p \neq 0$, we find that $\overline{S_A(\infty)}$ is systematically the largest in the CUE and the smallest in the CSE. This is consistent with the differences in the entangling power of individual gates obtained in our analytical considerations and hence retains the unconventional ordering by the symmetry index β. Figure 3.2 (b) verifies these trends by the sample-to-sample fluctuations var $S_A(\infty)$. Compared to the CUE, these fluctuations are suppressed in the other two ensembles, most noticeably so in the CSE. Figure 3.2 (c) substantiates this further in terms of the tripartite mutual information $\overline{\mathcal{I}_3}$ (2.46), defined for the three adjacent subsystems A, B, and C, each of size $L/4$ as schematically illustrated in Figure 2.4 (b). We again find a systematic shift between the different ensembles, consistent with the quantitative differences in the entanglement generation process.

At any fixed p, the dependence of the entanglement statistics on L further distinguishes an extensive volume-law scaling from an area-law scaling. In Figures 3.3 to 3.5, we analyse this for the different ensembles. Figure 3.3 plots the steady-state entanglement entropy $\overline{S_A(\infty)}$ as a function of the projective measurement rate p, where we now compare results for different system sizes L. In the absence of measurement ($p = 0$), we continue to consistently recover the Page result (2.44). As long as the projective measurement rate p remains small, the quasistationary entanglement entropy remains large and continues to increase linearly with system size L. Increasing the measurement rate further suppresses $\overline{S_A(\infty)}$ monotonically, until its behaviour becomes indicative of being independent of system size at sufficiently large measurement rates. For the system sizes that we study, this translates to an entanglement transition occurring at a characteristic critical measurement rate p_c for each of the ensembles. As we show next, when compared to the CUE, the value of p_c is slightly reduced in the COE and noticeably reduced in the CSE. For this, we first turn in Figure 3.4 to the sample-to-sample fluctuations var $S_A(\infty)$, which become large in the vicinity of the entanglement transition [147]. Compared to the CUE, these fluctuations are suppressed in the other two ensembles, whose locations of maximal fluctuations are shifted to smaller measurement rates, most noticeably so in the CSE.

Figure 3.5 quantifies this shift in terms of the ensemble-averaged tripartite mutual

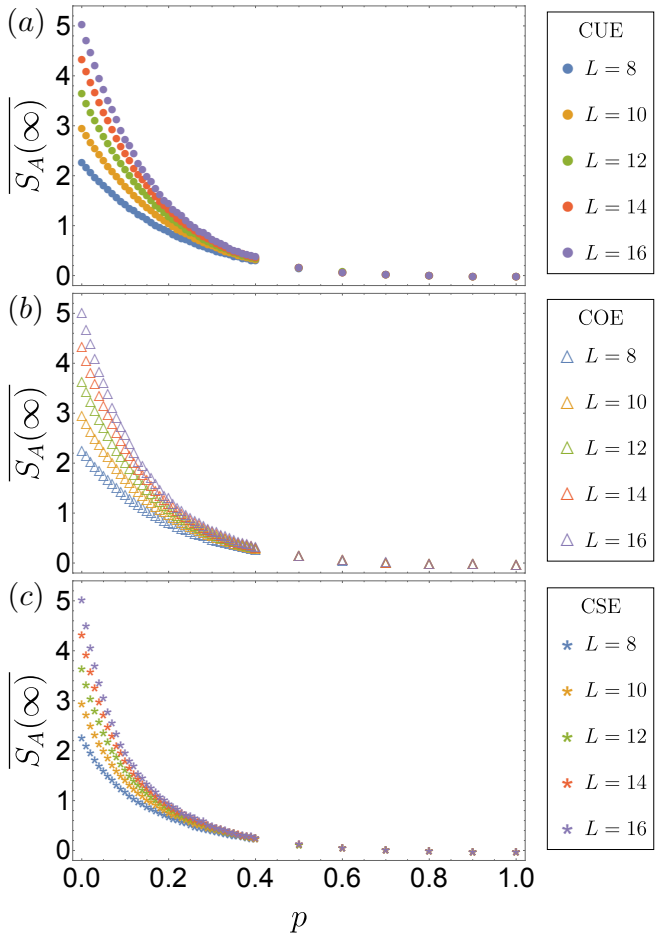

Figure 3.3: Quasistationary entanglement statistics of the bipartite entanglement entropy $\overline{S_A(\infty)}$ as in Figure 3.2 (a) but now comparing systems of size $8 \leq L \leq 16$ in each ensemble, (a) CUE, (b) COE, and (c) CSE. Each data point is obtained from 10^4 realisations (10^3 for $L = 16$).

information $\overline{\mathcal{I}_3}$ of three adjacent subsystems, each of size $L/4$. In this quantity, the transition is indicated by the crossing point between curves produced by different system sizes, which must necessarily have length L divisible by 4. Indeed, $\overline{\mathcal{I}_3}$ can be interpreted akin to an order parameter; in the limit of no measurement ($p = 0$), $\overline{\mathcal{I}_3}$ diverges to infinitely negative values for increasing system size, while it is expected to be a negative number close to zero in magnitude once the area-law phase has been established by frequent projective measurement. In the original hybrid unitary-projective circuits that

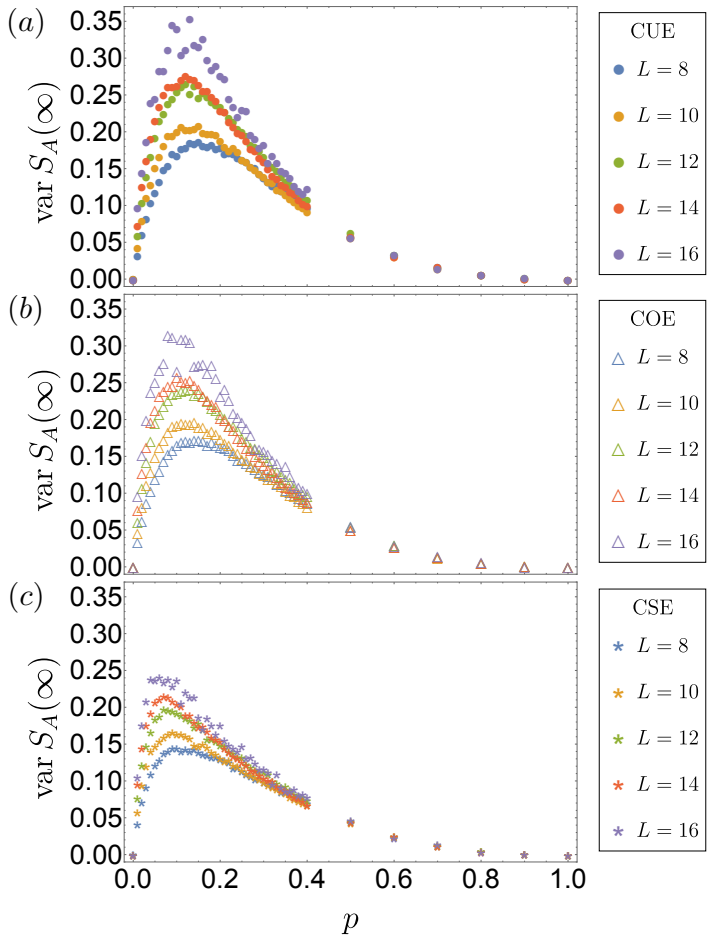

Figure 3.4: Quasistationary entanglement statistics of the fluctuations var $S_A(\infty)$ as in Figure 3.2 (b) but now comparing systems of size $8 \leq L \leq 16$ in each ensemble, (a) CUE, (b) COE, and (c) CSE. Each data point is obtained from 10^4 realisations (10^3 for $L = 16$).

serve as our reference, the crossing points between curves $\overline{\mathcal{I}_3}$ of different system sizes are found to have minimal finite-size drifts, which enables the reliable determination of the critical measurement rate with minimal scaling assumptions. (Conversely, for continuous-time models, crossings are found to drift with increasing system size [147, 184, 188, 244, 245].)

These features are indeed born out by the data in Figure 3.5. In each ensemble, the curves for different system sizes cross at a characteristic location, which then allow

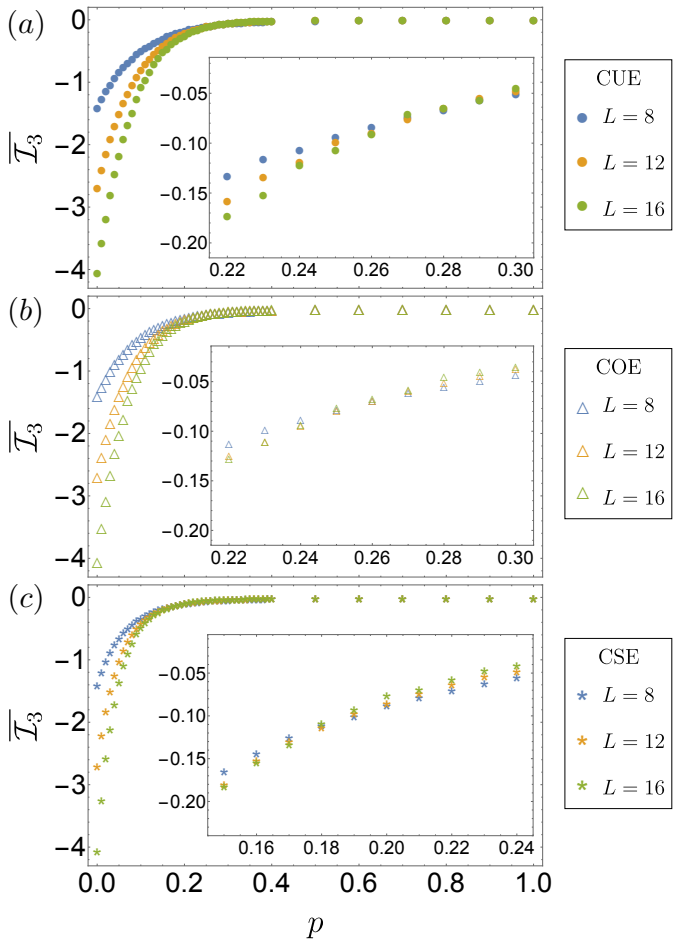

Figure 3.5: Quasistationary entanglement statistics of the tripartite mutual information $\overline{\mathcal{I}_3}$ as in Figure 3.2 (c) but now comparing systems of size $8 \leq L \leq 16$ in each ensemble, (a) CUE, (b) COE, and (c) CSE. The insets focus on the region where $\overline{\mathcal{I}_3}$ crosses for different system sizes, from which we extract an estimate for p_c characterising the measurement-induced entanglement transition. Each data point is obtained from 10^4 realisations (10^3 for $L = 16$).

for crude estimates of the respective critical measurement rate by best fitting quadratic curves to the data. For the studied system sizes, these estimates are given by $p_c \approx 0.27$ in the CUE, consistent with the literature [88], as well as $p_c \approx 0.25$ in the COE and $p_c \approx 0.18$ in the CSE. The ordering of these values therefore conforms once more to our general picture that, statistically, gates from the CUE generate the largest amount of entanglement and those from the CSE generate the smallest amount.

3.4 Summary

In this chapter, we applied RMT to analytically characterise the entanglement generated by unitary matrices taken from Dyson's three circular ensembles, representing gates with different behaviour under time-reversal symmetry, and then supplemented this by numerical investigations of the ensuing entanglement dynamics in hybrid unitary-projective quantum circuits built from these gates. Utilising a characteristic entanglement matrix, we found that gates from the CUE, which are conventionally invoked in these circuits, generate more local entanglement than gates from the COE or CSE, resulting in an unusual ordering of this characteristic in terms of the RMT symmetry index β. This results in a transition from an extensive volume-law scaling to a subextensive area-law scaling, which we found to persist for dynamics generated by the COE and CSE but to occur at a reduced critical rate of projective measurements for the system sizes that we numerically study. These results imply that ensuring *local* time-reversal symmetry on the level of individual gates can help to inhibit thermalisation in noisy settings, which is desirable in the storage and manipulation of quantum information. Besides shifting the critical rate of the transition, it remains to be seen if the dynamics generated by the COE and CSE can also modify the critical exponents of the entanglement transition. A reliable numerical analysis of the finite-size critical exponent, which might shed light on the symmetry classes of the transition, would, however, require system sizes beyond those accessible in numerical simulations.

By introducing the notion of locality and structure to RMT, random quantum circuits have materialised as a highly modifiable platform to investigate thermalisation and chaotic dynamics, and the underlying universal phenomena of quantum information and entanglement spreading. The simpler setting of zero-dimensional models (generically with all-to-all interactions, not restricted to be pairwise on a chain) is more tractable, and therefore promising for detailed insights into the scrambling mechanism and approach to ergodicity.

Chapter 4

Spectral chaos bounds from scaling theory of maximally efficient quantum-dynamical scrambling

4.1 Overview

Across a diverse range of settings in physics, a universal endpoint of *ergodic* dynamics can be defined in terms of random-matrix theory. The dynamical process that describes the evolution of complex quantum systems towards this ergodic endpoint—*scrambling*—is typically system-specific [69] but conjectured to acquire universal features when it is most efficient, as is the case for maximally chaotic systems [65, 72]. These emergent universal characteristics can be mathematically formulated as chaos bounds that govern, for instance, the behaviour of out-of-time-ordered correlators [48, 72] (Section 2.3.4.2). The latter are generally associated with operator scrambling, which, albeit typically conflated with, has recently been shown to be necessary but insufficient for quantum chaos [246]. Furthermore, studying the OTOC in isolation is not enough to fully discriminate between unitary evolution inducing scrambling and external noise responsible for decoherence in experiments [247, 248], motivating the study of other quantities. From a spectral perspective, strictly unitary evolution connects dynamics at different times [249–254], indicative that maximally ergodic long-time behaviour is (universally) linked to short-time scrambling dynamics.

In this chapter, we utilise this spectral perspective to develop a predictive single-parameter scaling theory for the efficient scrambling dynamics of maximally chaotic systems and apply this theory to obtain analytical benchmarks for their behaviour over all time scales, formalised as spectral chaos bounds. This uncovers universality in the language of a general framework that relates all statistical details to a single intrinsic parameter [255]. The scaling assumption is simple—we equate the only two invariants of the dynamics under the assumption that the Hilbert space has no further structure, i.e., that the dynamics are invariant under unitary basis changes. This ansatz integrates into a single-parameter version of a specific random-matrix ensemble, the Poisson kernel, which has been widely studied in static settings [13, 207, 256, 257] but here acquires a dynamical interpretation. The scaling predictions are matched by a privileged stochastic process, Dyson's Brownian motion, and serve as bounds for other dynamical scrambling scenarios, allowing one to quantify inefficient or incomplete scrambling on all time scales. As the scaling theory manifestly preserves all unitarity constraints, it emphasises the role of functional relations linking the short- and long-time dynamics, both in the universal regime as well as deviations away from it, from which we can draw broader conclusions about the approach to ergodicity in complex quantum matter.

This chapter is organised as follows. We begin by reviewing the connection between scrambling and chaos bounds in Section 4.2, and contrast the out-of-time-ordered correlators (Section 2.3.4.2), typically used to formulate these bounds, with the spectral form factor (Section 2.2.4.3), which is the focal quantity in our formulation in terms of spectral statistics. In Section 4.3, we develop the scaling theory and derive analytical forms of the spectral form factor for optimally efficient scrambling. In Section 4.4, we utilise the scaling framework to characterise specific processes and demonstrate that scaling expressions serve as sensitive chaos bounds. Finally, we draw our conclusions in Section 4.5. The technical details are given in Appendices B, C, and D.

4.2 Background and objective

4.2.1 Characterising scrambling

While complex quantum many-body dynamics vary greatly for different quantum systems, it is conjectured that there exists an upper bound on how quickly such systems can disperse, or *scramble*, local information into non-local degrees of freedom [48, 65, 71, 72]. As detailed in Section 2.3.4.2, a principal diagnostic tool to quantify these scrambling dynamics is the OTOC [48, 72]. The Maldacena-Shenker-Stanford bound conjectures that this correlator develops at most exponentially in time [72], and never faster than a universal Lyapunov exponent, setting a bound that is independent of the details of the system. This *chaos bound* is saturated by *fast scramblers*, thought to encompass systems such as black holes and the SYK model at low temperature [68, 73–76]. After the scrambling time, this initial exponential growth of the OTOC for chaotic systems [258–260] settles into saturation oscillations, whose amplitude is suppressed in the chaotic limit [175, 261–263], and generally displays non-universal behaviour [174, 264–267]. *Slow scramblers* fail to saturate this bound on all time scales, only attaining, e.g., logarithmical growth as in many-body localised systems [268–270], linear short-time growth as in weakly chaotic systems [173], or quadratic growth as in Luttinger liquids [174].

This interplay between universal and non-universal features replicates a common theme known from the study of spectral statistics. In this spectral setting, the key quantity to capture both the universal and system-specific aspects of the dynamics over all time scales is the SFF (2.36) discussed in Section 2.2.4.3, which can also be defined in the stroboscopic setting (2.37) and furthermore generalised to scenarios without periodic dynamics (2.39). In the CUE, one obtains the paradigmatic dip-ramp-plateau form (2.38). However, this result does not capture the details of the short-time scrambling dynamics itself. For complex quantum systems, $K(t)$ generally displays a dip over the scrambling regime, taking the value of unity at the minimum, followed by a ramp up to $K(t) \sim N$ until the Heisenberg time at which the discreteness of the level spectrum becomes resolved, which is then followed by a plateau. System-specific signatures can persist well into the ramp, while fast scramblers are expected to display universality already during the dip [50, 54, 65, 271].

In this chapter, our general objective is to combine these themes and establish universal benchmarks of efficient complex quantum dynamics in terms of the spectral information. This is paired with the conjecture that for efficient systems, this spectral information again recovers a strong degree of universality.

4.2.2 The SFF and unitarily invariant processes

Our main setting will be stochastic processes (2.10) in which the unitary matrix $U(t)$ generating the dynamics is updated incrementally by unitary matrices $u(t;dt) \simeq \mathbb{1}$ over a small time step dt, where the sole constraint imposed is that $u(t;dt)$ be invariant under unitary basis changes. These processes describe a large class of dynamics, among which we want to identify and characterise those that facilitate maximally efficient chaotic dynamics.

We prepare this discussion by adapting the spectral form factor to this setting. At any point of time t, this dynamical evolution can be equipped with a definite Heisenberg time by considering the instantaneous SFF (2.39) that analyses the moments of $U(t)$, thus probing the dynamics over all energy and time scales [3, 125, 126]. In the context of this chapter, it facilitates detailed analysis by giving us two time scales—the time t for the evolution along the scrambling dynamics, and the time nt resolving the spectral statistics established up to this point.

Our approach will allow us to relate these spectral correlators through the flow of a single scaling parameter that we introduce in the next section. To establish some early intuition for what we are aiming at, let us apply the definition (2.39) to any dynamical evolution (2.10) induced by ensembles of generators that are invariant under rotations $u(t;dt) \to W^\dagger u(t;dt)W$. Evaluating the average over W in the CUE, the first-order SFF incrementally updates as

$$K_1(t+dt) = K_1(t) + \frac{N^2 - \overline{|\operatorname{tr} u(t;dt)|^2}}{N^2-1}\,(1-K_1(t))\,, \tag{4.1}$$

where the overline here denotes averaging over the specific ensemble generating stochastic dynamics, resulting in an exponential decay to unity with the decay constant

$$\gamma_1 = \lim_{dt\to 0} dt^{-1}(N^2 - \overline{|\operatorname{tr} u(t;dt)|^2})/(N^2-1). \tag{4.2}$$

Within this class of unitarily invariant dynamics, distinct processes (each characterised by some $\overline{|\operatorname{tr} u(t;dt)|^2}$) are therefore characterised by different rates γ_1, which discriminate how efficiently they approach ergodic random-matrix behaviour. Moreover, it follows directly from the statistical definitions that the corresponding decay rates of the higher-order SFFs are constrained as $\gamma_n \leq n\gamma_1$.

Our specific objective is to turn such relations into spectral chaos bounds for the maximally efficient scrambling scenario, which abstracts away the arbitrary overall time scale of the dynamics. For this, we set out to formulate such bounds in a stricter fashion in terms of a single scaling parameter.

4.3 Scaling theory of the spectral form factor

4.3.1 Scaling ansatz

For maximally chaotic scrambling, we expect the dynamics to have minimal constraints. On the level of the incremental time evolution (2.10), this would include representative processes for which the generators $u(t;dt)$ are invariant under unitary basis changes. We now observe that on the level of the resulting dynamics $U(t)$ at finite times, there are two fundamental anti-Hermitian invariants, $U^\dagger \frac{dU}{dt}$ and $U - U^\dagger$, that are also invariant under unitary basis changes. Of these, the former extracts the generator of the time evolution, while the latter characterises the departure from the initial conditions. Constraining the description of these processes in terms of such invariants is in the spirit of the seminal scaling theory of localisation that relates the fluctuations in the conductance to the value of the conductance itself [255]. For maximally chaotic scrambling, where we expect the dynamics to have no further constraints, we therefore propose the scaling assumption

$$U - U^\dagger = g(t) U^\dagger \frac{dU}{dt} \equiv U^\dagger \frac{dU}{da}, \tag{4.3}$$

which equates these invariants in the ensemble sense up to a time-dependent factor $g(t)$. This scaling ansatz can be integrated by introducing the parameter

$$a(t) = \tanh\left[\operatorname{atanh}(a_0) - \int_{t_0}^{t} (1/g(t'))dt'\right], \tag{4.4}$$

which follows from setting $g(t)d/dt = (a^2 - 1)d/da$. The scaling ansatz (4.3) is then solved by the parameterised ensemble

$$U = (a\mathbb{1} + V)(\mathbb{1} + aV)^{-1}. \tag{4.5}$$

The originally assumed basis invariance is respected when V is uniformly distributed in the unitary group of degree N, hence taken from the CUE.

This ensemble is a single-parameter incarnation of the Poisson kernel, a matrix ensemble that previously appeared in stationary scattering settings subject to some constraint [13, 207, 256, 257], where its functional form is tied to a multiple-scattering expansion [215]. Here, we encounter it instead in the context of dynamics generated by a multiplicative composition law, where the dynamical flow of the scaling parameter $a(t)$ will be of central importance.

4.3.2 Interpretation of the scaling parameter

Our scaling assumption reduces the matrix-generated scrambling dynamics to a single dynamical scaling parameter a. In terms of this parameter, the ensemble (4.5) interpolates between action by the identity ($U = \mathbb{1}$) at $a = 1$ and the random unitary matrix $U = V$ at $a = 0$, i.e., the static ergodic endpoint defined by the CUE. For intermediate time, we can equate $a = N^{-1}\overline{\mathrm{tr}\, U}$ to characterise the motion of the centre of mass of the eigenvalues $\lambda_n \equiv \exp(i\phi_n)$, capturing their expansion on the unit circle as ergodicity is established. This centre-of-mass motion is illustrated in an individual realisation $U(t)$ in Figure 4.1. The cloud of eigenvalues, initially centred at unity, begins to disperse around the unit circle so that $N^{-1}\mathrm{tr}\, U$ performs a stochastic trajectory towards the origin—the RMT result—where the centre of mass of the eigenvalues is zero.

This motion is tied to a specific scaling of the density of states, which we will have to take into account in the application of the theory. The mean density of eigenvalues $\lambda_l \equiv \exp(i\phi_l)$ of the unitary time-evolution operator U can be obtained by first expressing

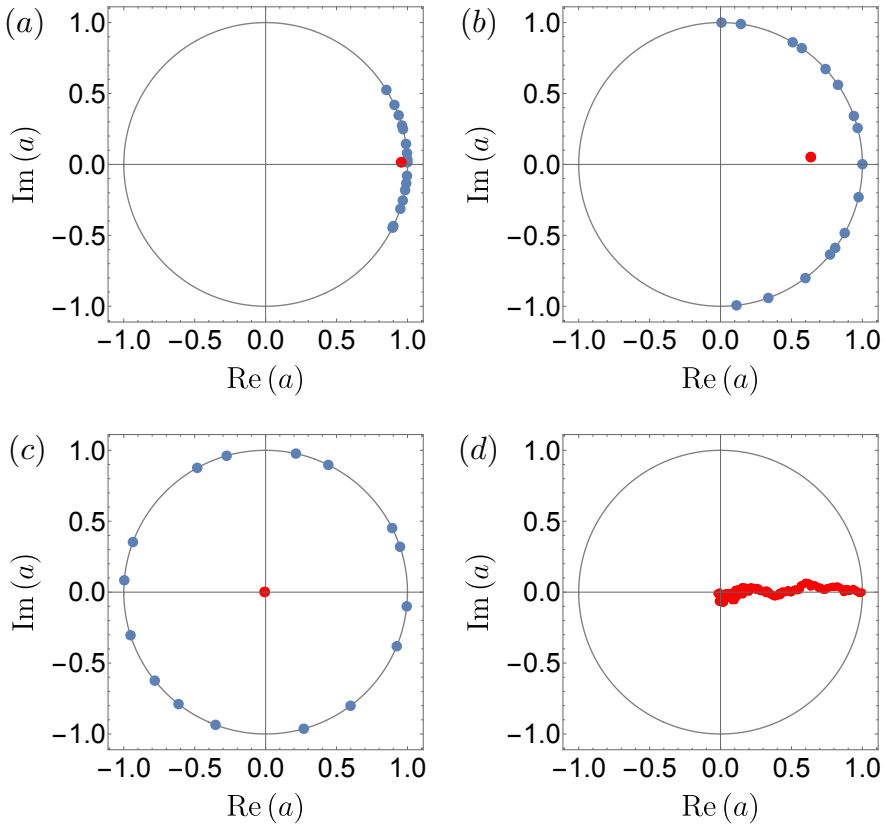

Figure 4.1: Interpretation of the spectral scaling parameter a as the centre of mass (red) of the eigenvalue distribution (blue), illustrated for a single time evolution generated by the multiplication of random unitary matrices of the form (2.13) ($N = 16$, $dt = 0.01$). Panels (a)-(c) show snapshots after 10, 100, and 1000 time steps, while panel (d) shows the complete centre-of-mass trajectory over 1000 time steps.

it in terms of the moments $A_n = N^{-1}\overline{\mathrm{tr}\, U^n}$, whereby

$$\rho(\phi) = \frac{1}{2\pi}\left(1 + 2\sum_{n=1}^{\infty} A_n \cos(n\phi)\right). \tag{4.6}$$

In the scaling theory, $A_n = a^n$ follows directly by expanding Eq. (4.5) into a geometric series and using the CUE average $\overline{V^m} = \delta_{0m}\mathbb{1}$. The first term

$$A_1 = a = N^{-1}\overline{\mathrm{tr}\, U} \tag{4.7}$$

recovers the interpretation of the scaling parameter as the centre of mass of the eigenvalue cloud. Summation of the series (4.6) then delivers the scaling mean density of states

$$\rho(\phi) = \frac{1}{2\pi} \frac{1-a^2}{1+a^2-2a\cos\phi}, \tag{4.8}$$

whose flow corresponds to the expansion of the eigenvalues.

The scaling ensemble (4.5) endows this expanding eigenvalue cloud with intrinsically universal spectral statistics, induced via the matrix-valued Möbius transformation

$$U' = \left(\frac{a'-a}{1-aa'}\mathbb{1} + U\right)\left(\mathbb{1} + \frac{a'-a}{1-aa'}U\right)^{-1} \tag{4.9}$$

between the ensembles with parameters a to a'. At the same time, the scaling parameter defines a specific unfolding procedure of the eigenvalues. For any pair of unitary matrices U and V related by (4.5), the eigenvalues $\mu_l = \exp(i\psi_l)$ of V determine the eigenvalues

$$\lambda_l = (a+\mu_l)/(1+a\mu_l) = \exp(i\phi_l) \tag{4.10}$$

of U. When V is sampled from the CUE, λ_l are eigenvalues distributed as in the Poisson kernel with the scaling mean density of states (4.8). This transformation can be inverted to translate the eigenvalues λ_l into uniformly distributed eigenvalues

$$\mu_l = (a-\lambda_l)/(a\lambda_l - 1), \tag{4.11}$$

constituting an unfolding procedure in which eigenvalues are unfolded to a uniform (CUE) distribution at any instant of time $t \neq 0$ in the evolution.

4.3.3 Derivation of the spectral form factor scaling predictions

Within the scaling ensemble (4.5), we can analytically analyse the SFF by expressing it in terms of the eigenvalues λ_l of U,

$$K_n = \overline{|\operatorname{tr} U^n|^2} = \sum_{lm} \lambda_l^n \lambda_m^{*n}. \tag{4.12}$$

To this end, we use the transformation (4.10) to recast the SFF in each realisation U explicitly in terms of the eigenvalues $\mu_l = e^{i\psi_l}$ of the corresponding CUE matrix V,

$$|\mathrm{tr}\, U^n|^2 = \sum_{lm} \left(\frac{a + e^{i\psi_l}}{1 + ae^{i\psi_l}} \frac{a + e^{-i\psi_m}}{1 + ae^{-i\psi_m}} \right)^n . \tag{4.13}$$

The joint distribution

$$P_{\mathrm{CUE}}(\{\psi\}) \propto \prod_{l<m} \left| e^{i\psi_l} - e^{i\psi_m} \right|^2 = \det \left(\sum_l \mu_l^{p-q} \right) \tag{4.14}$$

of these eigenvalues can be written as a product of two Vandermonde determinants, where the indices $q, p = 1, 2, ..., N$ label the rows and columns of the resulting determinant. While this does not factorise in terms of the eigenvalues μ_l, Ref. [123] establishes that the average of any completely symmetric function $f(\{\psi_l\})$ simplifies to

$$\overline{f(\{\psi_l\})} = \left(\prod_r \int_0^{2\pi} \frac{d\psi_r}{2\pi} \right) f(\{\psi_l\}) \det \left(\mu_p^{p-q} \right) . \tag{4.15}$$

Applied to the SFF, we then obtain

$$K_n = \left(\prod_r \int_0^{2\pi} \frac{d\psi_r}{2\pi} \right) \det(e^{i(p-q)\psi_q}) \times \sum_{lm} \left(\frac{a + e^{i\psi_l}}{1 + ae^{i\psi_l}} \right)^n \left(\frac{a + e^{-i\psi_m}}{1 + ae^{-i\psi_m}} \right)^n . \tag{4.16}$$

In this expression, the integrals over ψ_q can be performed independently of one another and pulled into the qth rows of the matrix in the determinant. Each of the diagonal terms $l = m$ in the sum gives a contribution of 1, while the off-diagonal terms $l \neq m$ give contributions

$$\det \begin{pmatrix} a^n & c_{m-l,n} \\ c_{m-l,n} & a^n \end{pmatrix} = a^{2n} - c_{m-l,n}^2, \tag{4.17}$$

where the integrals

$$c_{q,n} = \int_0^{2\pi} \frac{d\psi}{2\pi} \left(\frac{a + e^{-i\psi}}{1 + ae^{-i\psi}} \right)^n e^{i\psi q} \tag{4.18}$$

correspond to the coefficient $\propto v^q$ in the expansion of $(a + v)^n/(1 + av)^n$ in powers of v and hence are finite only for $m > l$.

Altogether, we arrive at

$$K_n = N + N(N-1)a^{2n} - \sum_{q=1}^{N}(N-q)c_{q,n}^2,$$
$$c_{q,n} = \frac{1}{q!}\frac{d^q}{dv^q}\left.\frac{(a+v)^n}{(1+av)^n}\right|_{v=0}. \tag{4.19}$$

The first term is due to each diagonal $l = m$ term contributing 1, summing to N overall. The second term is due to $(N^2 - N)$ distinct off-diagonal terms with $l \neq m$, each contributing a^{2n} from Eq. (4.17). The third then collects the contributions $-c_{q,n}^2$ from this equation over all possible combinations of m and l with fixed $q = m - l \geq 1$ permitted by the matrix of dimension N. Equation (4.19) recovers the standard CUE result for $a = 0$, where $c_{q,n} = \delta_{qn}$, such that K_n takes the form given in Eq. (2.38).

Equation (4.19) is our main result within the scaling theory. It expresses all orders of the SFF in terms of a single parameter, which has its independent interpretation as characterising the expansion of the eigenvalue cloud. Next, we will describe how this result can be utilised as a benchmark to analyse specific dynamical processes.

4.4 Applications

To establish how the scaling forms (4.19) of the SFF provide benchmarks for maximally ergodic dynamics, we describe how they can be used to distinguish the effects of efficient but incomplete scrambling, and inherently inefficient scrambling. We develop these features both within the scaling framework itself, as well as in the context of two specific stochastic processes.

4.4.1 Efficient but incomplete scrambling

First, we describe how the effects of incomplete scrambling up to a given time t are captured within the scaling approach. As mentioned above, the scaling forms (4.19) of the instantaneous SFF reduce to the CUE result (2.38) for $a = 0$, which defines the endpoint of the scrambling flow. The SFF then falls from $K_0 = N^2$ to $K_1 = 1$ before ramping up linearly to $K_N = N$ at the stroboscopic Heisenberg time N, after which it plateaus. Figure 4.2 (a) contrasts this behaviour of the instantaneous SFF (4.19) with the scenarios for finite values of a. Tuning the scaling parameter a away from 0—stopping the dynamics at time t short of maximally ergodic behaviour—results in curves that initially continue to dip, and then take a longer time to recover the plateau. Therefore, incomplete scrambling dynamics at short times are translated into a long-time signal in the form of a modified ramp, demonstrating the consequences of not having established fully ergodic dynamics for the remainder of the time evolution. The time over which the curves continue to dip defines an effective ergodic time, while the time it takes them to ramp up to the plateau defines an effective Heisenberg time. Crucially, within the scaling theory, these two time scales are directly linked via the scaling parameter a.

This link is emphasised by the scaling relation between these results. The transformation (4.9) directly transfers into self-similar correlations of the eigenvalues λ_l along the flow. Unfolding the spectrum to a uniform density with Heisenberg time N according to (4.11) collapses the SFF identically onto the RMT result, as illustrated in Figure 4.2 (b). Within the scaling ensemble, this collapse is exact, underlining both its scale invariance and single-parameter nature.

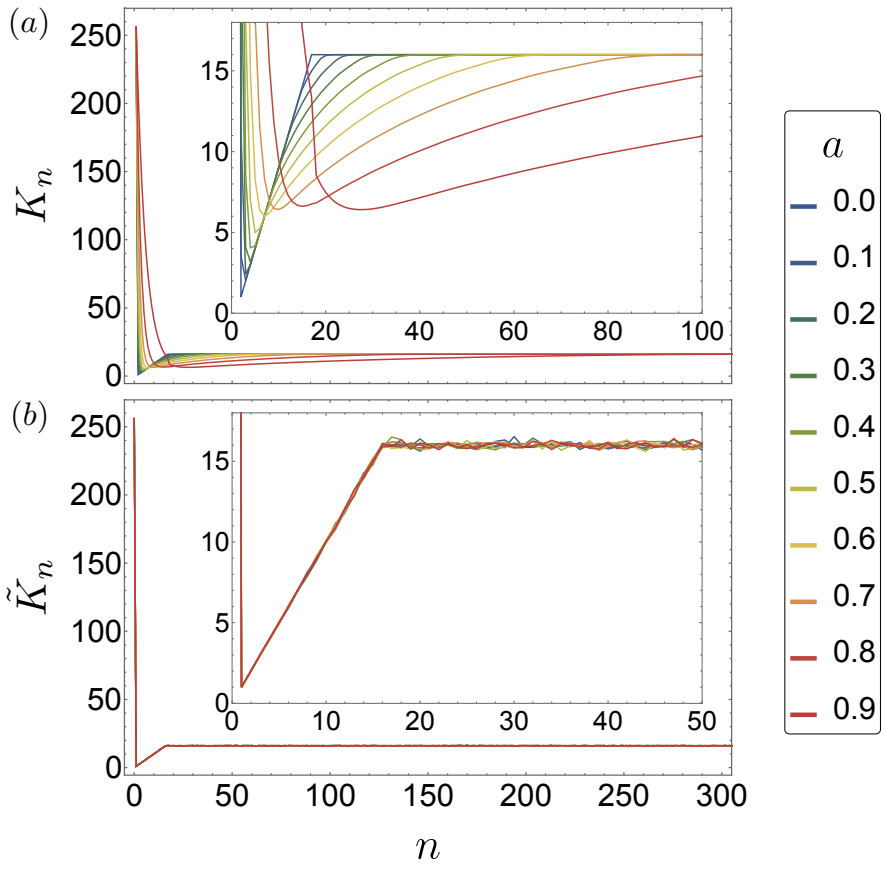

Figure 4.2: (*a*) Scaling predictions of the instantaneous form factor K_n for maximally efficient scrambling, Eq. (4.19), for $N = 16$, where a describes different points along the scrambling flow. All curves display the paradigmatic dip-ramp-plateau shape. For $a = 0$, scrambling is complete, and the curves follow the RMT predictions of an ergodic system. Finite values of a describe earlier times along scrambling dynamics, resulting in effective ergodic and Heisenberg times that are linked by the scaling parameter a. (*b*) Numerical sampling of the ensemble (10^4 realisations) confirms that the points along the scrambling flow are linked by the transformation (4.9), which implies self-similar statistics and the exact collapse onto the RMT result after unfolding the spectrum (denoted by the tilde) according to (4.11), corresponding to setting $a' = 0$ in Eq. (4.9).

4.4.2 Dyson's Brownian motion: a manifestation of efficient scrambling

We next turn to question whether this single-parameter behaviour within the ensemble can be replicated in a suitable unitary time evolution. Which dynamical process, if any, recovers the statistics of the scaling ensemble (4.5), parameterised by a single suitable time-dependent scaling parameter a? We argue that the answer lies in another paradigm of RMT, Dyson's Brownian motion (DBM).

DBM emerges as a natural candidate for fast scrambling in the context of quantum circuit models. These come in two main variants: random Haar circuits (e.g., [88, 89, 91, 151]) built out of fully ergodic gates from RMT (Section 2.4.1), and Brownian circuits [50, 67, 82, 210–213], built from gates with randomly chosen Hamiltonians $H(t)$ over small time steps dt (Section 2.4.2). Our scaling approach interpolates between both types of models for one of these gates, and so does the Brownian process applied for a finite time. This coincides with the DBM process defined in Section 2.4.2.1, in which the incremental updating unitary matrices (2.13) are generated by instantaneous Hamiltonians sampled from the GUE whose matrix elements satisfy Eq. (2.52) and are scaled according to Eq. (2.53) with $\kappa = 1$. The unitary time-evolution operator $U(t)$ then performs a random walk in the unitary group, sampling it uniformly according to the Haar measure.

Within this process, we find that the scaling parameter a decays exponentially from unity to zero, $a(t) = e^{-t/2}$, corresponding to a dimensionless decay rate $\gamma_0 = 1/2$. This is accompanied by an exponential decay $K_1(t) = (N^2-1)e^{-t}+1$ of the first-order SFF, describing the dip to unity with a decay rate $\gamma_1 = 2\gamma_0$, which agrees with the scaling prediction (4.19) up to corrections $O(N^{-2})$. The key question is whether the process recovers the complete spectral statistics encoded in the scaling forms (4.19) of K_n, and displays self-similar spectral correlations up to standard unfolding, as in the scaling theory itself.

This is analysed in Figure 4.3. The top panel shows the SFF after unfolding the DBM spectrum to the scaling mean density of states (4.8) (see Appendix C). We observe that this agrees with the scaling prediction (4.19) up to statistical fluctuations, over the whole range of the scaling parameter, hence over the complete scrambling dynamics. Furthermore, upon fully unfolding the spectrum to a uniform mean density in the

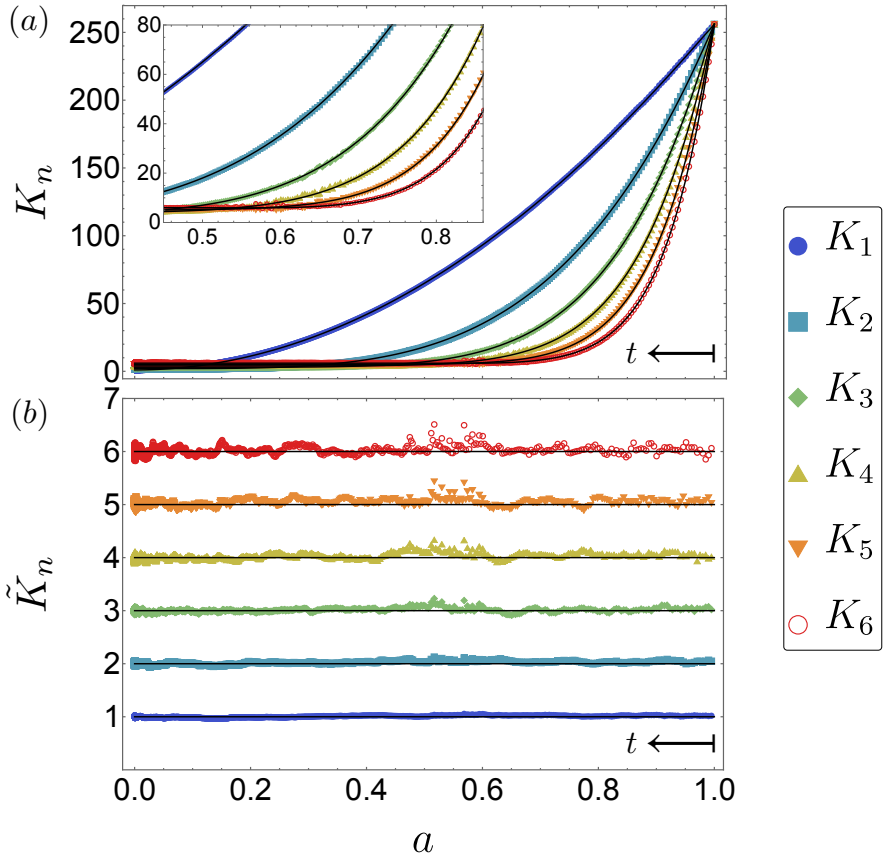

Figure 4.3: Scaling analysis of scrambling in the DBM process, generated by Eq. (2.13) ($N = 16$, $dt = 0.01$, 10^4 realisations). (a) Spectral form factors K_n after unfolding the spectrum to the scaling mean density of states (4.8) at $a(t) = e^{-t/2}$, as a function of a. There is agreement within statistical uncertainty with the analytical scaling predictions (4.19) (black curves). (b) Further unfolding the spectrum to uniform density (denoted by the tilde) collapses it onto the RMT prediction $K_n = n$, verifying that DBM generates self-similar spectral statistics along the complete scrambling dynamics.

bottom panel, we find perfect collapse of all data onto straight lines $K_n = n$, which establishes agreement with the scaling theory down to the level of self-similarity under the flow, again on all scales of a.

As we show next, this tight agreement —including the higher orders of the SFF—is a non-trivial statement about the DBM process, marking it out as a privileged model of fast scrambling among a wider class of dynamical models.

4.4.3 Deviations from efficient scrambling: formulation via chaos bounds

Our scaling ansatz (4.3) equates two unitarily invariant generators. This unitary invariance is also obeyed in DBM, and is the sole constraint in the derivation of the exponential decay of the first-order SFF (4.1) to unity with decay rate (4.2). Studying this decay of the SFF in isolation, one could be led to believe that all systems within this more general class of unitarily invariant processes exhibit maximally chaotic scrambling. A first hint that this may not be the case is given by the decay of the scaling parameter itself, where we again observe an exponential decay, but with a decay rate (see Appendix D)

$$\gamma_0 = \lim_{dt\to 0} (dt\, N)^{-1}(N - \overline{\operatorname{tr} u(t;dt)}) \tag{4.20}$$

that is not universally linked to γ_1 given by Eq. (4.2). Instead, the mathematical definitions of these quantities enforce the relation $\gamma_1 \leq 2\gamma_0$, again up to corrections $O(N^{-2})$. The scaling forms (4.19) satisfy this constraint tightly and its extension to the decay rates of the higher-order SFFs, $\gamma_n \leq 2n\gamma_0$. We can therefore view these scaling forms as lower bounds that are approached only for maximally scrambling dynamics, as represented, e.g., by DBM. Within the class of unitarily invariant processes, we can view these bounds for the decay of the nth-order SFF as the analogue of the chaos bounds on OTOCs, here obtained directly from the spectral statistics. Moreover, by further adapting our scaling analysis of the DBM process, we can take one further step and directly utilise the scaling forms (4.19) of the SFF as bounds that are expressed in terms of the scaling parameter a.

We exemplify this by modifying DBM, which mathematically corresponds to a Wiener process, into a Cauchy process that is obtained from generators

$$u(t;dt) = \left(\sqrt{1-dt}\mathbb{1} + V\right)\left(\sqrt{1-dt}V + \mathbb{1}\right)^{-1} \tag{4.21}$$

with V uniform in the unitary group of degree N. This composes generators from the scaling ensemble multiplicatively into a time-evolution operator, which differs from the self-similarity mapping (4.9) governing the maximally efficient scaling flow. For this process, we find again $\gamma_0 = 1/2$, while $\gamma_1 = 1 - N^{-1} + O(N^{-2})$ just falls short of the chaos bound stated above at any finite value of N.

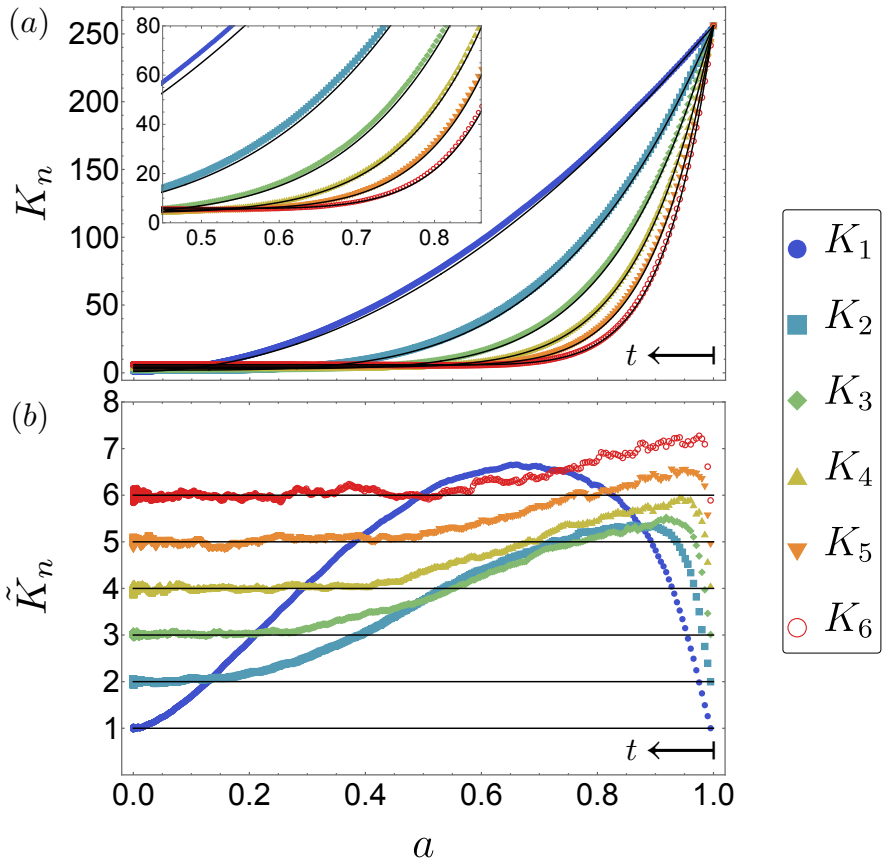

Figure 4.4: Scaling analysis of scrambling in the Cauchy process generated by Eq. (4.21) ($N = 16$, $dt = 0.01$, 10^4 realisations), in analogy to Figure 4.3. The SFF departs from the analytical scaling predictions (black curves), which now serve as lower bounds (a), and no longer display self-similar statistics along the flow, as verified by unfolding the spectrum to uniform density (b), again denoted by the tilde.

Figure 4.4 reports the full scaling analysis of the higher-order SSFs, where we exploit the fact that the Cauchy process shares the same mean level density as the scaling theory so that no unfolding is needed (see Appendix B). As shown in panel (a), this now shows clear deviations from our expectations for a maximally efficient process, with the results rising significantly above the bounds (4.19) set by the scaling theory plotted as a function of the scaling parameter a. Panel (b) shows that these deviations persist when the spectrum is unfolded to a uniform density, which reveals that the spectral correlations are not self-similar along the scrambling dynamics. The framework established in this chapter therefore allows us to distinguish the effects of efficient but yet incomplete scrambling to a time t, captured by a finite value of a—already present in Figures 4.2 and 4.3—and intrinsically inefficient scrambling, captured by the departure from the scaling bounds.

4.5 Summary

In summary, we developed a quantitatively predictive single-parameter scaling theory of maximally chaotic scrambling dynamics, which embodies self-similarity of the spectral correlations along the whole process. The theory is amenable to a complete analytical treatment, delivering bounds for the decay of the spectral correlations on all scales. These bounds are tightly met by Dyson's Brownian motion, which illuminates the physical content of the scaling theory and underlines the privileged nature of this process. Signatures of inefficient or incomplete scrambling in other scenarios are captured sensitively, revealing, for instance, that the purely exponential decay of spectral correlations observed by a wide class of scrambling models is in itself not a sufficient signature of maximally chaotic scrambling. The scaling theory also emphasises deeper conceptual features of general scrambling dynamics, such as the intimate link of short-time scrambling and long-time ergodicity enforced by the unitarity of this process. As chaotic scrambling is a fundamental tenet of complex quantum-matter phenomenology, this approach transfers to a wide range of physical domains. In the following chapter, we ask what happens when we constrain dynamics, for instance, by placing systems into different symmetry classes.

Chapter 5

Analytical approach to spectral correlations in Brownian Quantum Chaos

5.1 Overview

Chaotic quantum systems exhibit a strong degree of universality in their spectral statistics and dynamical correlation functions [16, 17, 35]. Strong arguments for this universality have been formulated in the context of single-particle systems that are disordered or chaotic in the classical limit [13, 15–17, 103, 272]. In the analogous picture for many-body systems [50, 53, 121, 273], the SYK model [73–79] has emerged as a paradigmatic setting since it adheres to the RMT predictions of the symmetry class determined by the number of Majorana fermions therein.

As detailed in Section 2.4.2.2, the BSYK model describes dynamics configured to have a stochastic time dependence, whose interactions drive the system into a featureless infinite-temperature state. Within RMT, the paradigm of these models is DBM (Section 2.4.2.1). For DBM generated by Hamiltonians from the GUE, exact results for the instantaneous spectral statistics have been established in the framework of orthogonal polynomials [126, 274, 275]. Stochastic models of this kind are generally known as Brownian models of quantum chaos, and a key question is again to which extent their spectral statistics are universal.

In this chapter, we develop an analytical approach to study the spectral statistics in Brownian models at instantaneous times and establish their universality when they are resolved on a single well-defined dynamical time scale that characterises the gradual evolution towards full RMT ergodicity within a given symmetry class. Our approach follows the spirit of the moment method of DBM [116] but significantly relaxes its assumptions to only require stochastically emergent basis invariance, which we argue to hold generically in zero-dimensional stochastic models. By explicitly evaluating ensemble averages in an incremental stochastic time step, we derive, for each symmetry class, a closed hierarchy of differential equations for the instantaneous SFF [2, 126], in which the time derivative of the nth order can be expressed in terms of instantaneous spectral correlators of order $m \leq n$. From this, we obtain exact analytical expressions of the time evolution of the instantaneous SFF and other spectral correlators, including those relevant for the ensemble-averaged OTOC, valid for all times and system sizes N.

We establish these results in detail as follows. In Section 5.2, we formulate the precise programme of our approach. We start by deriving the spectral hierarchy of the unitary DBM model in Section 5.3. This recovers the exact results for this symmetry class from the framework of orthogonal polynomials [126], extends them to a wider class of correlators, and allows us to determine their uniform asymptotics for large system sizes N at all times and orders. In Section 5.4, we extend these considerations to the orthogonal and symplectic symmetry classes, and establish exact and asymptotic results. In the next two sections, we turn to the question of universality in more general Brownian models. In Section 5.5, we rederive the same hierarchies under the significantly relaxed assumption of basis invariance, which we argue to hold generically in zero-dimensional Brownian models. In Section 5.6, we verify this universality for BSYK dynamics numerically, where we find precise agreement with the analytical predictions in all three symmetry classes. In Section 5.7, we show that the ensemble-averaged OTOC can be expressed analytically in terms of quantities derived at most from the second level of the spectral hierarchy. The discussion of the observed universality, Section 5.8, emphasises the significance of the U(1) invariance of the studied correlators. Our general conclusions are formulated in Section 5.9, while further details of the derivations are presented in Appendices E, F, and G. Appendix H includes a calculation of the OTOC in the scaling theory developed in Chapter 4.

5.2 Programme of this chapter

Section 2.2.4.3 describes how the SFF is a sensitive probe of dynamically induced correlations between energy levels and introduces its instantaneous version (2.39) in the setting of stochastic processes. In this chapter, we will employ this variant as a diagnostic of emergent ergodicity. Our main objective is to develop an approach that facilitates the direct analytic study of the instantaneous SFF (2.39) in the described Brownian models of quantum chaos and allows for their comparison in a unified framework that furthermore identifies the extent of universality in these and a whole range of related spectral correlators, as well as the role of symmetries both at finite and infinite times.

The key technical observation is that the incremental update

$$K_n(t+dt) \equiv \overline{|\operatorname{tr}[U(t+dt)]^n|^2} = \overline{|\operatorname{tr}[u(t;dt)U(t)]^n|^2}. \tag{5.1}$$

of the instantaneous SFF (2.39) under the stochastic evolution (2.10) can be evaluated in the limit that $dt \to 0$ and, when averaged over the ensemble, depends only on spectral correlators up to the given order n. This culminates in a spectral hierarchy: a closed set of linear first-order differential equations in which expressions for the nth order contain only terms up to and including the nth level. Even though the number of different correlators proliferates with n, these equations can be solved algebraically, which then enables us to derive exact and asymptotic expressions in all three standard Wigner-Dyson symmetry classes.

Notably, we will arrive at the same hierarchies in two different settings. The first setting is DBM, which is covered in Section 5.3 for the GUE and in Section 5.4 for the GOE and GSE. The second setting are models with stochastically emerging basis invariance, which we treat analytically in Section 5.5. The applicability of this concept to the BSYK model is discussed in Section 5.6.

As we show in Section 5.7, the lowest orders of the hierarchy also determine the ensemble-averaged OTOC, which we again determine and validate in all three symmetry classes. After developing these technical details, we will then be able to establish more general implications, in particular, about the extent of the observed universality, in Section 5.8.

Throughout these sections, we aim to give analytical results for the lowest orders of the hierarchy and illustrate these along with the higher orders in figures, as well as through comparison with data from the direct numerical implementation of the underlying Brownian models.

5.3 Spectral hierarchy for DBM with unitary symmetry

In this section, we first carry out the programme in detail for DBM in the GUE, in which the stepwise unitary updates (2.12) are generated by instantaneous Hamiltonians $H(t)$ that obey Eq. (2.52). These details will also serve as a starting point for the generalisations to the other symmetry classes in addition to basis-invariant models.

5.3.1 The first-order instantaneous SFF and averaging rules

We start our considerations with the first-order instantaneous SFF $K_1(t)$, hence for the index $n = 1$, which we will soon see to signify the level of this quantity in the spectral hierarchy. This subsection reproduces a key result from Chapter 4, whose derivation is given in Appendix D, but from the hierarchical perspective. We will see that because dynamics are equipped with an effective time scale, this approach is extendable to other symmetry classes.

With the dynamics generated by Eqs. (2.10) and (2.12), the ensemble average (5.1) over a single step of the stochastic evolution, expanded up to order dt, takes the form

$$\begin{aligned} K_1(t+dt) =& K_1(t) + dt\,\overline{\mathrm{tr}\,[H(t)U(t)]\ \mathrm{tr}\,[H(t)U^\dagger(t)]} \\ &- \frac{dt}{2}\left(\overline{\mathrm{tr}\,[H^2(t)U(t)]\ \mathrm{tr}\,U^\dagger(t)} + \overline{\mathrm{tr}\,U(t)\,\mathrm{tr}\,[H^2(t)U^\dagger(t)]}\right), \end{aligned} \tag{5.2}$$

where we can perform the average over the instantaneous Hamiltonians by applying Eqs. (2.52) and (2.53).

Evaluating these averages joins the two arguments of the traces in the second term

according to the rule

$$\overline{C_{AB}} \equiv \overline{\mathrm{tr}\,[H(t)A]\,\mathrm{tr}\,[H(t)B]} = \frac{\kappa}{N}\mathrm{tr}\,[AB], \tag{5.3}$$

which applies to any given matrices A and B that are independent of the instantaneous Hamiltonian. The counterpart of this rule performs the average over instantaneous Hamiltonians within the same trace operation and splits the argument into two,

$$\overline{D_{AB}} \equiv \overline{\mathrm{tr}\,[H(t)AH(t)B]} = \frac{\kappa}{N}\mathrm{tr}\,[A]\,\mathrm{tr}\,[B], \tag{5.4}$$

which we will need later when evaluating other quantities. Applying the averaging rule (5.3) to Eq. (5.2) gives

$$\begin{aligned} K_1(t+dt) &= K_1(t) + N^{-1}\kappa\, dt\, \overline{\mathrm{tr}\,[U(t)U^\dagger(t)]} - \kappa\, dt\, K_1(t) \\ &= K_1(t) + \kappa\, dt\,(1 - K_1(t))\,. \end{aligned} \tag{5.5}$$

Consequently, in the limit $dt \to 0$, we find the first-order linear differential equation

$$\frac{d}{dt}K_1(t) = \dot{K}_1(t) = \kappa\,(1 - K_1(t))\,, \tag{5.6}$$

which for the initial condition $K_1(0) = \overline{|\,\mathrm{tr}\,\mathbb{1}|^2} = N^2$ is solved by an exponential decay,

$$K_1(t) = (N^2 - 1)e^{-\kappa t} + 1. \tag{5.7}$$

We observe that $K_1(t) \to 1$ for large times, in agreement with the RMT prediction (2.38) for a fully ergodic system. The inverse rate $1/\kappa \sim t_{\mathrm{erg}}$ defines the effective time scale for the dynamics on which this ergodic limit is approached. We will develop a general interpretation of this time scale in Section 5.5.

5.3.2 The second-order instantaneous SFF and emergence of the hierarchy

We now turn to the second-order of the instantaneous SFF (2.39), whose incremental update (5.1) is given by

$$K_2(t+dt) \equiv \overline{|\mathrm{tr}\,[u(t;dt)U(t)]^2|^2}. \tag{5.8}$$

Expanding this expression again up to order dt and averaging over the instantaneous Hamiltonians according to the rules (5.3) and (5.4) gives

$$\begin{aligned} K_2(t+dt) =& K_2(t) + \kappa\, dt \Big[4 - 2K_2(t) \\ & - N^{-1}\left(\overline{\mathrm{tr}\,[U(t)]^2\,\mathrm{tr}\,U^\dagger(t)\,\mathrm{tr}\,U^\dagger(t)} + \overline{\mathrm{tr}\,U(t)\,\mathrm{tr}\,U(t)\,\mathrm{tr}\,[U^\dagger(t)]^2}\right)\Big]. \end{aligned} \tag{5.9}$$

Here, we encounter two new quantities that signal the start of an emerging hierarchical structure, which furthermore encompasses a more comprehensive set of correlators. To account for these quantities, we introduce the notation

$$\mathcal{K}_{\{.\},\{.\}}(t) = \mathcal{K}_{pq\ldots,rs\ldots}(t) = \overline{(\mathrm{tr}\,[U(t)]^p\,\mathrm{tr}\,[U(t)]^q\cdots\mathrm{tr}\,[U^\dagger(t)]^r\,\mathrm{tr}\,[U^\dagger(t)]^s\cdots)}, \tag{5.10}$$

where the sequences of integers specify the number of terms of the form $\mathrm{tr}\,[U(t)]^p$ or $\mathrm{tr}\,[U^\dagger(t)]^r$. By construction, the respective sums over the tallies $\{\cdot\}$ before and after the comma are equal to the same integer n, which enumerates the orders of the hierarchy. What was previously expressed as $K_n(t)$ therefore becomes $\mathcal{K}_{n,n}(t)$, while the new quantities appearing in Eq. (5.9) can now be written as

$$\mathcal{K}_{11,2}(t) = \overline{\mathrm{tr}\,U(t)\,\mathrm{tr}\,U(t)\,\mathrm{tr}\,[U^\dagger(t)]^2}, \tag{5.11}$$

$$\mathcal{K}_{2,11}(t) = \overline{\mathrm{tr}\,[U(t)]^2\,\mathrm{tr}\,U^\dagger(t)\,\mathrm{tr}\,U^\dagger(t)}, \tag{5.12}$$

so that Eq. (5.9) becomes

$$\mathcal{K}_{2,2}(t+dt) = \mathcal{K}_{2,2}(t) + \kappa\, dt\left[4 - 2\mathcal{K}_{2,2}(t) - N^{-1}\left(\mathcal{K}_{2,11}(t) + \mathcal{K}_{11,2}(t)\right)\right]. \tag{5.13}$$

The incremental updates of these new quantities $\mathcal{K}_{11,2}(t)$ and $\mathcal{K}_{2,11}(t)$ can again be evaluated using the averaging rules (5.3) and (5.4), where we also encounter the quantity $\mathcal{K}_{11,11}(t)$. Evaluating its derivative in the same manner then yields a closed set of first-order linear differential equations,

$$\begin{aligned}
\dot{\mathcal{K}}_{1,1}(t) &= \kappa\left[1 - \mathcal{K}_{1,1}(t)\right], \\
\dot{\mathcal{K}}_{2,2}(t) &= \kappa\left[4 - 2\mathcal{K}_{2,2}(t) - N^{-1}\left(\mathcal{K}_{2,11}(t) + \mathcal{K}_{11,2}(t)\right)\right], \\
\dot{\mathcal{K}}_{2,11}(t) &= \kappa\left[-2\mathcal{K}_{2,11}(t) - N^{-1}\left(\mathcal{K}_{11,11}(t) + \mathcal{K}_{2,2}(t) - 4\mathcal{K}_{1,1}(t)\right)\right], \\
\dot{\mathcal{K}}_{11,2}(t) &= \kappa\left[-2\mathcal{K}_{11,2}(t) - N^{-1}\left(\mathcal{K}_{11,11}(t) + \mathcal{K}_{2,2}(t) - 4\mathcal{K}_{1,1}(t)\right)\right], \\
\dot{\mathcal{K}}_{11,11}(t) &= \kappa\left[-2\mathcal{K}_{11,11}(t) + 4\mathcal{K}_{1,1}(t) - N^{-1}\left(\mathcal{K}_{2,11}(t) + \mathcal{K}_{11,2}(t)\right)\right].
\end{aligned} \tag{5.14}$$

In contrast to the single differential equation (5.6) for $n = 1$, this system of differential equations includes quantities of the first and second order and is thus hierarchical.

Since realisations in which $U(t)$ is replaced by $U^\dagger(t)$ are statistically equivalent, we observe the symmetry $\mathcal{K}_{pq\ldots,rs\ldots} = \mathcal{K}_{rs\ldots,pq\ldots}$ of all quantities under the exchange of the left and right indices. Accordingly, $\mathcal{K}_{2,11}(t) = \mathcal{K}_{11,2}(t)$ so that the dynamics of these two quantities are effectively described by the same equation. This reduces the cumulative number of equations for $n = 1$ and 2 from 5 to 4. These equations have to be solved according to the dynamical initial condition $U(0) = \mathbb{1}$, which translates to

$$\mathcal{K}_{1,1}(0) = N^2, \quad \mathcal{K}_{2,2}(0) = N^2, \quad \mathcal{K}_{11,2}(0) = \mathcal{K}_{2,11}(0) = N^3, \quad \mathcal{K}_{11,11}(0) = N^4. \tag{5.15}$$

Here, the power of N corresponds to the number of traces in Eq. (5.10) and hence equals the total number of indices. As the equations are furthermore linear, they can be solved exactly, from which we obtain

$$\begin{aligned}
K_2(t) = 2 + \frac{1}{4}\Big[&(N+1)(N-3)N^2 e^{\frac{2}{N}\kappa t} \\
&+ (N-1)(N+3)N^2 e^{-\frac{2}{N}\kappa t} - 2(N^2-1)(N^2-4)\Big] e^{-2\kappa t}.
\end{aligned} \tag{5.16}$$

While this expression is lengthy, it agrees precisely with the result from the theory of orthogonal polynomials [126, 274, 275] (see Appendix F).

5.3.3 Higher orders of the instantaneous SFF

It transpires that the principles developed above are all that is required to calculate the instantaneous SFF at all orders and determine a comprehensive set of additional correlators along with this. Using the general averaging rules (5.3) and (5.4) in conjunction with the notation (5.10), the incremental updates of these spectral correlators can be expressed conceptually as

$$\dot{\mathcal{K}}_{pq\ldots,rs\ldots}(t) = -\kappa n \mathcal{K}_{pq\ldots,rs\ldots}(t) \underbrace{-\frac{\kappa}{N}\left(+pq\mathcal{K}_{(p+q)..,rs\ldots}(t) - pr\mathcal{K}_{(p-r)q..,s\ldots}(t) + \ldots\right)}_{\text{from combining traces as in Eq. (5.3)}} \underbrace{-\frac{\kappa}{N}\left(\sum_{n=1}^{p-1}\frac{p}{2}\mathcal{K}_{n(p-n)q..,rs\ldots}(t) + \ldots + \sum_{n=1}^{r-1}\frac{r}{2}\mathcal{K}_{pq..,n(r-n)s\ldots}(t) + \ldots\right)}_{\text{from splitting traces as in Eq. (5.4)}} . \quad (5.17)$$

The factors $+pq$ and $-pr$ that appear in the process of combining traces reveal that it is convenient to think of the indices on either side of the comma to be of opposite sign, such that combining indices from the same side yields a positive sign, while combining indices from both sides yields a negative sign. Moving all indices to one side of the comma so that $\mathcal{K}_{pq\ldots,rs\ldots}(t) = \mathcal{K}_{pq\ldots(-r)(-s)\ldots}(t) \equiv \mathcal{K}_{(c_i)_{i=1}^m}(t)$, where m is the length of the combined index sequence, we can then compactly write the spectral hierarchy as

$$\dot{\mathcal{K}}_{(c_i)_{i=1}^m}(t) = -\kappa n \mathcal{K}_{(c_i)_{i=1}^m}(t) \underbrace{-\frac{\kappa}{N}\sum_{j<k} c_j c_k \mathcal{K}_{(c_i)_{i\neq j,k}(c_j+c_k)}(t)}_{\text{from combining traces as in Eq. (5.3)}} \underbrace{-\frac{\kappa}{N}\sum_j \frac{|c_j|}{2}\sum_{k=1}^{|c_j|-1}\mathcal{K}_{(c_i)_{i\neq j}(k\,\mathrm{sgn}\,c_j)(c_j-k\,\mathrm{sgn}\,c_j)}(t)}_{\text{from splitting traces as in Eq. (5.4)}} . \quad (5.18)$$

We see that the terms on the right-hand side never increase the order n of the correlator, while the order reduces whenever two indices $c_j + c_k = 0$ annihilate, which results in a constant factor $\mathrm{tr}\,\mathbb{1} = N$. Furthermore, we only encounter correlators in which the sum of signed indices

$$\sum_{i=1}^m c_i = 0 \quad (5.19)$$

vanishes, which means that all encountered correlators are U(1)-invariant (we return to the general significance of this feature at the end of this chapter, see Section 5.8). The description of this closed hierarchy of differential equations is then completed by the initial conditions

$$\mathcal{K}_{(c_i)_{i=1}^m}(0) = N^m, \tag{5.20}$$

where m is again the combined number of indices.

Applied directly to $n = 3$, we find that we must add the relations

$$\begin{aligned}
\dot{\mathcal{K}}_{3,3}(t) &= \kappa \left[9 - 3\mathcal{K}_{3,3}(t) - 6N^{-1}\mathcal{K}_{3,12}(t)\right], \\
\dot{\mathcal{K}}_{3,12}(t) &= \kappa \big[-3\mathcal{K}_{3,12}(t) \\
&\qquad -N^{-1}\left(3\mathcal{K}_{12,12}(t) + \mathcal{K}_{3,111}(t) + 2\mathcal{K}_{3,3}(t) - 6\mathcal{K}_{1,1} - 3\mathcal{K}_{2,2}(t)\right)\big], \\
\dot{\mathcal{K}}_{3,111}(t) &= \kappa \left[-3\mathcal{K}_{3,111}(t) - N^{-1}\left(3\mathcal{K}_{3,12}(t) + 3\mathcal{K}_{12,111}(t) - 9\mathcal{K}_{2,11}(t)\right)\right], \\
\dot{\mathcal{K}}_{12,12}(t) &= \kappa \big[-3\mathcal{K}_{12,12}(t) + 4\mathcal{K}_{1,1}(t) + \mathcal{K}_{2,2}(t) \\
&\qquad -2N^{-1}\left(\mathcal{K}_{12,111}(t) + 2\mathcal{K}_{3,12}(t) - 2\mathcal{K}_{2,11}(t)\right)\big], \\
\dot{\mathcal{K}}_{12,111}(t) &= \kappa \big[-3\mathcal{K}_{12,111}(t) + 3\mathcal{K}_{2,11}(t) \\
&\qquad -N^{-1}\left(\mathcal{K}_{111,111}(t) + 3\mathcal{K}_{12,12}(t) - 6\mathcal{K}_{11,11} + 2\mathcal{K}_{3,111}(t)\right)\big], \\
\dot{\mathcal{K}}_{111,111}(t) &= \kappa \left[-3\mathcal{K}_{111,111}(t) + 9\mathcal{K}_{1,1}(t) - 6N^{-1}\mathcal{K}_{12,111}(t)\right]
\end{aligned} \tag{5.21}$$

to the system of equations (5.14) obtained for level $n = 2$.

The symmetry in the left and right indices reduces what would have been the addition of 10 equations to the 6 given independent equations.[1] In order to solve the equations at the nth level, these equations are then combined cumulatively with all equations at lower levels $m < n$. The total number of independent differential equations at the nth level of this hierarchy proliferates with increasing n, as $1, 4, 10, 25, 53, 119, 239$, and so on. However, since the system of equations closes at every level, these equations can be solved exactly for any system size N, where the instantaneous SFF again agrees precisely with those from the theory of orthogonal polynomials (see Appendix F). The other correlators contain dynamical information

[1] More generally, the number of equations generated at the nth level is $x(x+1)/2$, where x is the number of integer partitions of n, and thus yields an integer sequence $s(n)$ describing the number of partitions of $2n$ that are sum-symmetric (Sequence A086737, OEIS Foundation Inc. (2025), The On-Line Encyclopedia of Integer Sequences, Published electronically at https://oeis.org).

and complete the description consistently, as we revisit later on in Sections 5.7 and 5.8.

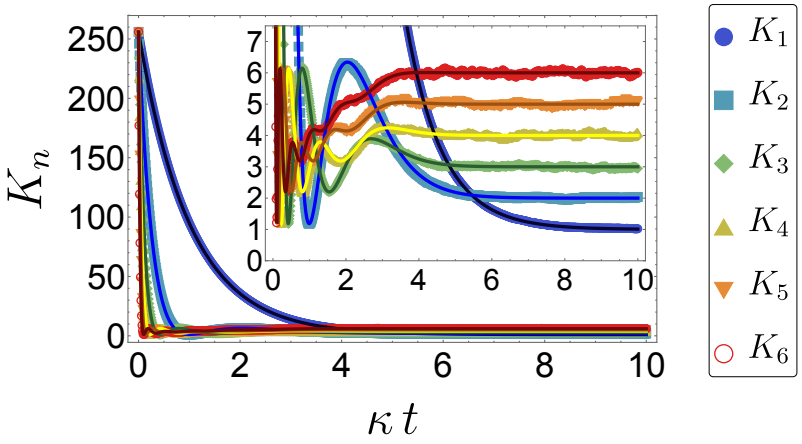

Figure 5.1: Comparison of the analytical solutions for the instantaneous SFF $K_n(t)$ for unitary DBM, obtained from the spectral hierarchy up to level $n = 6$, where $N = 16$ (solid coloured curves), with numerical sampling of the corresponding dynamics generated by DBM with Hamiltonians drawn from the GUE (data points, obtained from 10^4 realisations with $dt = 0.01$). The inset highlights the detailed agreement on intermediate time scales, as well the expected long-time behaviour, where $\lim_{t\to\infty} K_n(t) = n$ agrees with the CUE prediction, Eq. (2.38) with $1 \leq n \leq N$.

Figure 5.1 compares the resulting analytical expressions for the instantaneous SFF $K_n(t) = \mathcal{K}_{n,n}(t)$ from the spectral hierarchy up to level $n = 6$ with numerical data generated by DBM with instantaneous Hamiltonians drawn from the GUE, where the system size is set to $N = 16$. The analytic expressions precisely reproduce the non-monotonic structure observed in the numerical sampling of the DBM dynamics over all times and also reproduce the expected long-time behaviour that is consistent with the CUE result (2.38) for a completely ergodic system. As described in Appendix G, this long-time consistency with the CUE also applies to the other correlators appearing in the spectral hierarchy.

5.3.4 Uniform asymptotics for large system sizes

An immediate application of the spectral hierarchy is to determine the asymptotic form of the instantaneous SFF in the limit of large system sizes, $N \to \infty$. In each order, the SFF dips over short times from N^2 to $O(N^0)$ and the large-time limit plateaus

at values $O(N^1)$, so that this requires a systematic uniform expansion in t and N. This is a more difficult task than obtaining the same asymptotics for the connected part of the correlator [126], which is by construction only of order $O(N^0)$ but in more general settings involves non-universal contributions from the density of states — see Section 5.8 for further discussion of these points.

Using the spectral hierarchy, we achieve this uniform expansion by power counting the terms generated by the averaging rules (5.3) and (5.4), which then simplify in analogy to the RMT non-crossing approximation (see, e.g., [43]). Specifically, all terms that do not maximise the number of traces generated in the averaging rules reduce the power in N by at least two orders, hence a factor of $O(N^{-2})$, unless they are compensated by a trace of the identity matrix.

In leading order, this asymptotic constraint eliminates all averages from the averaging rule (5.3) unless $A = B^\dagger$. This leads, in the notation of Eq. (5.18), to the closed expression

$$\mathcal{K}^{(\infty)}_{(c_i)_{i=1}^m}(t) = \prod_{i=1}^{m} a_{|c_i|}(\kappa t) \tag{5.22}$$

of all encountered correlators in their leading order, where

$$a_p(s) = N e^{-sp/2} \sum_{k=0}^{p-1} \frac{(p-1)!}{(p-k-1)!k!(k+1)!} (-sp)^k. \tag{5.23}$$

For the instantaneous SFF, this captures the $O(N^2)$ leading-order behaviour as $K_n(t) \sim a_n^2(\kappa t)$, where explicitly

$$K_1^{(\infty)} = N^2 e^{-\kappa t}, \tag{5.24}$$

$$K_2^{(\infty)} = N^2 (1-\kappa t)^2 e^{-2\kappa t}, \tag{5.25}$$

$$K_3^{(\infty)} = N^2 \left(1 - 3\kappa t + \frac{3(\kappa t)^2}{2}\right)^2 e^{-3\kappa t}. \tag{5.26}$$

This provides a good description of the dip but not of the ramp and plateau.

The desired uniform approximation down to order $O(N^0)$ is obtained by using these leading-order expressions whenever the hierarchy branches according to the averaging

rule (5.3). This automatically guarantees that such branching occurs at most once, which makes the description correct to order $O(N^0)$. With this simple replacement, the system of differential equations becomes inhomogeneous but closes on each level. From this, we obtain uniform approximations of the form

$$K_1^{(u)}(t) = K_1^{(0)}, \tag{5.27}$$

$$K_2^{(u)}(t) = K_2^{(0)} + \frac{s^4 - 4s^3 - 9s^2}{3} e^{-2s}, \tag{5.28}$$

$$K_3^{(u)}(t) = K_3^{(0)} + \frac{3s^2}{8}\left(9s^4 - 54s^3 + 48s^2 - 56\right) e^{-3s}, \tag{5.29}$$

where $s = \kappa t$ and

$$K_n^{(0)} = K_n^{(\infty)} + n(1 - e^{-n\kappa t}) \tag{5.30}$$

accounts for the dip and plateau, while the remaining terms provide the detailed oscillations in the ramp.

These different levels of approximations are illustrated in Figure 5.2, where they are compared with the exact analytical results for $N = 16$. We see that while $K_n^{(0)}$ already captures most of the dynamical behaviour, a much more precise agreement is obtained from the uniform approximations $K_n^{(u)}$.

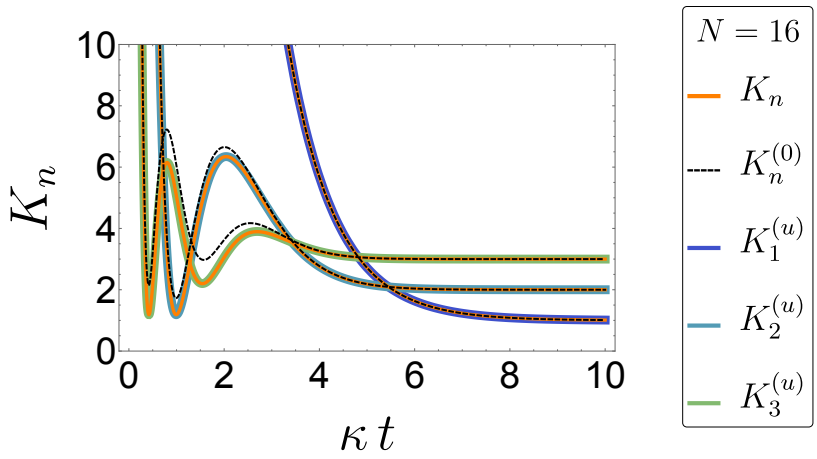

Figure 5.2: Comparison of the exact instantaneous SFF K_n (solid orange curves) with $K_n^{(0)}$, Eq. (5.30) (dashed black curves), and the more accurate uniform asymptotic approximations $K_n^{(u)}$, Eqs. (5.27)-(5.29) (solid coloured curves) for $N = 16$.

5.4 DBM with orthogonal and symplectic symmetry

We now extend the analytical treatment of the instantaneous SFF and related correlators to DBM in the other two standard symmetry classes, where the instantaneous Hamiltonians in Eq. (2.12) are drawn from the GOE or GSE, respectively. We will maintain the composition rule (2.10) in which time-reversal symmetry is broken dynamically by the stochastic variation of the Hamiltonian, even though it obeys time-reversal symmetry over each instantaneous time step. A template for this setting would be a system of electrons driven by stochastic electric field variations in the absence of magnetic fields. As we will expand upon further below, the CUE still determines the long-time limit of this dynamics. Alternatively, we could consider the Brownian motion in one of the corresponding circular ensembles (COE and CSE) itself, where the COE case would be obtained from the unitary dynamics with time-evolution operator denoted as $V(t)$ by setting $U(t) = V^T(t)V(t)$. The corresponding correlators are automatically included in the hierarchies in our settings, while, physically, the alternative settings correspond to the experimentally more challenging situation in which the stochastic signal is itself symmetric in time.

While the resulting hierarchies are much more involved, they remain closed and constitute a complete analytical description for all times t, orders n, and system sizes N. We first develop this for dynamics generated by the GOE and then show that the results for the GSE follow from a simple substitution rule, where one formally replaces the matrix dimension N by $-N$. Furthermore, we will confirm that all hierarchies obey the same long-time limit for finite N.

5.4.1 Orthogonal symmetry

In the orthogonal symmetric class, the instantaneous SFF updates in a similar fashion to that of the unitary class reported in the previous section but with additional terms and quantities that arise from the symmetric structure of the instantaneous GOE Hamiltonian, whose matrix elements satisfy Eq. (2.54). This modifies the GUE

averaging rules (5.3) and (5.4) to read

$$\overline{C_{AB}} = \frac{\kappa}{N+1}\left(\mathrm{tr}\,[AB] + \mathrm{tr}\,[AB^T]\right) \tag{5.31}$$

and

$$\overline{D_{AB}} = \frac{\kappa}{N+1}\left(\mathrm{tr}\,[A]\,\mathrm{tr}\,[B] + \mathrm{tr}\,[AB^T]\right). \tag{5.32}$$

Starting from the expansion (5.2), the first-order instantaneous SFF then updates according to

$$\mathcal{K}_{1,1}(t+dt) = (1-\kappa\,dt)\,\mathcal{K}_{1,1}(t) + \frac{\kappa\,dt}{N+1}\,(N+L(t))\,, \tag{5.33}$$

where

$$L(t) = \overline{\mathrm{tr}\,[U(t)U^*(t)]} \tag{5.34}$$

constitutes an additional spectral correlator for level $n = 1$ of the hierarchy, and the asterisk denotes complex conjugation. This new quantity incrementally updates—again using the rules (5.31) and (5.32) to evaluate the averages—according to

$$\begin{aligned} L(t+dt) &= \overline{\mathrm{tr}\,[U(t+dt)U^*(t+dt)]} \\ &= (1-\kappa\,dt)L(t) + \frac{\kappa\,dt}{N+1}\,(N+\mathcal{K}_{1,1}(t))\,. \end{aligned} \tag{5.35}$$

Altogether, we find the closed system of coupled first-order linear differential equations

$$\dot{\mathcal{K}}_{1,1}(t) = \kappa\,\left((N+1)^{-1}\,(N+L(t)) - \mathcal{K}_{1,1}(t)\right), \tag{5.36}$$

$$\dot{L}(t) = \kappa\left((N+1)^{-1}\,(N+\mathcal{K}_{1,1}(t)) - L(t)\right), \tag{5.37}$$

which for the initial conditions $\mathcal{K}_{1,1}(0) = \overline{|\,\mathrm{tr}\,\mathbb{1}|^2} = N^2$ and $L(0) = \overline{\mathrm{tr}\,\mathbb{1}} = N$ are solved by

$$\mathcal{K}_{1,1}(t) = 1 + \frac{N-1}{2}\left(N+2+Ne^{-\frac{2}{N+1}\kappa\,t}\right)e^{-\frac{N}{N+1}\kappa\,t}, \tag{5.38}$$

$$L(t) = 1 + \frac{N-1}{2}\left(N+2-Ne^{-\frac{2}{N+1}\kappa\,t}\right)e^{-\frac{N}{N+1}\kappa\,t}. \tag{5.39}$$

When compared to the GUE result, additional spectral correlators therefore arise due to the symmetric structure of the GOE Hamiltonians. Propagating these through the calculations of the higher-order instantaneous SFF means that the number of quantities on each level of the hierarchy proliferates at a much faster rate than in the GUE derivation. Nonetheless, the hierarchy closes at each level and can be solved analytically, as we expand in more detail for the level $n = 2$ in Appendix E, with $K_2(t)$ given in Eq. (E.34). The analytical results for the instantaneous SFF to levels $n = 1$ and 2 are plotted in Figure 5.3, where we set the system size $N = 8$. There is excellent agreement between the analytical predictions and the numerical data for DBM-generated dynamics with instantaneous Hamiltonians drawn from the GOE, while there exist clear differences when compared to the predictions for GUE dynamics.

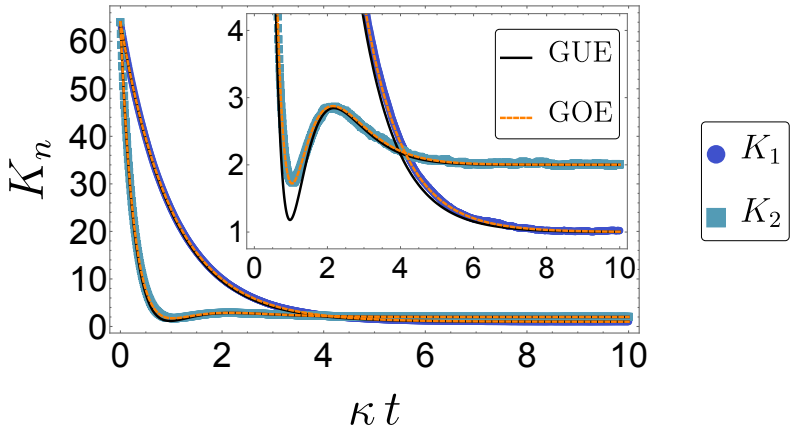

Figure 5.3: Numerical data for the instantaneous spectral form factor $K_n(t)$ with $n = 1, 2$ and $N = 8$ for DBM dynamics generated by instantaneous Hamiltonians from the GOE (data points) matches the analytical functions derived for the GOE (dashed curves), and differ clearly from the analytic expressions for the GUE (solid black curves, shown for reference). The DBM data is obtained from 10^4 realisations, with $dt = 0.01$.

5.4.2 Symplectic symmetry

As mentioned above, the results in the symplectic class can be obtained from the results in the orthogonal class by formally replacing the matrix dimension N by $-N$. Here, N refers to the full, even matrix dimension, not the size of the matrix expressed in terms of quaternions. From a general perspective, this relation between the two symmetry

classes is inherited from a similar relation between averages in the orthogonal $\mathrm{O}(N)$ and the compact symplectic group $\mathrm{Sp}(N/2)$ [276], whose significance we will demonstrate in our second setting (see Section 5.5). In the DBM setting, we can derive this substitution rule concretely by comparing the GOE averaging rules (5.31) and (5.32) with their GSE counterparts, which read

$$\overline{C_{AB}} = \frac{\kappa}{N-1}\left(\mathrm{tr}\,[AB] + \mathrm{tr}\,[AB^R]\right), \tag{5.40}$$

$$\overline{D_{AB}} = \frac{\kappa}{N-1}\left(\mathrm{tr}\,[A]\,\mathrm{tr}\,[B] - \mathrm{tr}\,[AB^R]\right). \tag{5.41}$$

Here, R denotes the quaternion conjugation given by Eq. (2.55), while the traces are the conventional matrix traces, not their quaternion modification. We now see that the averaging rules for the two ensembles are related by the formal replacements $N \to -N$, $T \to R$, and $\mathrm{tr} \to -\mathrm{tr}$. The same substitution rules then apply to the hierarchy equations and the initial conditions and, therefore, also to the instantaneous SFF itself.

In this way, we obtain, for instance, from Eq. (5.38), that the first-order instantaneous SFF in the symplectic DBM is given by

$$K_1(t) = 1 + \frac{N+1}{2}\left(N - 2 + Ne^{\frac{2}{N-1}\kappa t}\right)e^{-\frac{N}{N-1}\kappa t}, \tag{5.42}$$

while the analogous result for $n = 2$ is obtained by applying the same substitution to Eq. (E.34). As shown in Figure 5.4, these results again agree perfectly with numerical sampling of the DBM in this symmetry class.

5.4.3 Asymptotic relation between the three symmetry classes

While the analytical expressions of the instantaneous SFF display characteristic signatures in the three ensembles, they also share some common features. These are related to the fact that while the unitary increments $du(t;dt)$ generating the dynamics (2.10) obey specific symmetry constraints in the different ensembles, the resulting unitary evolution operator $U(t)$ at finite times is not constrained by these symmetries. This arises because the unitary increments $du(t;dt)$ in the orthogonal and symplectic symmetry class are confined to cosets, not groups. In the orthogonal class, the coset is formed by transposition-symmetric unitary matrices $du(t;dt) = du^T(t;dt)$,

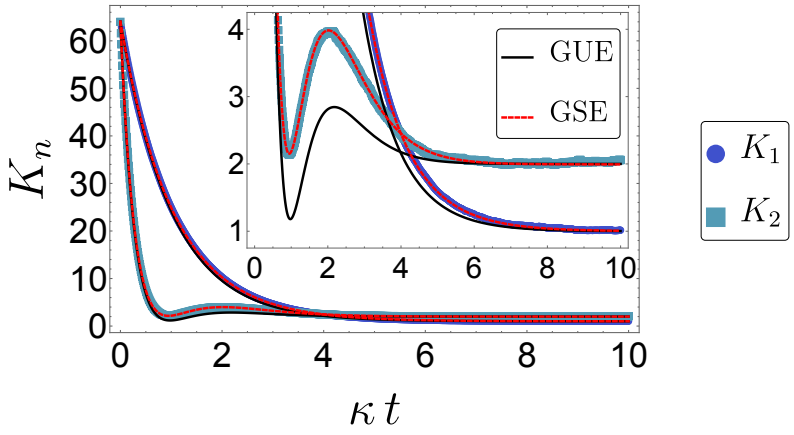

Figure 5.4: Analogous to Figure 5.3 but for DBM dynamics generated by instantaneous Hamiltonians from the GSE.

while in the symplectic symmetry class, the coset is that of self-dual unitary matrices $du(t;dt) = du^R(t;dt)$. However, both properties do not hold for products of elements from these cosets.

This results in the convergence of all three ensembles in the limit of long times $t \to \infty$, where all three dynamical versions of DBM converge to the CUE and hence cover all unitary matrices by the Haar measure. This is manifest in the analytical solutions, for instance, where $K_1(t) \to 1$ and $K_2(t) \to 2$ for the given analytical expressions in all three ensembles, and more generally can be verified from the stationary solutions of the spectral hierarchy in all symmetry classes.

It is instructive to compare this convergence for infinite times t with the limit of infinite system sizes $N \to \infty$ at finite times t. As in the unitary class (see Section 5.3.4) we can obtain both a simple leading behaviour and more precise uniform asymptotics by applying power counting to the averaging rules.

We start with the leading behaviour in the orthogonal class. Power counting then eliminates branching into the term $\mathrm{tr}\,[AB]$ from the averaging rule (5.31) unless $A = B^\dagger$ and branching into the term $\mathrm{tr}\,[AB^T]$ both in Eq. (5.31) and Eq. (5.32) unless $A = B^*$. The latter combinations can only occur from prior branching of the same form, which disconnects them asymptotically from the leading order of the instantaneous SFF. Therefore, this leading order coincides with that in the unitary class, see Eq. (5.22). By application of the stated formal substitution rules, the same argument then also holds

for the symplectic symmetry class.

Differences between the ensembles then appear when we consider the uniform approximation to order $O(N^0)$. The principles of the derivation remain the same as in the unitary class but have to be amended to include the leading orders of the newly generated terms. In the GOE, we obtain

$$K_1^{(u)}(t) = K_1^{(0)}(t) + s\left(1+\frac{s}{2}\right)e^{-s}, \tag{5.43}$$

$$K_2^{(u)}(t) = K_2^{(0)}(t) - 2N(1-s)^2e^{-2s} + \left[\frac{1}{3}(1+s)(3+3s-9s^2+5s^3)\right]e^{-2s} + 2(N-1)(1-s)e^{-3s} + e^{-4s}, \tag{5.44}$$

where $K_n^{(0)}(t)$ is given in Eq. (5.30) and $s = \kappa t$. The results for dynamics generated by the GSE then follow again by formally inverting the sign of N. The asymptotic expression for the first-order spectral form factor agrees between both ensembles, while for larger n the differences are of order $O(N^1)$.

5.5 Basis-invariant models

We now show that the same spectral hierarchies can be obtained under a significantly relaxed assumption, which makes them applicable to a much wider class of models with more complex statistical correlations of the Hamiltonian than in the Gaussian ensembles. For this, we consider Brownian models in which the unitary time-evolution operator $U(t)$ at any time is statistically invariant under a random unitary basis change $V(t)$, such that the transformed operator

$$U'(t) = V(t)U(t)V^\dagger(t) \tag{5.45}$$

occurs with the same probability in the ensemble.

This assumption is exact in DBM in all three symmetry classes, where $V(t)$ is chosen from the corresponding circular ensemble. More importantly, the same invariance should be well observed in a wide range of Brownian models since the matrices diagonalising the unitary generator $du(t;dt)$ are generally far from the identity, even when the generators themselves are arbitrarily close to the identity. Therefore, the

eigensystem is expected to become that of an ergodic system on a much shorter time scale than the ergodic time $t_{\text{erg}} \sim 1/\kappa$ that governs the evolution of the spectral statistics. Intuitively, this can be understood by noting that some finite time slice of the dynamics is produced by the multiplication of many incremental time steps dt (in a similar spirit to the CLT discussed in Section 2.2.3). We will verify this assertion in the next section for the BSYK model.

New forms of the DBM averaging rules in the different ensembles can then be obtained by considering the additional average over $V(t)$. We first work this out for the unitary symmetry class, where the DBM averaging rules are given by Eqs. (5.3) and (5.4), and then describe how the same process transfers to the other symmetry classes.

5.5.1 Unitary basis invariance

We note that the basis change (5.45) also applies in the same form to any power of $U(t)$ and $U^\dagger(t)$. Denoting any such combinations transforming in this way again as A and B, momentarily fixing H, the average over V from the CUE then gives

$$\begin{aligned} C_{AB} &\equiv \overline{\operatorname{tr}\,[HVAV^\dagger]\operatorname{tr}\,[HVBV^\dagger]} \\ &= \frac{1}{N^2-1}\left[\left(\operatorname{tr}\,[H^2]-\frac{1}{N}(\operatorname{tr} H)^2\right)\operatorname{tr}\,[AB]+\left((\operatorname{tr} H)^2-\frac{1}{N}\operatorname{tr}\,[H^2]\right)\operatorname{tr}\,[A]\operatorname{tr}\,[B]\right] \end{aligned} \tag{5.46}$$

and

$$\begin{aligned} D_{AB} &\equiv \overline{\operatorname{tr}\,[HVAV^\dagger HVBV^\dagger]} \\ &= \frac{1}{N^2-1}\left[\left(\operatorname{tr}\,[H^2]-\frac{1}{N}(\operatorname{tr} H)^2\right)\operatorname{tr}\,[A]\operatorname{tr}\,[B]+\left((\operatorname{tr} H)^2-\frac{1}{N}\operatorname{tr}\,[H^2]\right)\operatorname{tr}\,[AB]\right]. \end{aligned} \tag{5.47}$$

Averaging in the next step also over the Hamiltonian (without any further assumption of its specific ensemble and denoting this additional average again by an overline), we obtain

$$\overline{C_{AB}} = \frac{1}{N}\frac{N^2\mu-\lambda}{N^2-1}\operatorname{tr}\,[AB]+\frac{\lambda-\mu}{N^2-1}\operatorname{tr}\,[A]\operatorname{tr}\,[B] \tag{5.48}$$

and

$$\overline{D_{AB}} = \frac{1}{N}\frac{N^2\mu - \lambda}{N^2-1}\mathrm{tr}\,[A]\,\mathrm{tr}\,[B] + \frac{\lambda-\mu}{N^2-1}\mathrm{tr}\,[AB], \tag{5.49}$$

where all ensemble-specific information is captured by the quantities

$$\lambda = \overline{(\mathrm{tr}\,H)^2} \quad \text{and} \quad \mu = \frac{1}{N}\overline{\mathrm{tr}\,[H^2]}. \tag{5.50}$$

In the GUE, $\lambda = \mu = \kappa$ so that we recover the original DBM averaging rules (5.3) and (5.4).

We see that in comparison to these original rules, the revised rules contain a first part that only differs by a factor from the original rules and a second part that replicates the trace structure in the initial expression on the left-hand side. When we revisit the construction of the hierarchy with these revised rules, we see that this results in a minimal modification that amounts to a consistent redefinition of the ergodicity rate κ in terms of λ and μ.

This modification can be read off directly by comparing the original hierarchy structure (5.18) with the modified structure, which is given by

$$\begin{aligned}\dot{\mathcal{K}}_{(c_i)_{i=1}^m}(t) = {} & \underbrace{-\mu n \mathcal{K}_{(c_i)_{i=1}^m}(t)}_{\kappa \text{ replaced by } \mu} \underbrace{-\frac{\lambda-\mu}{N^2-1}\sum_{j<k} c_j c_k \mathcal{K}_{(c_i)_{i=1}^m}(t)}_{\text{retained trace structure in Eq. (5.48)}} \underbrace{-\frac{\lambda-\mu}{N^2-1}\sum_{j}\frac{|c_j|}{2}\sum_{k=1}^{|c_j|-1}\mathcal{K}_{(c_i)_{i=1}^m}(t)}_{\text{retained trace structure in Eq. (5.49)}} \\ & \underbrace{-\frac{\kappa}{N}\sum_{j<k} c_j c_k \mathcal{K}_{(c_i)_{i\neq j,k}(c_j+c_k)}(t)}_{\text{from combining traces in Eq. (5.48)}} \underbrace{-\frac{\kappa}{N}\sum_{j}\frac{|c_j|}{2}\sum_{k=1}^{|c_j|-1}\mathcal{K}_{(c_i)_{i\neq j}(k\,\mathrm{sgn}\,c_j)(c_j-k\,\mathrm{sgn}\,c_j)}(t)}_{\text{from splitting traces in Eq. (5.49)}}.\end{aligned} \tag{5.51}$$

The two sums in the second line arise from the first part of the modified rules, where the coefficient κ now takes the specific form

$$\kappa = \frac{N^2\mu - \lambda}{N^2-1}. \tag{5.52}$$

With this identification, these two sums then already agree with the original hierarchy.

The first line contains two additional sums, which arise from the new second parts of the two modified averaging rules. These are all proportional to the same correlator whose time derivative we are determining, which also appears in the very first term now with the coefficient μ. In these sums, the correlator occurs n^2 times multiplied with a positive sign [whenever two oppositely signed indices are combined, which amounts to taking one of n instances of H from a generator $u(t;dt)$ and pairing it with one of n instances of H from a generator $u^\dagger(t;dt)$] and $2\times n(n-1)/2$ times with a negative sign [these are the pairings of H from two generators $u(t;dt)$ or from two generators $u(t;dt)$]. Together with the contribution from the very first term, this combines into a factor

$$-n\mu + n\frac{\lambda-\mu}{N^2-1} = n\frac{\lambda-\mu+(1-N^2)\mu}{N^2-1} = -n\kappa, \tag{5.53}$$

where κ is the exact same combination of terms as in Eq. (5.52).

Altogether, we see that the entire hierarchy remains intact with this simple redefinition of κ, which holds irrespective of any further details of the ensemble of instantaneous Hamiltonians $H(t)$. We will return to the discussion of this renormalised ergodic rate after establishing its analogous form in the other two symmetry classes.

5.5.2 Orthogonal and symplectic invariance

Analogous considerations can be carried out in the orthogonal symmetry class, where we impose invariance under orthogonal transformations equipped with the Haar measure on $\mathrm{O}(N)$, and in the symplectic ensemble, where we impose invariance under symplectic transformations equipped with the Haar measure on $\mathrm{Sp}(N/2)$ (where N therefore still refers to the matrix size and hence has to be even; we also keep the conventional notion of a trace for this symmetry class).

The derivation can again be carried out on the level of the averaging rules. Carrying out the averages defined in Eqs. (5.46) and (5.47) with V from the COE, we find that

$$C_{AB} = \frac{N\,\mathrm{tr}\,[H^2]-(\mathrm{tr}\,H)^2}{N(N+2)(N-1)}(\mathrm{tr}\,[AB]+\mathrm{tr}\,[AB^T]) + \frac{(N+1)(\mathrm{tr}\,H)^2-2\,\mathrm{tr}\,[H^2]}{N(N+2)(N-1)}\mathrm{tr}\,[A]\,\mathrm{tr}\,[B] \tag{5.54}$$

and

$$D_{AB} = \frac{N \operatorname{tr}[H^2] - (\operatorname{tr} H)^2}{N(N+2)(N-1)}(\operatorname{tr}[A]\operatorname{tr}[B] + \operatorname{tr}[AB^T]) + \frac{(N+1)(\operatorname{tr} H)^2 - 2\operatorname{tr}[H^2]}{N(N+2)(N-1)}\operatorname{tr}[AB] \tag{5.55}$$

are instead relevant. Averaging next also over the instantaneous Hamiltonian, the rules (5.31) and (5.32) for orthogonal DBM therefore become replaced by

$$\overline{C_{AB}} = \frac{N^2\mu - \lambda}{N(N+2)(N-1)}(\operatorname{tr}[AB] + \operatorname{tr}[AB^T]) + \frac{(N+1)\lambda - 2N\mu}{N(N+2)(N-1)}\operatorname{tr}[A]\operatorname{tr}[B] \tag{5.56}$$

$$\overline{D_{AB}} = \frac{N^2\mu - \lambda}{N(N+2)(N-1)}(\operatorname{tr}[A]\operatorname{tr}[B] + \operatorname{tr}[AB^T]) + \frac{(N+1)\lambda - 2N\mu}{N(N+2)(N-1)}\operatorname{tr}[AB], \tag{5.57}$$

where λ and μ remain defined as in Eq. (5.50).

As in the unitary case, these modified rules contain a part that replicates the original rules (5.31) and (5.32) with a modified coefficient κ, which now takes the form

$$\kappa = \frac{N+1}{N(N+2)(N-1)}(N^2\mu - \lambda), \tag{5.58}$$

Furthermore, the modified rules contain again an additional part that replicates the trace structure of the terms that have been averaged, which gives rise to the same modification of κ when fed into the hierarchy. This follows in analogy to Eq. (5.53), where terms now combine according to

$$-n\mu + n\frac{(N+1)\lambda - 2N\mu}{N(N+2)(N-1)} = -n\kappa. \tag{5.59}$$

By an analogous calculation, we have verified that for invariance under symplectic basis changes, the averaging rules again carry over by the replacements $N \to -N$, $\operatorname{tr} \to -\operatorname{tr}$, and $T \to R$.

5.5.3 Brief summary of the main result

Summarising all three cases, we find that basis invariance results in the same spectral hierarchy as that from DBM, where the generalised ergodicity rate can be written as

$$\kappa = \gamma(N^2\mu - \lambda). \tag{5.60}$$

Here, λ and μ (5.50) are determined by the statistics of the instantaneous Hamiltonian, while

$$\begin{aligned} \gamma &= \frac{1}{(N+1)(N-1)} && \text{(unitary class)}, \\ \gamma &= \frac{N+1}{N(N+2)(N-1)} && \text{(orthogonal class)}, \\ \gamma &= \frac{N-1}{N(N+1)(N-2)} && \text{(symplectic class)}. \end{aligned} \tag{5.61}$$

We note that in all cases, this coefficient corresponds to a Weingarten function [276, 277].

$$\gamma = \overline{|V_{lm}|^2 |V_{l'm'}|^2} = \mathrm{Wg}([1][1]) \tag{5.62}$$

in the corresponding group, which involves two different matrix elements that are not related by any symmetry.

5.5.4 Consistency with DBM

The assumption of basis invariance holds manifestly in DBM. To establish consistency between both versions of the hierarchy, we make use of the detailed definitions of the Gaussian ensembles in Section (2.4.2.1). We then have, from the definitions (5.50) and the property (2.53), the identity $\mu = \kappa$, where κ is at this stage to be interpreted as the coefficient defining the Gaussian ensembles. Furthermore, from the detailed definitions

of these ensembles we also have

$$\begin{aligned} \lambda &= \mu && \text{(GUE)}, \\ \lambda &= \frac{2N}{N+1}\mu && \text{(GOE)}, \\ \lambda &= \frac{2N}{N-1}\mu && \text{(GSE)}. \end{aligned} \tag{5.63}$$

Inserting these expressions along with Eq. (5.61) into Eq. (5.60), we recover in all cases that generalised rate the coincides with the original coefficient κ appearing in the definitions of the Gaussian ensembles.

5.6 BSYK dynamics

We now investigate the applicability of the spectral hierarchy to the Brownian SYK model. For this, we first establish the analytical expression of the generalised ergodicity rate and then compare the ensuing predictions for the instantaneous SFF with the numerical implementation of the model, where we cover all three symmetry classes by varying the number of fermions M, as described in Section 2.4.2.2.

5.6.1 Ergodicity rate κ

To obtain the generalised ergodicity rate (5.60) in the BSYK model, we need to determine the coefficients λ and μ defined in Eq. (5.50). The structure of the BSYK Hamiltonian (2.58) entails that each realisation of it is traceless, $\operatorname{tr} H = 0$, so that $\lambda = 0$ vanishes identically. The coefficient μ then follows from the variance (2.59) of the instantaneous coupling tensor, where we have to account for the number of its independent elements (defined by the number of ways one can choose q from M). This gives

$$\mu = \frac{1}{q^2}\binom{M}{q}\frac{(q-1)!}{M^{q-1}}, \tag{5.64}$$

which ties this coefficient to the degree of sparseness in the model. The effective ergodicity rate is then given by

$$\kappa = N^2\gamma\mu, \tag{5.65}$$

where $N = 2^{(M/2)-1}$ is the size of a statistically independent block of the Hamiltonian, and γ is taken from Eq. (5.61) with the symmetry class determined by the number of fermions M.

5.6.2 Comparison of numerical and analytical results

As mentioned earlier, we will set $q = 4$. In keeping with our desire to test these analytical predictions in the non-trivial regime, we will furthermore focus on models with only moderately large numbers of fermions, which allows us to resolve statistically significant differences between the ensembles.

Figure 5.5 shows the numerically obtained time dependence of the instantaneous SFF $K_n(t)$ in analogy to Figure 5.1 but for numerical dynamics obtained from the BSYK model with $M = 10$ Majorana fermions. This value of M places the system into the unitary symmetry class, for which the Hamiltonian of dimension $2N = 2^5$ can be brought into block-diagonal form where each block is of dimension $N = 16$. As in Figure 5.1, we observe excellent agreement with the analytical predictions, with a small deviation only visible in K_2.

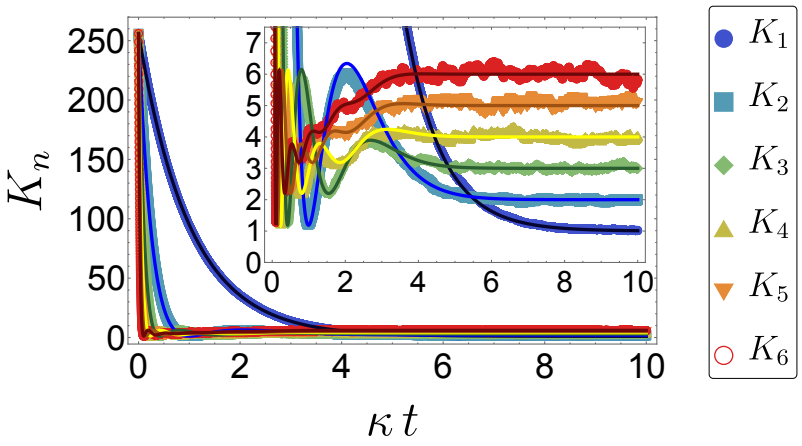

Figure 5.5: Comparison of the analytical predictions (solid coloured curves) for the instantaneous SFF $K_n(t)$ with data for BSYK-generated dynamics with $M = 10$ Majorana fermions, where the instantaneous Hamiltonians belong to unitary symmetry class. Data is generated from 10^3 realisations, with $dt = 0.01$.

Figure 5.6 displays numerical data for the BSYK model with $M = 8$ Majorana

fermions, for which the system is in the orthogonal symmetry class. Instead with the analytical predictions for this case, already shown and contrasted to the unitary case in Figure 5.3, we now compare this data with GOE DBM numerical data generated for the corresponding matrix dimension $N = 8$. We obtain excellent agreement between both Brownian models, which establishes the universality of their spectral correlations now also on the level of the models. Note that we would observe the same agreement if we had plotted the analytical curves instead.

Figure 5.7 is analogous to Figure 5.6 but for the symplectic class, which here is realised for $M = 12$ Majorana fermions ($N = 32$). Again, we observe excellent agreement between the BSYK and DBM data, which perfectly coincide with the analytical predictions of the spectral hierarchy for this class, see Figure 5.4.

Importantly, in all these cases we would have observed noticeable discrepancies if we had equated the ergodicity rate in the BSYK model naively as $\kappa = \mu$.

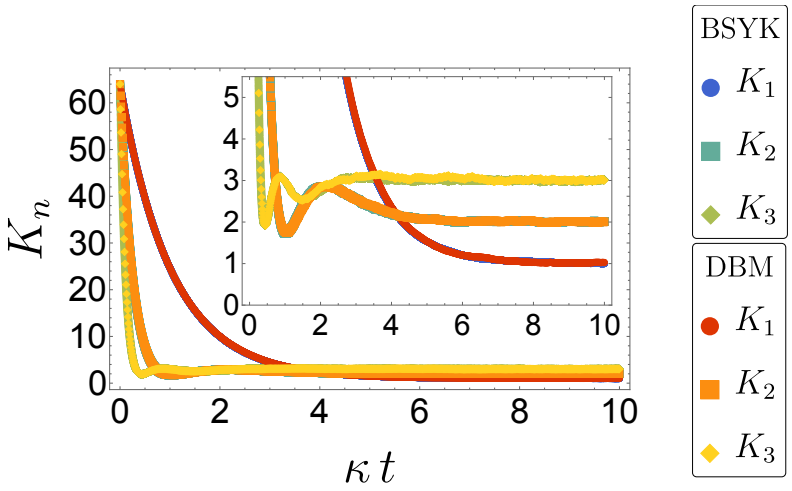

Figure 5.6: Comparison of numerical data for the instantaneous SFF $K_n(t)$ for BSYK-generated dynamics of $M = 8$ Majorana fermions, where the instantaneous Hamiltonians belong to the orthogonal symmetry class, and DBM-generated dynamics by GOE Hamiltonians of dimension $N = 8$. Data is generated for $dt = 0.01$, over 10^4 realisations.

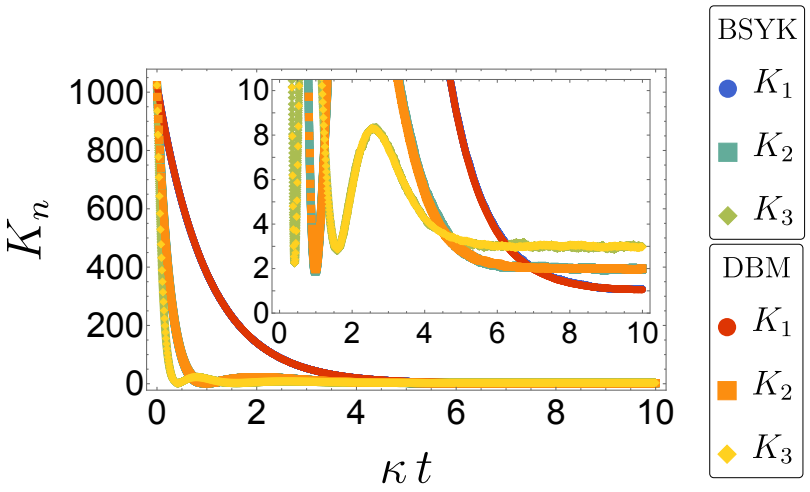

Figure 5.7: Analogous to Figure 5.6 but for the symplectic class, as realised in BSYK-generated dynamics with $M = 12$ Majorana fermions and GSE DBM with $N = 32$. Data is generated for $dt = 0.01$, over 10^4 realisations for DBM and 10^3 realisations for BSYK.

5.7 The out-of-time-ordered correlator (OTOC)

We now consider the relevance of the correlators appearing in the spectral hierarchy for dynamical correlations. Specifically, we address this in terms of out-of-time-ordered correlators (OTOCs), which serve as a common dynamical diagnostic of many-body quantum chaos as detailed in Section 2.3.4.2. In the particular setting of quantum-chaotic dynamics, the ballistic behaviour of the OTOC at early times allows for the extraction of a Lyapunov exponent, which facilitates the formulation of chaos bounds that have been found to be saturated both in black holes and in the SYK model [72–75]. We will see that in the Brownian models, ensemble-averaged versions of these correlators can be expressed directly in terms of quantities from the first two levels of the spectral hierarchy.

In the stochastic setting (2.10), we consider the OTOC (2.47) for two generic observables $V(0) = v$ and $W(t) = U^\dagger(t) w U(t)$, where the expectation value is evaluated in the infinite-temperature state. Taking the ensemble average, we then build up the

OTOC from the quantities

$$\begin{aligned} F(t) &= \overline{\text{tr }[vU^\dagger(t)wU(t)vU^\dagger(t)wU(t)]}, \\ G(t) &= \overline{\text{tr }[v^2U^\dagger(t)w^2U(t)]}, \\ \mathcal{O}(t) &= 2\left(G(t) - F(t)\right). \end{aligned} \tag{5.66}$$

The OTOC $\mathcal{O}(t)$ then probes the correlation of the time-evolved operator $w(t) = U^\dagger(t)wU(t)$ with the operator v for dynamics starting in an infinite-temperature state.

5.7.1 Stationary reference point

As a reference point, we first consider the case that v and w are two independent random observables, which for concreteness we model by taking them from the GUE with normalisation $\overline{v^2} = \overline{w^2} = \mathbb{1}$. The statistical properties of w then transfer unchanged to the time-evolved observable $W(t)$ so that the OTOC is independent of time. This can be made manifest by carrying out the averages explicitly, from which we find

$$\begin{aligned} \overline{F} &= \overline{\text{tr }[vwvw]} = \frac{1}{N} \\ \overline{G} &= \overline{\text{tr }[v^2w^2]} = N \\ \overline{\mathcal{O}} &= 2\left(N - \frac{1}{N}\right). \end{aligned} \tag{5.67}$$

This sets our expectations for the general behaviour of the OTOC in the long-time limit, in analogy to the status of the CUE result (2.38) for the SFF.

5.7.2 OTOC dynamics

Non-trivial dynamics are observed for the OTOC of a time-evolved operator with itself, which we obtain by equating $v = w$. Proceeding identically to the construction of the spectral hierarchy in the previous sections, one can consider the incremental updates of the quantities (5.66) under the stochastic evolution (2.10) and derive a system of first-order linear differential equations, which closes under the assumption of basis invariance. This evaluation is simplified by utilising this basis invariance from the outset, where one finds again convergence with the Gaussian ensembles. Implementing

this programme again for v from the GUE with $\overline{v^2} = \mathbb{1}$, the ensemble-averaged functions then take the form

$$\begin{aligned}
\overline{F(t)} &= \frac{1}{N^2}\left(\overline{\mathrm{tr}\,[U(t)]^2(\mathrm{tr}\,U^\dagger(t))^2} + \overline{\mathrm{tr}\,[U^\dagger(t)]^2(\mathrm{tr}\,U(t))^2}\right) + \frac{1}{N} = \frac{1}{N^2}\left(2\mathcal{K}_{11,2}(t) + N\right), \\
\overline{G(t)} &= N + \frac{1}{N}\left(1 + \overline{\mathrm{tr}\,U(t)\,\mathrm{tr}\,U^\dagger(t)}\right) = N + \frac{1}{N}\left(1 + \mathcal{K}_{1,1}(t)\right), \\
\overline{\mathcal{O}(t)} &= 2N + \frac{2}{N}\mathcal{K}_{1,1}(t) - \frac{4}{N^2}\mathcal{K}_{11,2}(t) = 2N\left(1 + \frac{\mathcal{K}_{1,1}(t)}{N^2} - \frac{2\mathcal{K}_{11,2}(t)}{N^3}\right).
\end{aligned} \tag{5.68}$$

We see that indeed, as advertised above, the OTOC $\overline{\mathcal{O}}$ becomes expressed in terms of quantities from the first two levels of the spectral hierarchy ($n = 1, 2$). Notably, this also includes the correlator $\mathcal{K}_{11,2}(t)$.

Further evaluation depends on the symmetry class of the unitary evolution. In the unitary class, where the hierarchy is determined by the differential equations (5.14) with initial conditions (5.15), we find

$$\mathcal{K}_{11,2}(t) = \frac{N^2}{4}\left((N-1)(N+3)e^{-\frac{2}{N}\kappa t} - (N+1)(N-3)e^{\frac{2}{N}\kappa t}\right)e^{-2\kappa t}, \tag{5.69}$$

which delivers the analytical prediction for the OTOC in this symmetry class when combined with Eq. (5.7) for $\mathcal{K}_{1,1}(t) = K_1(t)$. The corresponding result for the orthogonal symmetry class is given by Eq. (E.35), while the result for the symplectic symmetry class follows by applying the previously stated substitution rules.

In the limit of large N, the OTOC turns out to be of order $O(N^1)$ for all times. This simplifies its asymptotic analysis, for which we only need the leading orders $K^{(\infty)}(t)$ specified in Eqs. (5.22) and (5.23). From this, we obtain the asymptotic prediction

$$\overline{\mathcal{O}^{(\infty)}(t)} = 2N\left(1 + e^{-\kappa t} + 2(\kappa t - 1)e^{-2\kappa t}\right), \tag{5.70}$$

which then applies in the same form to all three symmetry classes.

Figure 5.8 depicts the time behaviour of the ensemble-averaged OTOC $\overline{\mathcal{O}}$ in (*a*) DBM- and (*b*) BSYK-generated dynamics for varying system dimensions, covering again the three different symmetry classes. With time scaled according to the analytically determined ergodicity rate κ, the numerical data agree perfectly well both between the two models and with the analytical predictions from (5.68). In all cases, the OTOC

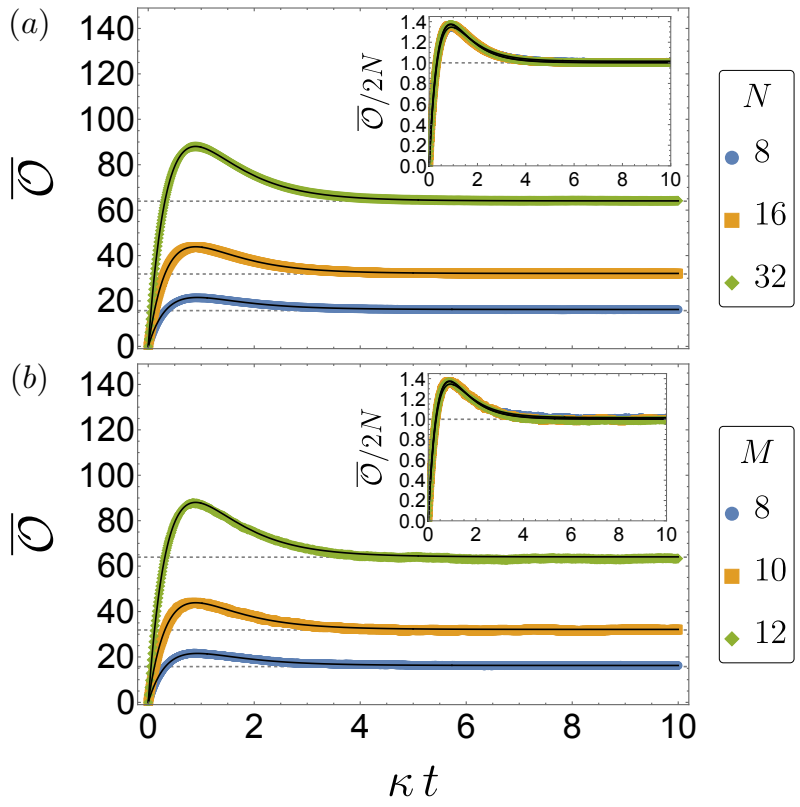

Figure 5.8: The OTOC $\overline{\mathcal{O}}$ calculated numerically for (a) DBM dynamics generated by Hamiltonians sampled from the GOE with dimension $N = 8$, the GUE with dimension $N = 16$, and the GSE with dimension $N = 32$, as well as (b) BSYK dynamics generated by $M = 8$, 10, and 12 Majorana fermions, whose Hamiltonians can be decomposed into 2 blocks each of dimension $N = 8, 16$, and 32 (blue circles, orange squares, and green diamonds, respectively), plotted as a function of rescaled time, where κ is given by Eq. (5.64). This is contrasted with the analytic solutions (5.68) derived in the setting of DBM (solid black curves). The inset demonstrates data collapse when $\overline{\mathcal{O}}$ is rescaled by $2N$, which corresponds to its asymptotic value for large N and t. Data is generated over 10^4 and 10^3 realisations, respectively (10^2 for BSYK with $M = 10$ and 12).

tends over time to the stationary value $\overline{\mathcal{O}}$ given in Eq. (5.67), which is indicated by the dashed lines. The respective insets show this numerical data normalised by $2N$. The resulting data collapse demonstrates that even though the chosen matrix dimensions are relatively small, the results for the different symmetry classes closely follow the asymptotic prediction (5.70), where all differences between the ensembles fall within statistical bounds.

5.8 The broader picture

The previous section highlights the significance of all spectral correlators encountered in this chapter, beyond those that define the instantaneous SFF itself. To conclude these considerations, we adopt an even broader perspective and set out to delineate the boundaries of the encountered universality in these spectral correlations. We will argue that these boundaries themselves align closely with all spectral correlators that form the spectral hierarchy. Our argument rests on the role of time-local U(1) invariance in the Brownian models. As emphasised earlier, all correlators within the hierarchy obey this invariance. In the unitary case, this invariance is manifest in the index sum rule (5.19), while more generally it follows from the averaging rules in all classes.

This invariance is also manifest in the universal form (5.60) of the ergodicity rate κ. In this expression, we can recast the ensemble-specific data as

$$N^2\mu - \lambda = N\,\overline{\mathrm{tr}\,[H_0^2]} \equiv N^2\mu_0, \tag{5.71}$$

where $H_0 = H - \frac{\mathrm{tr}\,H}{N}\mathbb{1}$ is the traceless part of the Hamiltonian. Therefore, all ensembles in which the Hamiltonians are amended by arbitrarily time-dependent additional contributions $\varphi(t)\mathbb{1}$ are equivalent, and this holds even when these additions are correlated in time. In the dynamics, these additional contributions then again integrate into an arbitrarily correlated U(1) phase, which however drops out of all of the correlators within the hierarchy.

We illustrate the relevance of this observation by identifying two closely related non-universal properties. The first property is the density of states of the instantaneous eigenvalues on the unit circle, which can be analysed in terms of its moments

$$A_n = \overline{\mathrm{tr}\,U^n(t)}. \tag{5.72}$$

We see that these moments formally correspond to unbalanced correlators $\mathcal{K}_{n,\cdot}(t)$, in which only one of the two sets of indices appears. These moments are manifestly not invariant under arbitrary U(1) transformations. Indeed, they can all be made to vanish by averaging over the global phase, which results in a flat density of states on the unit circle. In a Brownian model, this can be achieved on a freely chosen time scale by

amending the Hamiltonians as mentioned above, while leaving all correlators within the hierarchy unchanged.

The second closely related property is the connected part of the SFF, given by

$$S_n(t) = K_n(t) - A_n^2(t). \tag{5.73}$$

This connected part has been the focus of previous studies of unitary DBM, where it is more directly amendable to an analytical treatment as it removes the contributions of order N^2. However, utilising this connected part only, we would not be able to establish the observed universality of spectral correlations beyond DBM as it then mixes in the non-universal information from the density of states. Indeed, we see immediately from its definition (5.73) that the connected part does not obey U(1) invariance in the context of these more general models.

A concrete manifestation can be established directly by inspecting A_1, which in our models obeys the differential equation

$$\dot{A}_1 = -\frac{\mu}{2} A_1(t) \tag{5.74}$$

with initial condition $A_1(t) = N$. This is solved by $A_1(t) = Ne^{-\mu t/2}$, which introduces μ as an additional rate to describe statistical quantities outside the spectral hierarchy.

On the other hand, the leading order asymptotics of these moments in DBM also appear in our analysis, see Eq. (5.22). This suggests that a larger degree of universality also encompassing these quantities could possibly be reinstated by a suitable unfolding of the spectrum (which we expressly did not require for the quantities captured in our framework). Furthermore, one may consider U(1)-invariant versions of these moments, which could be based on the traceless parts of the instantaneous Hamiltonians.[2]

Finally, we recall that the universality of properties within the hierarchy still rests on an assumption, namely that of rapidly established basis invariance. We argued this to be observed for a wide class of models based on the fact that the matrices diagonalising the instantaneous unitary operators $du(t; dt)$ are generally far away from the identity. It furthermore follows that under the composition of two time steps, the new set of eigenstates is generally a non-perturbative combination of the eigenstates

[2]Such moments should be connected with the analysis of DBM on SU(N), see [278].

from each step. This stochastically emergent basis invariance is manifest in DBM and numerically well observed in the BSYK model. However, it is of course easy to come up with structured Brownian models that develop basis invariance on scales that compete with the ergodic time, with (non-zero-dimensional) Brownian circuits being a prime example of such models in the literature [50]. An open question following on from our results, therefore, is to identify the exact range of Brownian models that develop basis invariance on quasi-instantaneous time scales.

5.9 Summary

In this chapter, we described an analytical approach to obtain exact expressions for correlators that describe the instantaneous spectral statistics in zero-dimensional Brownian models of quantum chaos. These correlators are organised into a hierarchy, which includes the instantaneous SFF as well as other correlators that feature, e.g., in ensemble-averaged OTOCs. We established the universality of these spectral correlations encompassing all systems that rapidly develop statistical basis invariance and carried this out in each of the three standard Wigner-Dyson symmetry classes. This property applies exactly to DBM and agrees excellently with numerical data in the BSYK model.

To develop this picture, we presented a specific derivation for DBM and a general derivation that exploits stochastically emergent basis invariance according to the symmetry class in more generic Brownian models. The latter scenario results in the same hierarchy with a suitably renormalised ergodic time, whose general form we established in terms of the ensemble of instantaneous Hamiltonians, while its specific form can be determined analytically in the BSYK model.

We also explored the broader significance of these findings. By examining the assumptions of our derivations we clarify that the observed universality is confined to correlators that obey U(1) invariance. This is manifest in the OTOC and instantaneous SFF, but not, for instance, when one investigates only its connected part. While this makes determining the statistics for large system sizes N in principle more challenging, our approach allows us to establish these asymptotics uniformly in time and N.

Chapter 6

Summary and outlook

This thesis provides a statistical description for a broad range of stochastic time evolutions that effectively model complex many-body quantum scrambling dynamics. Specifically, we studied stochastic models for complex many-body quantum systems and the emergence of universal features in spectral correlations in their dynamical approach to ergodicity, addressing how symmetry and additional structure may constrain scrambling dynamics and how this is reflected in spectral properties.

Our central objective stems from the emergence of random-matrix theory as a natural description that captures universal features of a diverse range of complex quantum systems, enabling one to focus on overarching features of the system like dimensionality and symmetry. On the other hand, there are many open questions pertaining to complex many-body quantum dynamics, where understanding the scrambling mechanism has broad importance and implications. In addition to providing insight into the thermalisation of a quantum state under unitary time evolution, further understanding the approach towards ergodicity could clarify the connection between chaos and fast computation [279] and set new bounds on transport coefficients [161, 280, 281]. More direct applications in the quantum computing setting include the development of robust systems and mitigation against decoherence.

In Chapter 3, we studied the imposition of time-reversal symmetry on entanglement dynamics in random quantum circuits built from gates taken from the circular ensembles of Dyson's Threefold Way. Given the analytic intractability of the full hybrid unitary-projective circuit dynamics, we employed a statistical measure of entangling

power, formulated via a characteristic entanglement matrix that inherits its statistical behaviour from the circular ensembles, in order to analytically quantify the difference between these circuits on the local level. By introducing this measure, we gained an intuitive understanding of the full circuit entanglement dynamics, where we found time-reversal-symmetric gates to have a reduced entangling power when compared to non-time-reversal-symmetric gates, which subsequently shifted the MIET towards lower critical measurement rates for the system sizes studied. The role of symmetry classes could be extended to circuits composed of randomly drawn Clifford gates (*not* endowed with Haar measure), which have been studied extensively [89, 184–190]. While the Clifford group can be generated by time-reversal symmetric gates, it includes non-time-reversal-symmetric gates. Hence, a random uniform sampling of the Clifford group would be akin to the unitary ensemble, while the COE equivalent could be identified by the subset of the group consisting of time-reversal symmetric elements. Furthermore, the symmetries could also be imposed globally for finite iterations of the circuit, implying relations between gates in different layers. Zooming out, the study of quantum circuit dynamics is also relevant to quantum information science, in addition to the experimental drive to develop quantum simulators and qubit systems that realise and exploit entanglement and many-body phases to solve hard scientific problems (see Ref. [282] for a topical review). Remarkably, this has already been realised as a technological advantage, where an IBM experiment on the MIET utilised gates constrained to the CSE [182]. From a more general perspective, this motivates the understanding of how quantum information spreads across a system and the efficiency of this scrambling process. In the later chapters, we studied the evolution of complex many-body systems towards a chaotic, ergodic phase via their spectral statistics. For this, our central diagnostic tool is the SFF, which combines universal signatures of the symmetry class with a high sensitivity to system-specific spectral features [17, 42, 123].

In Chapter 4, we developed a single-parameter scaling theory for the spectral statistics in maximally efficient scrambling, which embodies the exact self-similarity of the spectral correlations along the complete scrambling dynamics towards the ergodic RMT endpoint. We showed that our scaling theory is exactly matched by DBM, further motivating the study of zero-dimensional Brownian models of quantum chaos. For other scrambling scenarios, the scaling theory's predictions serve as bounds, allowing one to

quantify inefficient or incomplete scrambling on all time scales.

In Chapter 5, we extended this framework in the setting of zero-dimensional Brownian models whose spectral statistics are amenable to an exact analytical treatment. We demonstrated that these spectral correlations appear as part of a closed hierarchy of differential equations that can be formulated for all system sizes and in each of the three standard symmetry classes defined with respect to time-reversal symmetry. This hierarchy of equations allows us to further express the ensemble-averaged OTOC in terms of spectral information. To appreciate the generality of these results, it is instructive to emphasise that the spirit of our approach has been to consider stochastic processes where the sole constraint is that the incremental updates are invariant under unitary transformations (basis rotations), which therefore describes a large class of dynamics. Subsequently, our key finding was that the spectral hierarchy applies exactly and in the same form to DBM and all systems with stochastically emerging basis invariance, where the model-dependent information is subsumed in a single dynamical time scale. We further verified this universality numerically for the BSYK model, for which we find perfect agreement with the analytical predictions of the symmetry class determined by the number of Majorana fermions. This results in a complete analytical description of the spectral correlations, enabling us to identify which correlations are universal in a large class of models, and leaves open investigation into other zero-dimensional Brownian models of quantum chaos.

Altogether, these results give a statistical description of complex many-body quantum scrambling dynamics in different scenarios within the broad stochastic setting. Specifically, our results delineate the boundaries of universal spectral statistics over a large range of stochastic models of quantum chaos and make them amenable to a systematic analytical treatment in all three standard Wigner-Dyson symmetry classes. These results can therefore serve as a useful benchmark to observe deviations from universality in more structured or constrained models. A further natural, yet detailed, extension of our results would be the extension to the Tenfold Way [31, 33], which also includes charge conjugation symmetry (as observed in superconductors [31]) and chiral symmetry (as observed, e.g., by the Dirac operator [283]) aspects. This would then also allow for the examination of the scope of topological protection, which is both of fundamental interest and of technological importance.

Appendix A

Joint eigenvalue distribution in the ensemble $\mathbf{A}^2$

To obtain the eigenvalue statistics of the characteristic entanglement matrix V, Eq. (3.6), for U in the CSE in Chapter 3, we reformulate the ensemble as in Eq. (3.20) and then apply the Brownian motion approach to the matrix $A = iW^T JW$. Consider the stochastic process generated by

$$W \to \left(\mathbb{1} - i(\delta t)^{1/2} G - \frac{\delta t}{2} G^2\right) W \left(\mathbb{1} - i(\delta t)^{1/2} H - \frac{\delta t}{2} H^2\right) \tag{A.1}$$

$$\equiv W + \delta W, \tag{A.2}$$

where δt is an infinitesimal parameter and we only keep terms up to $O(\delta t)$. Here H and G are independent random Hermitian matrices from the Gaussian Unitary Ensemble (GUE), characterised by $\overline{G_{kl}} = \overline{H_{kl}} = \overline{G_{kl} H_{mn}} = 0$ and $\overline{G_{kl} G_{mn}} = \overline{H_{kl} H_{mn}} = N^{-1} \delta_{kn} \delta_{lm}$. Some key averages that we need are

$$\overline{HMH} = N^{-1} \mathrm{tr}\, M, \quad \overline{HMH^*} = N^{-1} M^T, \tag{A.3}$$

for any fixed matrix M. These expressions imply $\overline{G^2} = \overline{H^2} = \mathbb{1}$, while cross-terms $\overline{GMH} = 0$, and allow us to set

$$\delta W = -i(\delta t)^{1/2}(GW + WH) - \delta t W, \tag{A.4}$$

as this captures all the finite contributions to averages calculated later on. This process samples the unitary group with the Haar measure. Furthermore, if W is itself from the Haar measure the process is stationary.

Our reference point is the well-known Brownian motion for the eigenvalues λ_n of W itself [7], which results in the standard CUE joint probability distribution. In perturbation theory (second order in $(\delta t)^{1/2}$ so that we stay accurate in $O(\delta t)$), the eigenvalues change as

$$\delta\lambda_n = \langle n|\delta W|n\rangle + \sum_{m\neq n} \frac{\langle n|\delta W|m\rangle\langle m|\delta W|n\rangle}{\lambda_n - \lambda_m}. \tag{A.5}$$

On average, with the help of the formulas above we then have

$$\overline{\delta\lambda_n} = -\delta t \left(\lambda_n + \frac{2}{N}\sum_{m\neq n}\frac{\lambda_n\lambda_m}{\lambda_n-\lambda_m}\right). \tag{A.6}$$

Furthermore, we obtain the correlator

$$\overline{\delta\lambda_n\delta\lambda_m} = -\delta t\frac{2}{N}\lambda_n^2\delta_{nm}. \tag{A.7}$$

We now introduce these averages as drift and diffusion terms into a Fokker-Planck equation, which tells us how the eigenvalue distribution changes,

$$\frac{\partial}{\partial t}P = -\sum_n \frac{\partial}{\partial\lambda_n}\left(\frac{\overline{\delta\lambda_n}}{\delta t} - \frac{1}{2}\frac{\partial}{\partial\lambda_n}\frac{\overline{(\delta\lambda_n)^2}}{\delta t}\right)P. \tag{A.8}$$

In the stationary situation, where W is from the CUE Haar measure, the probability distribution must be stationary, too, meaning that the right-hand side must vanish. This is indeed fulfilled, term by term, for the CUE probability distribution

$$P(\{\lambda_n\}) \propto \prod_{n<m}|\lambda_n-\lambda_m|^2\sum_k\lambda_k^{-1}. \tag{A.9}$$

(Note that $\lambda_k^{-1}d\lambda_k \propto d\varphi_k$ so that this transforms to the standard eigenphase distribution $P(\{\varphi_n\}) \propto \prod_{n<m}|e^{i\varphi_n}-e^{i\varphi_m}|^2$.)

Now we compare this to the eigenvalue distribution of the matrix A^2 related to the CSE, as defined in Eq. (3.20). We will denote the eigenvalues of $A = iW^T JW$ itself as μ_n, and those of A^2 as $\lambda_n = \mu_n^2$. A key point is that for any eigenstate $|n\rangle$,

$$A|n\rangle = \mu_n|n\rangle, \tag{A.10}$$

there is a partner state $|\bar{n}\rangle$, obtained by taking the complex conjugate of all components, which has the opposite eigenvalue,

$$A|\bar{n}\rangle = -\mu_n|\bar{n}\rangle. \tag{A.11}$$

For A^2, this implies that $\lambda_n = \lambda_{\bar{n}}$, and so all these eigenvalues are doubly degenerate. We also have to take this degeneracy into account in the Brownian motion, which we first formulate for the eigenvalues μ_n. For instance, in the second-order term, we find contributions such as $\langle n|AH|m\rangle\langle m|AH|n\rangle = \mu_n\mu_m/N$ and $\langle n|AH|m\rangle\langle m|H^*A|n\rangle = \mu_n^2\delta_{m\bar{n}}/N$, where the latter cancels the former for $m = \bar{n}$. Furthermore, we can combine the contributions of the remaining pairs $m, \bar{m} \neq n$, and hence only sum over one representative in each pair [we write this as a sum over the pairs $(m, \bar{m})$]. Carrying this out in detail gives

$$\overline{\delta\mu_n} = -\delta t \left(2(1-1/N)\mu_n + \frac{8}{N} \sum_{\substack{(m,\bar{m}) \\ \neq(n,\bar{n})}} \frac{\mu_n\mu_m^2}{\mu_n^2 - \mu_m^2} \right), \tag{A.12}$$

$$\overline{\delta\mu_n\delta\mu_m} = -\delta t \frac{4}{N}\mu_n\mu_m(\delta_{nm} + \delta_{\bar{n}m}). \tag{A.13}$$

Next, we transform this to the corresponding expression of the squared eigenvalues

(carefully expanding into second order using Ito calculus),

$$\overline{\delta\lambda_n} = 2\overline{\delta\mu_n}\mu_n + \overline{(\delta\mu_n)^2} \tag{A.14}$$

$$= -4\delta t\left(\lambda_n + \frac{2}{N/2}\sum_{m\neq n}\frac{\lambda_n\lambda_m}{\lambda_n-\lambda_m}\right), \tag{A.15}$$

$$\overline{\delta\lambda_n\delta\lambda_m} = 4\mu_n\mu_m\overline{\delta\mu_n\delta\mu_m} \tag{A.16}$$

$$= -4\delta t\frac{2}{N/2}\lambda_n^2\delta_{nm}, \tag{A.17}$$

with indices confined to run over distinct eigenvalues only. We interpret this as the drift and diffusion coefficients in a Brownian motion of $N/2$ numbers, each standing for a pair of eigenvalues, whose joint distribution is again found from the stationarity condition of the corresponding Fokker-Planck equation. But up to an overall factor of 4, the drift and diffusion terms are just the same as in the CUE with $N \to N/2$, and this overall factor drops out of the stationarity condition. Therefore, for U in the CSE, the joint probability distribution of the distinct eigenvalues λ_n of V coincides with that of CUE matrices with dimension $N/2$. In the main text, we apply this result to the case where V is a 4×4 matrix.

Appendix B

Mean density of states

In Chapter 4, we give the derivation of the scaling mean density of states. In order to obtain the mean density of eigenvalues $\lambda_l \equiv \exp(i\phi_l)$ of the unitary time-evolution operator U in the other processes, we follow a similar argument: first expressing it in terms of the moments $A_n = N^{-1}\overline{\mathrm{tr}\, U^n}$, and then applying Eq. (4.6). Recall that in the scaling theory, $A_n = a^n$ follows directly by expanding Eq. (4.5) into a geometric series, and using the CUE average $\overline{V^m} = \delta_{0m}\mathbb{1}$. Summation of the series (4.6) then delivers the scaling mean density of states (4.8).

We now treat the other scenarios. In the Cauchy process, we can apply the same expansion to the generator (4.21) so that the moments update as $A_n \to (1-dt)^{n/2}A_n$ over each time step. In the continuum limit $dt \to 0$, we then obtain $A_n = \exp(-nt/2) \equiv a^n(t)$, where the scaling parameter $a(t) = \exp(-t/2)$ now explicitly depends on time. In terms of this parameter, the mean density of states then takes the same analytical form (4.8) as in the scaling theory itself, while as a function of time, it can be written as

$$\rho(\phi) = \frac{1}{2\pi}\frac{\sinh t/2}{(\cosh t/2 - \cos\phi)}. \tag{B.1}$$

This matches numerical sampling at various times in the evolution, as shown in Fig. B.1.

In Dyson's Brownian motion (DBM), we perform the Gaussian averages in the generator (2.13) in the large-N limit to obtain the recursive differential equations $dA_n/dt = -(n/2)A_n - \sum_{l=1}^{n-1}(n/2)A_lA_{n-l}$, which are initialised by $A_1(t) \equiv a(t) = \exp(-t/2)$ and $A_n(0) = 1$. The explicit time dependence of the moments then follows

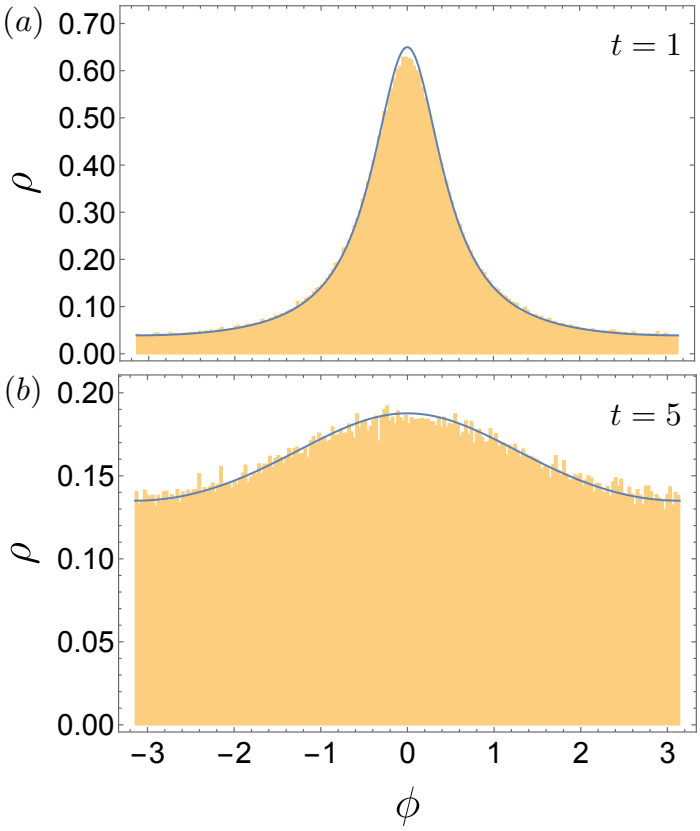

Figure B.1: Comparison of the analytical density of states (B.1) for the Cauchy process (curves) and data from numerical sampling the process (histograms) at (*a*) $t = 1$, and (*b*) $t = 5$. Data generated over 10^4 realisations for matrix dimension $N = 32$.

as

$$\begin{aligned} A_n &= \exp(-nt/2) \sum_{m=0}^{n-1} \frac{(n-1)!}{m!(m+1)!(n-1-m)!} (-tn)^m \\ &= \exp(-nt/2)\, {}_1F_1(1-n, 2, nt), \end{aligned} \tag{B.2}$$

with a hypergeometric function ${}_1F_1$. As illustrated in Fig. B.2, for intermediate times the series (4.6) converges numerically to a shape that resembles the Wigner semicircle, while for later times it describes the flattening out to a uniform distribution. The figure also illustrates that in all cases, the derived mean density of states conforms well to the empirical distribution obtained by random sampling of the ensembles.

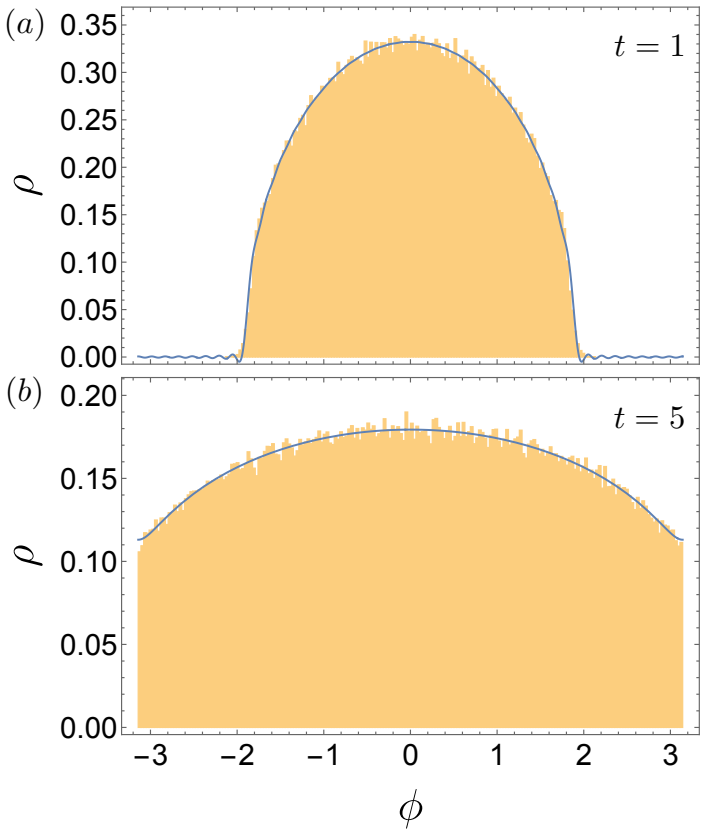

Figure B.2: Analogous to Fig. B.1, but for the Dyson Brownian motion process, where the analytical density of states is obtained by substituting the coefficients Eq. (B.2) into Eq. (4.6).

Appendix C

Unfolding procedures

Our unfolding procedures in Chapter 4 are based on the direct algebraic relation of the Poisson kernel (4.5) to the CUE [284], in which the eigenvalues are distributed uniformly on the unit circle.

1. For any pair of unitary matrices U, V related by $U = (a\mathbb{1} + V)/(\mathbb{1} + aV)$, the eigenvalues $\mu_l = \exp(i\psi_l)$ of V determine the eigenvalues

$$\lambda_l = (a + \mu_l)/(1 + a\mu_l) = \exp(i\phi_l) \tag{C.1}$$

   of U. This is given as Eq. (4.10) in the main text.

2. If the eigenvalues μ_l are obtained from matrices V of the CUE, then λ_l are eigenvalues distributed as in the Poisson kernel, with the scaling mean density of states (4.8).

3. This transformation can be inverted to translate eigenvalues λ_l distributed with the scaling mean density of states (4.8) into uniformly distributed eigenvalues

$$\mu_l = (a - \lambda_l)/(a\lambda_l - 1), \tag{C.2}$$

   which is given in the main text as Eq. (4.11).

We can utilise these relations directly to unfold the eigenvalues in the Poisson kernel into a uniform density of states, by applying the transformation (C.2) individually to all

eigenvalues. Furthermore, as the density of states (B.1) in the Cauchy process coincides with the scaling density of states (4.8) of the Poisson kernel with $a(t) = \exp(-t/2)$, we can unfold the spectra from this process by the same transformation (C.2). Finally, no unfolding is required to compare the original spectral statistics in these two cases for a given value of a. As shown in the main text, despite this agreement of the mean density of states, the spectral fluctuations captured by the instantaneous spectral form factor (SFF) K_n differ between these ensembles, both before and after unfolding.

In the DBM process, we utilise the integrated density of states

$$\psi_l = \int_{min\{\phi\}}^{\phi_l} \rho(\phi)\, d\phi \tag{C.3}$$

to unfold the eigenphases at each incremental step in the generated dynamics to a uniform distribution. We then apply the transformation (C.1) to unfold these eigenvalues to the scaling density of states (4.8). As shown in the main text for this process, the spectral fluctuations captured by the SFF then agree with the scaling predictions (4.19).

Appendix D

Unitarily invariant processes

In this final appendix for Chapter 4, we derive the exponential decay laws

$$a(t) = \exp(-\gamma_0 t), \tag{D.1}$$

$$K_1(t) = (N^2 - 1)\exp(-\gamma_1 t) + 1, \tag{D.2}$$

of the scaling parameter and first-order SFF in unitarily invariant processes, along with their respective decay rates (4.20) and (4.2). These expressions hold for any process in which the ensemble of stochastic generators $u(t; dt)$ are invariant under the replacement $u(t; dt) \to W^\dagger u(t; dt)W$ with an arbitrary fixed matrix W. The decay laws can then be derived by performing an auxiliary average over a suitable matrix ensemble of W, for which we choose the CUE.

We start by considering the evolution of the scaling parameter over one incremental time step,

$$a(t + dt) = N^{-1}\overline{\operatorname{tr} U(t + dt)} = N^{-1}\overline{\operatorname{tr} u(t; dt)U(t)} \tag{D.3}$$

$$= N^{-1}\overline{\operatorname{tr} W^\dagger u(t; dt)WU(t)}, \tag{D.4}$$

where the last line invokes the stated invariance condition. We next introduce the diagonalised forms $U(t) = XDX^\dagger$, $u(t; dt) = xdx^\dagger$, where D and d contain the eigenvalues of these matrices, while X and x are unitary matrices formed by the

corresponding eigenvectors. This gives

$$a(t+dt) = N^{-1}\overline{\operatorname{tr} w^\dagger dw D} = N^{-1}\overline{\sum_{lm} |w_{lm}|^2 d_l D_m} \tag{D.5}$$

with the combined unitary matrix $w = x^\dagger W X$, which inherits the CUE distribution from W. The auxiliary average over this matrix then follows from a well-known geometric argument, which we recapitulate here for completeness. As w is a unitary matrix of dimension N, its columns (or rows) form an orthonormal basis in $\mathbb{C}^N$ so that by normalisation and permutation symmetry of the basis indices

$$\sum_l |w_{lm}|^2 = 1 \to \overline{\sum_l |w_{lm}|^2} = 1 \to \overline{|w_{lm}|^2} = 1/N. \tag{D.6}$$

As a result,

$$a(t+dt) = N^{-2}\overline{\sum_{lm} d_l D_m} = N^{-1}\overline{\operatorname{tr} u(t;dt)}\, a(t) \tag{D.7}$$

factorises, corresponding to an incremental change

$$da(t) = \frac{\overline{\operatorname{tr} u(t;dt)} - N}{N}\, a(t). \tag{D.8}$$

For $dt \to 0$, this yields the universal exponential decay law (D.1), where the decay constant

$$\gamma_0 = \lim_{dt\to 0} (dt\, N)^{-1} (N - \overline{\operatorname{tr} u(t;dt)}), \tag{D.9}$$

recovers Eq. (4.20).

Analogously, we can write the increment of the form factor as

$$\begin{aligned} K_1(t+dt) =& \overline{|\operatorname{tr} u(t;dt) U(t)|^2} = \overline{|\operatorname{tr} w^\dagger\, d\, w D|^2} \\ =& \sum_{l,m,s,p} \overline{d_l D_m D_p^* d_s^* |w_{lm}|^2\, |w_{sp}|^2}. \end{aligned} \tag{D.10}$$

In the auxiliary average over w, we then split terms according to the index combinations

$$\begin{aligned}\overline{|w_{lm}|^4} &= \frac{2}{N(N+1)},\\ \overline{|w_{lm}|^2|w_{lp}|^2} = \overline{|w_{ml}|^2|w_{pl}|^2} &= \frac{1}{N(N+1)} \quad (m \neq p),\\ \overline{|w_{lm}|^2|w_{sp}|^2} &= \frac{1}{N^2-1} \quad (l \neq s, m \neq p).\end{aligned} \tag{D.11}$$

This sums up to

$$\begin{aligned}K_1(t+dt) &= \frac{\overline{|\operatorname{tr} u|^2}\operatorname{tr} U^\dagger U + \overline{\operatorname{tr} u^\dagger u}\,|\operatorname{tr} U|^2}{N(N+1)} + \frac{(\overline{\operatorname{tr} u^\dagger u} - \overline{|\operatorname{tr} u|^2})(\operatorname{tr} U^\dagger U - |\operatorname{tr} U|^2)}{N^2-1}\\ &= K_1(t) + \frac{N^2 - \overline{|\operatorname{tr} u(t;dt)|^2}}{N^2-1}(1-K_1(t)),\end{aligned} \tag{D.12}$$

where we momentarily suppressed the time arguments of $u(t;dt)$ and $U(t)$, and then used the unitarity of these matrices. This recovers Eq. (4.1) in the main text, and in the continuum limit $dt \to 0$ results in the exponential decay law (D.2), where the constant

$$\gamma_1 = \lim_{dt\to 0} dt^{-1}(N^2 - \overline{|\operatorname{tr} u(t;dt)|^2})/(N^2-1) \tag{D.13}$$

is in agreement with Eq. (4.2).

D.0.1 Application to Dyson's Brownian motion

In the DBM process, the generators (2.13) are expressed in terms of Hamiltonians H from the Gaussian Unitary Ensemble (GUE), satisfying

$$\overline{H_{lm}} = 0, \quad \overline{H_{kl}H_{mn}} = N^{-1}\delta_{kn}\delta_{lm}, \tag{D.14}$$

implying $\overline{H^2} = \mathbb{1}$. For the determination of the rates γ_0 and γ_1 in the continuum limit, we can expand the generator as

$$u(t;dt) = \mathbb{1} - i\sqrt{dt}H - dtH^2/2, \tag{D.15}$$

upon which

$$\overline{\operatorname{tr} u(t;dt)} = N(1 - dt/2), \tag{D.16}$$

$$\overline{|\operatorname{tr} u(t;dt)|^2} = N^2 - (N^2 - 1)dt. \tag{D.17}$$

Equations (4.20) and (4.2) in the main text (replicated above as Eqs. (D.9) and (D.13)) then deliver the decay rates

$$\gamma_0 = 1/2, \quad \gamma_1 = 1. \tag{D.18}$$

For completeness, we verify these decays by explicitly averaging in the ensemble, without using the unitary invariance. For the scaling parameter, we obtain

$$\begin{aligned} a(t + dt) &= a(t) - i\sqrt{dt}N^{-1}\overline{\operatorname{tr} HU(t)} - \frac{dt}{2}a(t) \\ &= (1 - dt/2)a(t), \end{aligned} \tag{D.19}$$

such that incrementally,

$$\frac{da}{dt} = -\frac{1}{2}a(t). \tag{D.20}$$

From the initial condition $a(0) = 1$, we then recover the exponential decay $a(t) = e^{-t/2}$ with decay constant $\gamma_0 = 1/2$.

For the first-order SFF, we arrive at

$$\begin{aligned} K_1(t + dt) &= K_1(t) + dt\,\overline{\operatorname{tr} HU^\dagger(t) \operatorname{tr} HU(t)} - \frac{dt}{2}(\overline{\operatorname{tr} H^2U^\dagger(t) \operatorname{tr} U(t)} + \overline{\operatorname{tr} U^\dagger(t) \operatorname{tr} U(t)H^2}) \\ &= K_1(t) + N^{-1}dt\,\overline{\operatorname{tr} U(t)U^\dagger(t)} - dtK_1(t) \\ &= K_1(t) + (1 - K_1(t))dt. \end{aligned} \tag{D.21}$$

Therefore, incrementally,

$$\frac{d}{dt}K_1(t) = 1 - K_1(t), \tag{D.22}$$

which for the initial condition $K_1(0) = \overline{|\operatorname{tr} \mathbb{1}|^2} = N^2$ is indeed solved by an exponential decay

$$K_1(t) = (N^2 - 1)e^{-t} + 1, \tag{D.23}$$

with decay constant $\gamma_1 = 1$.

D.0.2 Application to the Cauchy process

In the Cauchy process, we can exploit the correspondence between the generators (4.21) and the Poisson kernel (4.5) when $a = \sqrt{1-dt}$, now taken with $dt \to 0$ to obtain matrices close to the identity that then are composed multiplicatively. Transferring Eq. (4.7) to the setting of these generators, we find

$$\overline{u(t;dt)} = \sqrt{1-dt}\mathbb{1}. \tag{D.24}$$

Equation (4.20) then determines the decay constant $\gamma_0 = 1/2$, which matches with the decay rate in the DBM.

The determination of the decay rate γ_1 for the first-order SFF $K_1(t)$ is considerably more involved. We start by expanding

$$u(t;dt) = \frac{\beta\mathbb{1}+V}{\beta V+\mathbb{1}} = (\beta\mathbb{1}+V)\sum_{n=0}^{\infty}(-\beta V)^n \tag{D.25}$$

with $\beta = \sqrt{1-dt}$ so that

$$\begin{aligned}\overline{|\operatorname{tr} u(t;dt)|^2} = &\underbrace{\overline{\operatorname{tr}\left(\beta\mathbb{1}\sum_{n=0}^{\infty}(-\beta V)^n\right)\operatorname{tr}\left(\beta\mathbb{1}\sum_{m=0}^{\infty}(-\beta V^\dagger)^m\right)}}_{A}\\
&+\underbrace{\overline{\operatorname{tr}\left(\beta\mathbb{1}\sum_{n=0}^{\infty}(-\beta V)^n\right)\operatorname{tr}\left(V^\dagger\sum_{m=0}^{\infty}(-\beta V^\dagger)^m\right)}}_{B}\\
&+\underbrace{\overline{\operatorname{tr}\left(V\sum_{n=0}^{\infty}(-\beta V)^n\right)\operatorname{tr}\left(\beta\mathbb{1}\sum_{m=0}^{\infty}(-\beta V^\dagger)^m\right)}}_{C}\\
&+\underbrace{\overline{\operatorname{tr}\left(V\sum_{n=0}^{\infty}(-\beta V)^n\right)\operatorname{tr}\left(V^\dagger\sum_{m=0}^{\infty}(-\beta V^\dagger)^m\right)}}_{D}\end{aligned} \tag{D.26}$$

breaks up into four structurally similar terms. In each of these terms, only combinations of V and $V^\dagger$ raised to the same power make finite contributions to the average, where,

for instance,

$$A = \beta^2 \sum_{n=0}^{\infty} (-\beta)^{2n} \overline{|\operatorname{tr} V^n|^2} \equiv \sum_{n=0}^{\infty} \beta^{2n+2}\, k_n. \tag{D.27}$$

Here,

$$k_n = \overline{|\operatorname{tr} V^n|^2} = \begin{cases} N^2 \delta_{n,0} + n & \text{for } 0 \leq n \leq N \\ N & \text{for } n > N \end{cases} \tag{D.28}$$

is the form factor in the CUE. Analogously, we find

$$B = C = -\sum_{n=0}^{\infty} \beta^{2n+2}\, k_{n+1}, \tag{D.29}$$

$$D = \sum_{n=0}^{\infty} \beta^{2n}\, k_{n+1}. \tag{D.30}$$

Combining these results, we have

$$\overline{|\operatorname{tr} u(t;dt)|^2} = \sum_{n=0}^{\infty} \beta^{2n} \left(\beta^2\, k_n - 2\beta^2\, k_{n+1} + k_{n+1}\right). \tag{D.31}$$

With the CUE form factors (D.28), we then obtain

$$\begin{aligned} \overline{|\operatorname{tr} u(t;dt)|^2} &= 1 - \beta^{2N} + N^2\beta^2 \\ &= 1 + N^2(1-dt) - (1-dt)^N, \end{aligned} \tag{D.32}$$

where we reinstated the definition $\beta = \sqrt{1-dt}$ in the final line. The decay rate $\gamma_1 = N/(N+1)$ follows from Eq. (4.2) by expanding this result for small dt.

In the Cauchy process, the first-order SFF therefore decays more slowly than in maximally efficient scrambling dynamics. In Fig. 4.4 of the main text, we extend this analysis to the higher-order SFFs and quantify this in terms of deviations from the scaling bounds.

Appendix E

Second-order instantaneous SFF in GOE and GSE DBM

In DBM generated by the GOE or GSE, the number of correlators at each level of the hierarchy proliferates rapidly due to the additional terms in the averaging rules (5.31) and (5.32). To illustrate the complexity, but eventual feasibility, of the calculations, we here work through the construction of the second level of the hierarchy in the GOE, in a similar fashion to the first level in Section 5.4.1 of the main text.

For reference, let us summarise the first level of the hierarchy in the GOE concisely as

$$a \equiv K_1(t) = \mathcal{K}_{1,1}(t) = \overline{\operatorname{tr} U(t) \operatorname{tr} U^\dagger(t)}, \tag{E.1}$$

$$b \equiv L(t) = \overline{\operatorname{tr}\, [U(t)U^*(t)]}, \tag{E.2}$$

such that Eqs. (5.36) reduce to

$$\begin{aligned} \dot{a} &= \kappa\, (\nu\, (N + b) - a)\,, \\ \dot{b} &= \kappa\, (\nu\, (a + N) - b)\,. \end{aligned} \tag{E.3}$$

Here the time dependency of a and b is implied, and we have introduced $\nu = (N+1)^{-1}$

for brevity. The initial conditions $a(0) = N^2$, $b(0) = N$, then determine the solutions

$$a = 1 + \frac{N-1}{2}\left(N + 2 + Ne^{-2\nu\kappa t}\right)e^{-N\nu\kappa t}, \tag{E.4}$$

$$b = 1 + \frac{N-1}{2}\left(N + 2 - Ne^{-2\nu\kappa t}\right)e^{-N\nu\kappa t}. \tag{E.5}$$

For the second level, we anchor the hierarchy again at the instantaneous SFF, now denoted by

$$c \equiv K_2(t) = \mathcal{K}_{2,2}(t). \tag{E.6}$$

Using the GOE averaging rules, this quantity evolves as

$$\dot{K}_2 = \kappa\left(-2\underbrace{K_2(t)}_{=c} - 2(N+1)^{-1}\left(\underbrace{\mathcal{K}_{11,2}(t)}_{=d} + \underbrace{\overline{\mathrm{tr}\,[U(t)U^T(t)]\,\mathrm{tr}\,[U^\dagger(t)]^2}}_{=e}\right) + 4(N+1)^{-1}\left(N + \underbrace{\overline{\mathrm{tr}\;[U(t)U(t)U^*(t)U^*(t)]}}_{=f}\right)\right), \tag{E.7}$$

or more compactly

$$\dot{c} = \kappa\left(-2\,c - 2\nu\,(d+e) + 4\,\nu\;(N+f)\right), \tag{E.8}$$

where we also encounter

$$d \equiv \mathcal{K}_{11,2}(t) = \overline{\mathrm{tr}\,U(t)\,\mathrm{tr}\,U(t)\,\mathrm{tr}\,[U^\dagger(t)]^2} = \overline{\mathrm{tr}\,[U(t)]^2\,\mathrm{tr}\,U^\dagger(t)\,\mathrm{tr}\,U^\dagger(t)} = \mathcal{K}_{2,11}(t) \tag{E.9}$$

$$e \equiv \overline{\mathrm{tr}\,[U(t)]^2\,\mathrm{tr}\,[U^\dagger(t)U^*(t)]} = \overline{\mathrm{tr}\;[U(t)U^T(t)]\;\mathrm{tr}\,[U^\dagger(t)]^2} \tag{E.10}$$

$$f \equiv \overline{\mathrm{tr}\,[U(t)]^2[U^*(t)]^2}. \tag{E.11}$$

In these equations, we used the invariance of $U \to U^\dagger$ or U^* to equate equivalent terms.

Treating the above quantities in a similar fashion to a, b, and c, we find that we

also have to include the correlators

$$g = \overline{\operatorname{tr} U(t) \operatorname{tr} U(t) \operatorname{tr} U^\dagger(t) \operatorname{tr} U^\dagger(t)}, \tag{E.12}$$

$$h = \overline{\operatorname{tr} U(t) \operatorname{tr} U(t) \operatorname{tr} \left[U^\dagger(t) U^*(t)\right]}, \tag{E.13}$$

$$i = \overline{\operatorname{tr} U(t) \operatorname{tr} \left[U(t) U^*(t) U^*(t)\right]}, \tag{E.14}$$

$$j = \overline{\operatorname{tr} \left[U(t) U^T(t)\right] \operatorname{tr} \left[U^\dagger(t) U^*(t)\right]}, \tag{E.15}$$

$$l = \overline{\operatorname{tr} \left[U(t) U^*(t)\right] \operatorname{tr} \left[U(t) U^*(t)\right]}, \tag{E.16}$$

$$m = \overline{\operatorname{tr} U(t) \operatorname{tr} U^\dagger(t) \operatorname{tr} \left[U(t) U^*(t)\right]}, \tag{E.17}$$

$$n = \overline{\operatorname{tr} \left[U(t) U^*(t) U(t) U^*(t)\right]}, \tag{E.18}$$

$$o = \overline{\operatorname{tr} \left[U(t) U^T(t) U^\dagger(t) U^*(t)\right]}. \tag{E.19}$$

Working through the construction for all these quantities, we arrive at the system of linear differential equations

$$\dot{a} = \kappa \left(\nu \left(N + b\right) - a\right), \tag{E.20}$$

$$\dot{b} = \kappa \left(\nu \left(a + N\right) - b\right), \tag{E.21}$$

$$\dot{c} = \kappa \left(\nu \left(-2(d + e) + 4(N + f)\right) - 2c\right), \tag{E.22}$$

$$\dot{d} = \kappa \left(\nu \left(-c - e - g - h + 4(a + i)\right) - 2d\right), \tag{E.23}$$

$$\dot{e} = \kappa \left(\nu \left(8b - h - j\right) - 3e\right), \tag{E.24}$$

$$\dot{f} = \kappa \left(\nu \left(c + l + 2N\right) - 2f\right), \tag{E.25}$$

$$\dot{g} = \kappa \left(\nu \left(-2(d + h) + 4(Na + m)\right) - 2g\right), \tag{E.26}$$

$$\dot{h} = \kappa \left(\nu \left(8a - e - j\right) - 3h\right), \tag{E.27}$$

$$\dot{i} = \kappa \left(\nu \left(a + b + d + n\right) - 2i\right), \tag{E.28}$$

$$\dot{j} = \kappa \left(8N\nu - 4j\right) \qquad \text{(closes)}, \tag{E.29}$$

$$\dot{l} = \kappa \left(\nu(2f + 2m - 2n - 2o + 2N(b + 1)) - 2l\right), \tag{E.30}$$

$$\dot{m} = \kappa \left(\nu(g + l + N(a + b)) - 2m\right), \tag{E.31}$$

$$\dot{n} = \kappa \left(\nu(-2l - 2o + 4(i + b)) - 2n\right), \tag{E.32}$$

$$\dot{o} = \kappa \left(\nu(-j - o + 4(a + b)) - 3o\right) \qquad \text{(closes indirectly)}. \tag{E.33}$$

These are then solved with their initial values corresponding to the initial condition

$U(t = 0) = \mathbb{1}$. This gives, from the expressions for c and d, the second-order instantaneous form factor

$$\begin{aligned} K_2(t) = 2 &+ \frac{1}{6}(N-3)N(N+1)(N+2)\cosh(4\nu\kappa t)\, e^{-2\kappa t} \\ &+ (N-1)\left((N+2)e^{-\nu\kappa t} - Ne^{\nu\kappa t}\right) e^{-3\kappa t} + e^{-4\kappa t} \\ &- \frac{1}{12}(N-1)\left[\left(N^3+7N^2-12N-24\right) e^{2\nu\kappa t}\right. \\ &\qquad \left. + \left(N^3-5N^2-12N+12\right) e^{-2\nu\kappa t}\right] e^{-2\kappa t}, \end{aligned} \tag{E.34}$$

and the correlator

$$\begin{aligned} \mathcal{K}_{11,2}(t) = &- \frac{1}{6}(N-3)N(N+1)(N+2)\sinh(4\nu\kappa t)e^{-2\kappa t} \\ &+ (N-1)(N+2)e^{-(3+\nu)\kappa t} + e^{-4\kappa t} \\ &+ \frac{1}{12}(N-1)\left[(N-2)\left(N^2+9N+6\right) e^{-2\nu\kappa t} - N\left(N^2-5N-12\right) e^{2\nu\kappa t}\right] e^{-2\kappa t} \end{aligned} \tag{E.35}$$

that appears in the expression (5.68) for the ensemble-averaged OTOC.

We note that the long-time asymptotics of these expressions still agree with the CUE. Furthermore, results for the GSE follow from the replacement rules given in Section 5.4.

Appendix F

Results from the theory of orthogonal polynomials

We report here the exact results for the instantaneous spectral statistics and the truncated two-point correlation for Brownian motion over the $U(N)$ group as defined by Eqs. (2.10) and (2.12). The most recent results have been obtained from the theory of orthogonal polynomials, in Ref. [126]. It is worth noting that the earliest results on Brownian motion over the unitary group focused on the distributions of the group elements [218–220], while the seminal work from Dyson [7] addresses the Brownian motion of the eigenvalues, which is of interest here.

Consider the Brownian motion defined by Eqs. (2.10) and (2.12) in an N-dimensional Hilbert space. For a unitary matrix $U(t)$ at generic time t, with eigenvalues $\{e^{ix_m(t)}\}_{j=1}^{N}$, $-\pi < x_m(t) \leq \pi$, let us define the eigenvalue density $\rho_{(1),N}(x;t)$, the two-point correlation function $\rho_{2,(N)}(x,y;t)$ and the truncated two-point correlation function

$\rho^T_{2,(N)}(x,y;t)$ as

$$\begin{aligned}
\rho_{(1),N}(x;t) &\equiv \overline{\sum_{m=1}^{N}\delta(x-x_m(t))}, \\
\rho_{2,(N)}(x,y;t) &\equiv \overline{\sum_{m\neq n=1}^{N}\delta(x-x_m(t))\delta(y-x_n(t))}, \\
\rho^T_{2,(N)}(x,y;t) &\equiv \rho_{2,(N)}(x,y;t)-\rho_{(1),N}(x;t)\rho_{(1),N}(t;t).
\end{aligned} \tag{F.1}$$

The averages of the unitary evolution are related to the Fourier components of the spectral density and the spectral two-point function. Specifically, introducing the moments of the eigenvalues as [126]

$$m_k^{(N)}(t) \equiv \frac{1}{N}\int_{-\pi}^{\pi}\rho_{(1),N}(x;t)e^{-ikx}dx, \tag{F.2}$$

one has

$$\overline{\mathrm{tr}\,[U(t)]^k} = Nm_k^{(N)}(t). \tag{F.3}$$

Analogously, the instantaneous spectral form factor $K_n(t)$ introduced in Eq. (2.39) is related to the Fourier transform of the two-point spectral function via

$$K_k(t) = S_N(k;t) + N^2|m_k^{(N)}(t)|^2, \tag{F.4}$$

where

$$S_N(k;t) \equiv N + \int_{-\pi}^{\pi}dx\int_{-\pi}^{\pi}dy e^{ik(x-y)}\rho^T_{(2),N}(x,y;t). \tag{F.5}$$

Therefore, the SFF $K_n(t)$ is determined by the connected part $S_N(k;t)$ of the SFF and the spectral density moments $m_k^{(N)}(t)$; see also Eq. (5.73).

Exact results for the spectral density moments have been obtained in [274, 275], and recently reproduced using the cyclic Pòlya ensemble structure [126]. They can be expressed as

$$m_k^{(N)}(t) = q^{k(N+k-1)}{}_2F_1(1-N,1-k;2;1-q^{-2k}), \tag{F.6}$$

where $q = e^{-t/2N}$ and ${}_2F_1(a,b;c;z)$ is the Gaussian hypergeometric function. The exact

result for the truncated SFF obtained in Ref. [126] reads

$$S_N(k;t) = \min(N,k) - q^{2k^2+2k(N-1)} \sum_{j=0}^{k-1}\sum_{l=0}^{k-1} q^{-2k(j+l)}(-1)^{j+l} \times \frac{\Gamma(N+k-j)\Gamma(N+k-l)}{\Gamma(N-j)\Gamma(N+j)\Gamma(l+1)\Gamma(N-l)\Gamma(k-j)\Gamma(k-l)\Gamma(j+l-N-k+1)^2}, \tag{F.7}$$

which also admits the equivalent integral form

$$S_N(k;t) = \min(k,N) - q^{2k^2+2k(N-1)}(kN)^2 \times \int_0^\infty s\, e^{-s(N+k-1)} \left({}_2F_1(1-N,1-k;-(k-1+N);q^{-2k}e^s)\right)^2 ds. \tag{F.8}$$

The latter expression can be used to obtain the large-N asymptotic expansion for the connected part of the SFF at fixed k, which gives

$$\lim_{N\to\infty} S_N(k;t) = k - e^{-tk}\int_0^\infty s e^{-s}\left(L_{k-1}^{(1)}(kt+s)\right)^2 ds, \tag{F.9}$$

where $L_s^{(a)}(z)$ are the Laguerre polynomials. Analogously, one can establish the large-N expansion of the moments $m_k^{(N)} = A_n/N$, whose leading order follows from Eq. (5.23). Carried out to order $O(N^0)$, these expansions combine to agree with the asymptotics for the SFF obtained from the hierarchy equations, as given in Eq. (5.27). Note that the hierarchy equations also yield exact and asymptotic expansions for the additional correlations $\mathcal{K}_{pq\ldots,rs\ldots}(t)$ defined in Eq. (5.47).

Appendix G

Stationary solutions in the unitary hierarchy

As discussed in Chapter 5, the instantaneous SFF converges in the long-time limit, in all three symmetry classes, to the RMT prediction (2.38) for an ergodic system with unitary invariance, where the unitary time-evolution operators $U(t)$ are taken from the CUE.

This agreement in the ergodic limit also extends to the long-time behaviour of the other quantities $\mathcal{K}_{\{\cdot\},\{\cdot\}}(t)$ appearing in the hierarchy, for which the CUE results have been established as well [123, 285, 286]. These results can be expressed compactly as

$$\overline{\prod_{j=1}^{k}\left(\text{tr }[U]^j\right)^{a_j}\left(\text{tr }[U^\dagger]^j\right)^{b_j}} = \delta_{ab}\prod_{j=1}^{k} j^{a_j} a_j!, \tag{G.1}$$

where $a = (a_1, ...a_k)$ and $b = (b_1, ...b_k)$ are two integer sequences, while the overline denotes the averaging of U in the CUE. These expressions are consistent with the stationary solutions of the spectral hierarchy, which is determined by setting all time derivatives to zero. In particular, we recover that only balanced quantities (5.10) of the form $\{\cdot\}_{\text{LHS}} = \{\cdot\}_{\text{RHS}}$ tend to non-zero stationary values. These values furthermore correspond to Eq. (G.1) when we identify a_j with the number of times an integer j appears in the index sequence $\{\cdot\}_{\text{LHS}}$.

This behaviour is further illustrated in Figure G.1, which depicts the analytical

solutions of all quantities in the unitary spectral hierarchy to level $n = 2$. These solutions are obtained Eqs. (5.14) paired with the initial conditions (5.15), and evaluated for $N = 16$. All balanced terms tend to integer values: the first- and second-order SFF $\mathcal{K}_{1,1}(t)$ and $\mathcal{K}_{2,2}(t)$, tend to 1 and 2, as already discussed above, while $\mathcal{K}_{11,11}(t)$ tends to 2, as dictated by Eq. (G.1). Both $\mathcal{K}_{11,2}(t)$ and $\mathcal{K}_{2,11}(t)$ are unbalanced in their indices, thus tend to zero, and coincide by way of symmetry, thus overlaid.

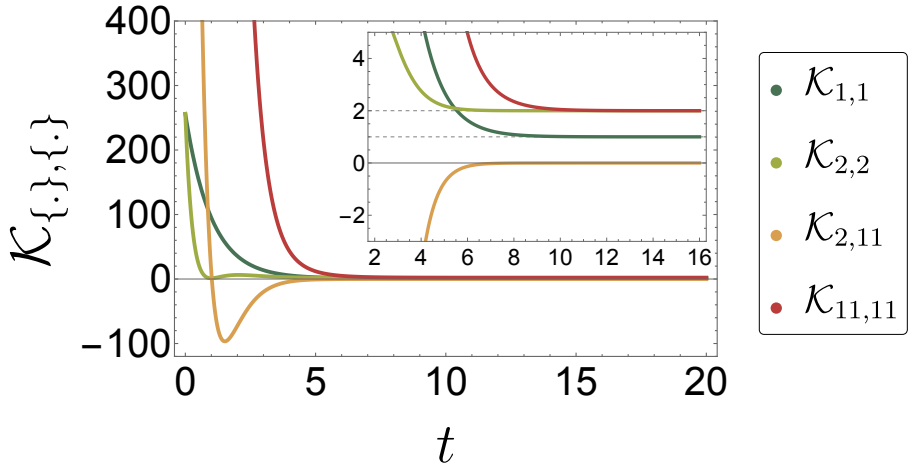

Figure G.1: Analytical solutions of all correlators appearing in unitary spectral hierarchy up to level $n = 2$, for system size $N = 16$. The SFF $\mathcal{K}_{n,n}(t)$ (light and dark greens) tends to n at longer times, as indicated by the grey dashed lines. The correlator $\mathcal{K}_{11,11}(t)$ (red) is the only other quantity at this level that tends to a non-zero stationary value, given by 2. The correlator $\mathcal{K}_{2,11}(t)$ (orange), and equivalently $\mathcal{K}_{11,2}(t)$, decays to 0. All these long-time asymptotics agree with the general CUE result (G.1).

Appendix H

Scaling theory of the OTOC

This appendix combines results from Chapters 4 and 5. Specifically, we evaluate the ensemble-averaged OTOC given by Eq. (5.68) in the spectral hierarchy presented in Chapter 5 for DBM generated by instantaneous Hamiltonians sampled from the GUE, here, in the scaling theory for maximally efficient quantum-dynamical scrambling developed in Chapter 4.

Chapter 4 derives the result (4.19) for the instantaneous SFF $K_n(t)$ in the scaling theory. At second-order, the DBM GUE spectral hierarchy includes one other unique correlator due to symmetry in the indices, namely Eq. (5.11) that we here reproduce

$$\mathcal{K}_{11,2}(t) = \overline{\operatorname{tr} U(t) \operatorname{tr} U(t) \left[\operatorname{tr} U^{\dagger}(t)\right]^2}. \tag{H.1}$$

As in the calculation of the SFF in the scaling theory presented in Section 4.3.3, we use the transformation (4.10) to express $\mathcal{K}_{11,2}$ within the scaling ensemble (4.5) as

$$\mathcal{K}_{11,2} = \left(\prod_r \int_0^{2\pi} \frac{d\psi_r}{2\pi}\right) \det(e^{i(p-q)\psi_q}) \times \sum_{lmn} \left(\frac{a + e^{i\psi_l}}{1 + ae^{i\psi_l}}\right) \left(\frac{a + e^{i\psi_m}}{1 + ae^{i\psi_m}}\right) \left(\frac{a + e^{-i\psi_n}}{1 + ae^{-i\psi_n}}\right)^2, \tag{H.2}$$

where the indices $q, p = 1, 2, ..., N$ label the rows and columns of the resulting determinant. Pulling the integrals over ψ_q into the qth rows of the matrix in the determinant, we can split the sum over the indices l, m, and n and treat the different scenarios. Each of the 'diagonal' cases $l = m = n$ contribute 1 to the sum, contributing

N overall. When $l = m \neq n$, Eq. (5.11) reduces to the form $\mathcal{K}_{2,2} - N$, that is, Eq. (4.16) when $n = 2$, where we must subtract N to account for the scenario $l = m = n$. Similarly, the cases $l \neq m = n$ and $l = n \neq m$ both reduce Eq. (5.11) to the form $\mathcal{K}_{1,1} - N$, that is, Eq. (4.16) when $n = 1$, again remembering to avoid double counting the case $l = m = n$. Finally, we must consider the case $l \neq n \neq m$, where in analogy to the SFF calculation, we must now consider a 3×3 matrix determinant. Thus, Eq. (H.2) reduces to the form

$$\mathcal{K}_{11,2} = \underbrace{\sum_{l=m=n} 1}_{=N} + \underbrace{\sum_{l=m\neq n} \cdot}_{=\mathcal{K}_{2,2}-N} + \underbrace{\sum_{l=n\neq m \text{ or } l\neq m=n} \cdot}_{=2(\mathcal{K}_{1,1}-N)} + \sum_{l\neq m\neq n} \cdot \quad , \tag{H.3}$$

where the last scenario corresponding to $l \neq m \neq n$ is the sum over matrix determinants of the form

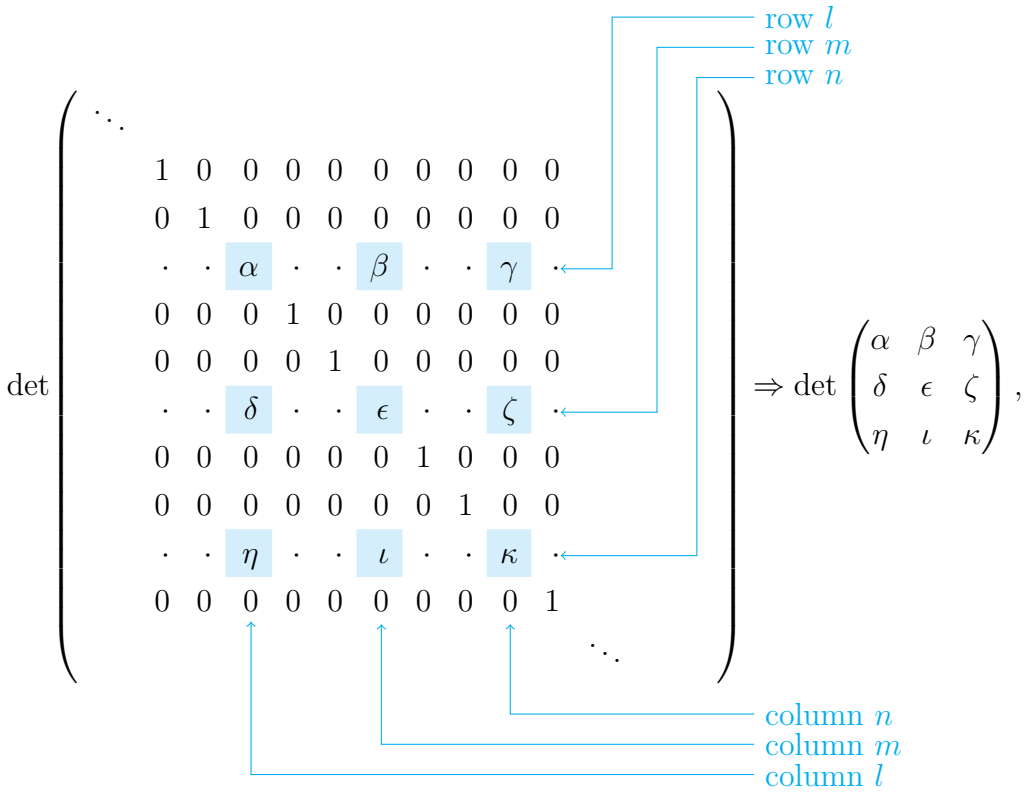

where $\cdot$ denotes some finite element that is in general non-zero. Explicitly, each 'off-diagonal' term in the sum $l \neq m \neq n$ has the form

$$\det \begin{pmatrix} a & (1-a^2)\,(-a)^{-l+m-1} & (1-a^2)\,(-a)^{-l+n-1} \\ (1-a^2)\,(-a)^{l-m-1} & a & (1-a^2)\,(-a)^{-m+n-1} \\ \{(a^2-1)\,(-a)^{-l+n-2} & \{(a^2-1)\,(-a)^{-m+n-2} & a^2 \\ \times[a^2(-l+n+1) & \times[a^2(-m+n+1) & \\ +l-n+1]\} & +m-n+1]\} & \end{pmatrix} \tag{H.4}$$

In order to determine the specific contributions, we must treat all possible orderings of the indices l, m, n. For $l < m < n$,

$$\det \begin{pmatrix} a & \cdot & \cdot \\ 0 & a & \cdot \\ \cdot & \cdot & a^2 \end{pmatrix}, \tag{H.5}$$

which upon summing over all permitted indices, delivers the same contribution as the case $m < l < n$,

$$\det \begin{pmatrix} a & 0 & \cdot \\ \cdot & a & \cdot \\ \cdot & \cdot & a^2 \end{pmatrix}. \tag{H.6}$$

Likewise, the contributions from the cases $l < n < m$

$$\det \begin{pmatrix} a & \cdot & \cdot \\ 0 & a & 0 \\ \cdot & 0 & a^2 \end{pmatrix} \tag{H.7}$$

and $m < n < l$,

$$\det \begin{pmatrix} a & 0 & 0 \\ \cdot & a & \cdot \\ 0 & \cdot & a^2 \end{pmatrix}, \tag{H.8}$$

respectively, are the same.

Similarly, contributions from $n < l < m$,

$$\det \begin{pmatrix} a & \cdot & 0 \\ 0 & a & 0 \\ 0 & 0 & a^2 \end{pmatrix} = a^4, \tag{H.9}$$

and $n < m < l$,

$$\det \begin{pmatrix} a & 0 & 0 \\ \cdot & a & 0 \\ 0 & 0 & a^2 \end{pmatrix} = a^4 \tag{H.10}$$

reduce to the same form.

Evaluating the index summations subject to the constraints in each case, we find that Eq. (H.3) reduces to

$$\mathcal{K}_{11,2} = N^2 a^4 \left(N + a^{2N-6}(1 - a^4) \right), \tag{H.11}$$

where we have used the result (4.19) to evaluate

$$\begin{aligned} \mathcal{K}_{1,1} &= 1 + a^2 N^2 - a^{2N} \\ \mathcal{K}_{2,2} &= 2 + a^4 N^2 - a^{-2+2N}(2a^2 + (-1 + a^2)^2 N^2). \end{aligned} \tag{H.12}$$

Altogether, we arrive at the OTOC in the scaling theory

$$\overline{\mathcal{O}(t)} = 2N \left(1 + \frac{a^2 N^2 - a^{2N} + 1}{N^2} - \frac{2\left(a^{2N} - a^{2N+4} + a^6 N\right)}{a^2 N} \right). \tag{H.13}$$

As depicted in Figure H.1, when applied to the OTOC (5.68), we find good agreement between the analytical result for the scaling theory and numerical data for the Poisson kernel, valid for $a = e^{-t/2}$.

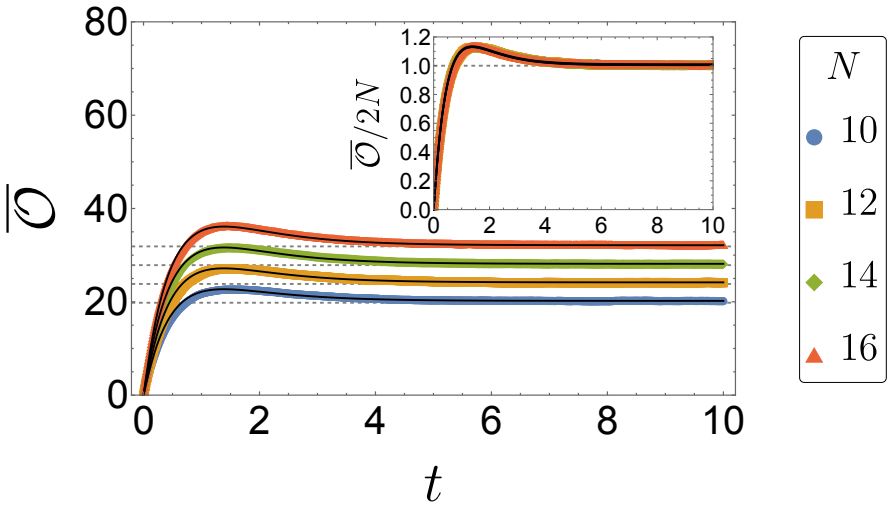

Figure H.1: Comparison of the analytical prediction for the OTOC in the scaling theory obtained from inserting Eqs. (H.11) and (H.12) into Eq. (5.68), and numerical data for the Poisson kernel, in analogy to Figure 5.8. Data is generated over 10^4 realisations for various system sizes N.

References

[1] T. Kalsi, A. Romito, and H. Schomerus, "Three-fold way of entanglement dynamics in monitored quantum circuits", Journal of Physics A: Mathematical and Theoretical **55**, 264009 (2022).

[2] T. Kalsi, A. Romito, and H. Schomerus, "Spectral chaos bounds from scaling theory of maximally efficient quantum-dynamical scrambling", arXiv:2310.11355 [quant-ph] (2024).

[3] T. Kalsi, A. Romito, and H. Schomerus, "Hierarchical analytical approach to universal spectral correlations in Brownian Quantum Chaos", arXiv:2410.15872 [cond-mat.mes-hall] (2024).

[4] E. P. Wigner, "Characteristic Vectors of Bordered Matrices with Infinite Dimensions", The Annals of Mathematics **62**, 548 (1955).

[5] E. P. Wigner, "Characteristic Vectors of Bordered Matrices with Infinite Dimensions II", The Annals of Mathematics **65**, 203 (1957).

[6] E. P. Wigner, "On the Distribution of the Roots of Certain Symmetric Matrices", The Annals of Mathematics **67**, 325 (1958).

[7] F. J. Dyson, "A Brownian-Motion Model for the Eigenvalues of a Random Matrix", Journal of Mathematical Physics **3**, 1191–1198 (1962).

[8] F. J. Dyson, "Statistical Theory of the Energy Levels of Complex Systems. I, II, III", Journal of Mathematical Physics **3**, 140–156 (1962).

[9] F. J. Dyson, "The Threefold Way. Algebraic Structure of Symmetry Groups and Ensembles in Quantum Mechanics", Journal of Mathematical Physics **3**, 1199–1215 (1962).

[10] E. P. Wigner, "Random Matrices in Physics", SIAM Review **9**, 1–23 (1967).

[11] M. Mehta, *Random matrices and the statistical theory of energy levels* (Academic Press, New York, NY, 1967).

[12] T. A. Brody, J. Flores, J. B. French, P. A. Mello, A. Pandey, and S. S. M. Wong, "Random-matrix physics: spectrum and strength fluctuations", Reviews of Modern Physics **53**, 385–479 (1981).

[13] C. W. J. Beenakker, "Random-matrix theory of quantum transport", Reviews of Modern Physics **69**, 731–808 (1997).

[14] T. Guhr, A. Müller–Groeling, and H. A. Weidenmüller, "Random-matrix theories in quantum physics: common concepts", Physics Reports **299**, 189–425 (1998).

[15] E. Akkermans and G. Montambaux, *Mesoscopic Physics of Electrons and Photons* (Cambridge University Press, Cambridge, 2007).

[16] H.-J. Stöckmann, *Quantum Chaos* (Cambridge University Press, Cambridge, 1999).

[17] F. Haake, S. Gnutzmann, and M. Kuś, *Quantum Signatures of Chaos*, 4th ed. (Springer International Publishing, Cham, 2018).

[18] J. M. Deutsch, "Quantum statistical mechanics in a closed system", Physical Review A **43**, 2046–2049 (1991).

[19] M. Srednicki, "Chaos and quantum thermalization", Physical Review E **50**, 888–901 (1994).

[20] R. Nandkishore and D. A. Huse, "Many-body localization and thermalization in quantum statistical mechanics", Annual Review of Condensed Matter Physics **6**, 15–38 (2015).

[21] L. D'Alessio, Y. Kafri, A. Polkovnikov, and M. Rigol, "From quantum chaos and eigenstate thermalization to statistical mechanics and thermodynamics", Advances in Physics **65**, 239–362 (2016).

[22] F. Borgonovi, F. M. Izrailev, L. F. Santos, and V. G. Zelevinsky, "Quantum chaos and thermalization in isolated systems of interacting particles", Physics Reports **626**, 1–58 (2016).

[23] D. A. Abanin, E. Altman, I. Bloch, and M. Serbyn, "Colloquium: Many-body localization, thermalization, and entanglement", Reviews of Modern Physics **91**, 21001 (2019).

[24] L. P. Kadanoff, "Scaling and universality in statistical physics", Physica A: Statistical Mechanics and its Applications **163**, 1–14 (1990).

[25] A. Z. Patashinskiĭ, V. L. Pokrovskiĭ, and P. J. Shepherd, *Fluctuation theory of phase transitions: covering second-order phase transitions, scale and conformal invariance, algebras of fluctuating quantities, degenerate systems, critical dynamics, epsilon expansions, renormalization group, and applications*, International series in natural philosophy; v. 98 (Pergamon Press, Oxford, 1979).

[26] P. Di Francesco, P. Mathieu, and D. Sénéchal, *Conformal Field Theory* (Springer New York, New York, NY, 1997).

[27] S. Sachdev, *Quantum Phase Transitions*, 2nd ed. (Cambridge University Press, Cambridge, 2011).

[28] M. J. Lax, W. Cai, and M. Xu, *Random Processes in Physics and Finance*, Oxford finance series (Oxford University Press, Oxford, 2013 - 2006).

[29] K. Jacobs, *Stochastic Processes for Physicists: Understanding Noisy Systems* (Cambridge University Press, Cambridge, 2010).

[30] G. Schehr, A. Altland, Y. V. Fyodorov, N. O'Connell, and L. F. Cugliandolo, *Stochastic Processes and Random Matrices: Lecture Notes of the Les Houches Summer School: Volume 104, July 2015* (Oxford University Press, 2017).

[31] A. Altland and M. R. Zirnbauer, "Nonstandard symmetry classes in mesoscopic normal-superconducting hybrid structures", Physical Review B **55**, 1142–1161 (1997).

[32] A. Kitaev, "Periodic table for topological insulators and superconductors", AIP Conference Proceedings **1134**, 22–30 (2009).

[33] S. Ryu, A. P. Schnyder, A. Furusaki, and A. W. W. Ludwig, "Topological insulators and superconductors: tenfold way and dimensional hierarchy", New Journal of Physics **12**, 065010 (2010).

[34] E. J. Bergholtz, J. C. Budich, and F. K. Kunst, "Exceptional topology of non-Hermitian systems", Reviews of Modern Physics **93**, 015005 (2021).

[35] O. Bohigas, M. J. Giannoni, and C. Schmit, "Characterization of Chaotic Quantum Spectra and Universality of Level Fluctuation Laws", Physical Review Letters **52**, 1–4 (1984).

[36] N. Rosenzweig and C. E. Porter, ""Repulsion of Energy Levels" in Complex Atomic Spectra", Physical Review **120**, 1698–1714 (1960).

[37] J.-P. Bouchaud and M. Potters, "Financial applications of random matrix theory: a short review", in *The Oxford Handbook of Random Matrix Theory* (Oxford University Press, Oxford, 2015).

[38] H. Sompolinsky, A. Crisanti, and H. J. Sommers, "Chaos in Random Neural Networks", Physical Review Letters **61**, 259–262 (1988).

[39] K. Rajan and L. F. Abbott, "Eigenvalue Spectra of Random Matrices for Neural Networks", Physical Review Letters **97**, 188104 (2006).

[40] M. L. Mehta and M. Gaudin, "On the density of Eigenvalues of a random matrix", Nuclear Physics **18**, 420–427 (1960).

[41] M. V. Berry and M. Tabor, "Level clustering in the regular spectrum", Proceedings of the Royal Society of London. Series A, Mathematical and Physical Sciences **356**, 375–394 (1977).

[42] R. E. Prange, "The Spectral Form Factor Is Not Self-Averaging", Physical Review Letters **78**, 2280–2283 (1997).

[43] E. Brézin and S. Hikami, "Spectral form factor in a random matrix theory", Physical Review E **55**, 4067–4083 (1997).

[44] M. Sieber and K. Richter, "Correlations between periodic orbits and their rôle in spectral statistics", Physica Scripta **2001**, 128 (2001).

[45] S. Müller, S. Heusler, P. Braun, F. Haake, and A. Altland, "Semiclassical Foundation of Universality in Quantum Chaos", Physical Review Letters **93**, 014103 (2004).

[46] S. Müller, S. Heusler, P. Braun, F. Haake, and A. Altland, "Periodic-orbit theory of universality in quantum chaos", Physical Review E **72**, 046207 (2005).

[47] A. M. García-García and J. J. M. Verbaarschot, "Spectral and thermodynamic properties of the Sachdev-Ye-Kitaev model", Physical Review D **94**, 126010 (2016).

[48] J. S. Cotler, G. Gur-Ari, M. Hanada, J. Polchinski, P. Saad, S. H. Shenker, D. Stanford, A. Streicher, and M. Tezuka, "Black holes and random matrices", Journal of High Energy Physics **2017**, 118 (2017).

[49] J. Cotler, N. Hunter-Jones, J. Liu, and B. Yoshida, "Chaos, complexity, and random matrices", Journal of High Energy Physics **2017**, 48 (2017).

[50] H. Gharibyan, M. Hanada, S. H. Shenker, and M. Tezuka, "Onset of random matrix behavior in scrambling systems", Journal of High Energy Physics **2018**, 124 (2018).

[51] P. Saad, S. H. Shenker, and D. Stanford, "A semiclassical ramp in SYK and in gravity", arXiv:1806.06840 [hep-th] (2019).

[52] A. Chan, A. De Luca, and J. T. Chalker, "Solution of a Minimal Model for Many-Body Quantum Chaos", Physical Review X **8**, 041019 (2018).

[53] P. Kos, M. Ljubotina, and T. Prosen, "Many-Body Quantum Chaos: Analytic Connection to Random Matrix Theory", Physical Review X **8**, 021062 (2018).

[54] A. Chan, A. De Luca, and J. T. Chalker, "Spectral Statistics in Spatially Extended Chaotic Quantum Many-Body Systems", Physical Review Letters **121**, 060601 (2018).

[55] B. Bertini, P. Kos, and T. Prosen, "Exact Spectral Form Factor in a Minimal Model of Many-Body Quantum Chaos", Physical Review Letters **121**, 264101 (2018).

[56] A. J. Friedman, A. Chan, A. De Luca, and J. T. Chalker, "Spectral Statistics and Many-Body Quantum Chaos with Conserved Charge", Physical Review Letters **123**, 210603 (2019).

[57] D. Yang, A. Grankin, L. M. Sieberer, D. V. Vasilyev, and P. Zoller, "Quantum non-demolition measurement of a many-body Hamiltonian", Nature Communications **11**, 775 (2020).

[58] L. K. Joshi, A. Elben, A. Vikram, B. Vermersch, V. Galitski, and P. Zoller, "Probing Many-Body Quantum Chaos with Quantum Simulators", Physical Review X **12**, 011018 (2022).

[59] K. Richter, J. D. Urbina, and S. Tomsovic, "Semiclassical roots of universality in many-body quantum chaos", Journal of Physics A: Mathematical and Theoretical **55**, 453001 (2022).

[60] C. B. Dağ, S. I. Mistakidis, A. Chan, and H. R. Sadeghpour, "Many-body quantum chaos in stroboscopically-driven cold atoms", Communications Physics **6**, 136 (2023).

[61] H. Dong, P. Zhang, C. B. Dag, Y. Gao, N. Wang, J. Deng, X. Zhang, J. Chen, S. Xu, K. Wang, Y. Wu, C. Zhang, F. Jin, X. Zhu, A. Zhang, Y. Zou, Z. Tan, Z. Cui, Z. Zhu, F. Shen, T. Li, J. Zhong, Z. Bao, H. Li, Z. Wang, Q. Guo, C. Song, F. Liu, A. Chan, L. Ying, and H. Wang, "Measuring Spectral Form Factor in Many-Body Chaotic and Localized Phases of Quantum Processors", Physical Review Letters **134**, 010402 (2025).

[62] M. C. Gutzwiller, *Chaos in Classical and Quantum Mechanics* (Springer New York, New York, NY, 1990).

[63] S. Strogatz, *Nonlinear Dynamics and Chaos: With Applications to Physics, Biology, Chemistry, and Engineering*, 3rd ed. (CRC Press, Boca Raton, FL, 2024).

[64] P. Hayden and J. Preskill, "Black holes as mirrors: quantum information in random subsystems", Journal of High Energy Physics **2007**, 120–120 (2007).

[65] Y. Sekino and L. Susskind, "Fast scramblers", Journal of High Energy Physics **2008**, 065 (2008).

[66] W. Brown and O. Fawzi, "Scrambling speed of random quantum circuits", arXiv:1210.6644 [quant-ph] (2013).

[67] N. Lashkari, D. Stanford, M. Hastings, T. Osborne, and P. Hayden, "Towards the fast scrambling conjecture", Journal of High Energy Physics **2013**, 22 (2013).

[68] S. H. Shenker and D. Stanford, "Black holes and the butterfly effect", Journal of High Energy Physics **2014**, 67 (2014).

[69] P. Hosur, X.-L. Qi, D. A. Roberts, and B. Yoshida, "Chaos in quantum channels", Journal of High Energy Physics **2016**, 4 (2016).

[70] M. P. Fisher, V. Khemani, A. Nahum, and S. Vijay, "Random Quantum Circuits", Annual Review of Condensed Matter Physics **14**, 335–379 (2023).

[71] S. Xu and B. Swingle, "Scrambling Dynamics and Out-of-Time-Ordered Correlators in Quantum Many-Body Systems", PRX Quantum **5**, 010201 (2024).

[72] J. Maldacena, S. H. Shenker, and D. Stanford, "A bound on chaos", Journal of High Energy Physics **2016**, 106 (2016).

[73] A. Kitaev, *A simple model of quantum holography (part 1)*, Talk at KITP, https://online.kitp.ucsb.edu/online/entangled15/kitaev/, University of California, Santa Barbara, CA, 2015.

[74] S. Sachdev and J. Ye, "Gapless spin-fluid ground state in a random quantum Heisenberg magnet", Physical Review Letters **70**, 3339–3342 (1993).

[75] J. Maldacena and D. Stanford, "Remarks on the Sachdev-Ye-Kitaev model", Physical Review D **94**, 106002 (2016).

[76] J. Polchinski and V. Rosenhaus, "The spectrum in the Sachdev-Ye-Kitaev model", Journal of High Energy Physics **2016**, 1–25 (2016).

[77] D. Bagrets, A. Altland, and A. Kamenev, "Sachdev–Ye–Kitaev model as Liouville quantum mechanics", Nuclear Physics B **911**, 191–205 (2016).

[78] D. Bagrets, A. Altland, and A. Kamenev, "Power-law out of time order correlation functions in the SYK model", Nuclear Physics B **921**, 727–752 (2017).

[79] V. Rosenhaus, "An introduction to the SYK model", Journal of Physics A: Mathematical and Theoretical **52**, 323001 (2019).

[80] S. W. Hawking, "Breakdown of predictability in gravitational collapse", Physical Review D **14**, 2460–2473 (1976).

[81] D. N. Page, "Information in black hole radiation", Physical Review Letters **71**, 3743–3746 (1993).

[82] S. H. Shenker and D. Stanford, "Stringy effects in scrambling", Journal of High Energy Physics **2015**, 132 (2015).

[83] A. Blommaert, T. G. Mertens, and H. Verschelde, "The Schwarzian theory — a Wilson line perspective", Journal of High Energy Physics **2018**, 22 (2018).

[84] A. Blommaert, T. G. Mertens, and H. Verschelde, "Fine structure of Jackiw-Teitelboim quantum gravity", Journal of High Energy Physics **2019**, 66 (2019).

[85] D. A. Trunin, "Pedagogical introduction to the Sachdev–Ye–Kitaev model and two-dimensional dilaton gravity", Physics-Uspekhi **64**, 219 (2021).

[86] Y.-Z. You, A. W. W. Ludwig, and C. Xu, "Sachdev-Ye-Kitaev model and thermalization on the boundary of many-body localized fermionic symmetry-protected topological states", Physical Review B **95**, 115150 (2017).

[87] J. Liu, "Spectral form factors and late time quantum chaos", Physical Review D **98**, 086026 (2018).

[88] B. Skinner, J. Ruhman, and A. Nahum, "Measurement-Induced Phase Transitions in the Dynamics of Entanglement", Physical Review X **9**, 031009 (2019).

[89] Y. Li, X. Chen, and M. P. A. Fisher, "Measurement-driven entanglement transition in hybrid quantum circuits", Physical Review B **100**, 134306 (2019).

[90] A. Chan, R. M. Nandkishore, M. Pretko, and G. Smith, "Unitary-projective entanglement dynamics", Physical Review B **99**, 224307 (2019).

[91] Y. Li, X. Chen, and M. P. A. Fisher, "Quantum Zeno effect and the many-body entanglement transition", Physical Review B **98**, 205136 (2018).

[92] A. Nahum, J. Ruhman, S. Vijay, and J. Haah, "Quantum Entanglement Growth under Random Unitary Dynamics", Physical Review X **7**, 031016 (2017).

[93] B. Bertini, P. Kos, and T. Prosen, "Random Matrix Spectral Form Factor of Dual-Unitary Quantum Circuits", Communications in Mathematical Physics **387**, 597–620 (2021).

[94] S. J. Garratt and J. T. Chalker, "Local Pairing of Feynman Histories in Many-Body Floquet Models", Physical Review X **11**, 021051 (2021).

[95] J. J. Sakurai and J. Napolitano, *Modern Quantum Mechanics* (Cambridge University Press, Cambridge, 2020).

[96] D. J. Griffiths and D. F. Schroeter, *Introduction to Quantum Mechanics* (Cambridge University Press, London, 2018).

[97] J. von Neumann, *Mathematische Grundlagen der Quantenmechanik* (Springer Berlin Heidelberg, Berlin, Heidelberg, 1996).

[98] J. von Neumann, *Mathematical Foundations of Quantum Mechanics*, edited by N. A. Wheeler (Princeton University Press, Princeton, 2018).

[99] K. Jacobs, *Quantum Measurement Theory and its Applications* (Cambridge University Press, Cambridge, 2014).

[100] H. M. Wiseman and G. J. Milburn, *Quantum measurement and control* (Cambridge University Press, Cambridge, 2009).

[101] M. A. Nielsen and I. L. Chuang, *Quantum Computation and Quantum Information* (Cambridge University Press, Cambridge, June 2012).

[102] J. Wishart, "The Generalised Product Moment Distribution in Samples from a Normal Multivariate Population", Biometrika **20A**, 32 (1928).

[103] K. Efetov, *Supersymmetry in Disorder and Chaos* (Cambridge University Press, Cambridge, 1999).

[104] Y. Imry, "Active Transmission Channels and Universal Conductance Fluctuations", Europhysics Letters **1**, 249–256 (1986).

[105] B. L. Al'tshuler and B. I. Shklovskii, "Repulsion of energy levels and conductivity of small metal samples", Zhurnal Èksperimental'noi i Teoreticheskoi Fiziki **91**, 234 (1986).

[106] B. Altshuler, P. A. Lee, and R. A. Webb, *Mesoscopic Phenomena in Solids*, Modern problems in condensed matter sciences; v. 30 (North Holland, Amsterdam, 1991).

[107] C. Porter, *Statistical Theories of Spectra: Fluctuations; a Collection of Reprints and Original Papers, with an Introductory Review*, Perspectives in Physics (Academic Press, 1965).

[108] P. L. Hsu, "On the distribution of roots of certain determinantal equations", Annals of Eugenics **9**, 250–258 (1939).

[109] D. N. Nanda, "Distribution of a Root of a Determinantal Equation", The Annals of Mathematical Statistics **19**, 47–57 (1948).

[110] M. Hamermesh, *Group Theory and Its Application to Physical Problems*, Addison Wesley Series in Physics (Dover Publications, 1989).

[111] K. Zyczkowski and M. Kus, "Random unitary matrices", Journal of Physics A: Mathematical and General **27**, 4235–4245 (1994).

[112] F. Mezzadri, "How to generate random matrices from the classical compact groups", Notices of the American Mathematical Society **54**, 592–604 (2007).

[113] J. Ginibre, "Statistical Ensembles of Complex, Quaternion, and Real Matrices", Journal of Mathematical Physics **6**, 440–449 (1965).

[114] M. R. Zirnbauer, "Symmetry Classes", arXiv:1001.0722 [math-ph] (2010).

[115] H. Fischer, *A History of the Central Limit Theorem* (Springer New York, New York, NY, 2011).

[116] T. Tao, *Topics in random matrix theory*, Graduate studies in mathematics; v. 132 (American Mathematical Society, Providence, R.I, 2012).

[117] L. Pastur and M. Shcherbina, "Universality of the local eigenvalue statistics for a class of unitary invariant random matrix ensembles", Journal of Statistical Physics **86**, 109–147 (1997).

[118] P. Deift, T. Kriecherbauer, K. T-R McLaughlin, and S. Venakides, "Asymptotics for polynomials orthogonal with respect to varying exponential weights", International Mathematics Research Notices **1997**, 759 (1997).

[119] L. Erdős, S. Péché, J. A. Ramírez, B. Schlein, and H.-T. Yau, "Bulk universality for Wigner matrices", Communications on Pure and Applied Mathematics **63**, 895–925 (2010).

[120] T. Tao and V. Vu, "Random Matrices: Universality of Local Eigenvalue Statistics up to the Edge", Communications in Mathematical Physics **298**, 549–572 (2010).

[121] O. Bouverot-Dupuis, S. Pappalardi, J. Kurchan, A. Polkovnikov, and L. Foini, "Random matrix universality in dynamical correlation functions at late times", arXiv:2407.12103 [cond-mat.stat-mech] (2024).

[122] A. K. Das, C. Cianci, D. G. A. Cabral, D. A. Zarate-Herrada, P. Pinney, S. Pilatowsky-Cameo, A. S. Matsoukas-Roubeas, V. S. Batista, A. del Campo, E. J. Torres-Herrera, and L. F. Santos, "Proposal for many-body quantum chaos detection", arXiv:2401.01401 [cond-mat.stat-mech] (2024).

[123] F. Haake, M. Kus, H.-J. Sommers, H. Schomerus, and K. Zyczkowski, "Secular determinants of random unitary matrices", Journal of Physics A: Mathematical and General **29**, 3641–3658 (1996).

[124] H. Singh, B. A. Ware, R. Vasseur, and A. J. Friedman, "Subdiffusion and Many-Body Quantum Chaos with Kinetic Constraints", Physical Review Letters **127**, 230602 (2021).

[125] P. Kos, B. Bertini, and T. Prosen, "Chaos and Ergodicity in Extended Quantum Systems with Noisy Driving", Physical Review Letters **126**, 1–190601 (2021).

[126] P. J. Forrester, M. Kieburg, S.-H. Li, and J. Zhang, "Dip-ramp-plateau for Dyson Brownian motion from the identity on $U(N)$", Probability and Mathematical Physics **5**, 321–355 (2024).

[127] M. V. Berry, "Quantizing a classically ergodic system: Sinai's billiard and the KKR method", Annals of Physics **131**, 163–216 (1981).

[128] S. W. McDonald and A. N. Kaufman, "Spectrum and Eigenfunctions for a Hamiltonian with Stochastic Trajectories", Physical Review Letters **42**, 1189–1191 (1979).

[129] G. Casati, F. Valz-Gris, and I. Guarnieri, "On the connection between quantization of nonintegrable systems and statistical theory of spectra", Lettere al Nuovo Cimento **28**, 279–282 (1980).

[130] M. V. Berry and M. Robnik, "Statistics of energy levels without time-reversal symmetry: Aharonov-Bohm chaotic billiards", Journal of Physics A: Mathematical and General **19**, 649–668 (1986).

[131] M. Robnik and M. V. Berry, "False time-reversal violation and energy level statistics: the role of anti-unitary symmetry", Journal of Physics A: Mathematical and General **19**, 669–682 (1986).

[132] H. Friedrich and H. Wintgen, "The hydrogen atom in a uniform magnetic field — An example of chaos", Physics Reports **183**, 37–79 (1989).

[133] D. Poilblanc, T. Ziman, J. Bellissard, F. Mila, and G. Montambaux, "Poisson *vs.* GOE Statistics in Integrable and Non-Integrable Quantum Hamiltonians", Europhysics Letters **22**, 537–542 (1993).

[134] K. Richter, *Semiclassical Theory of Mesoscopic Quantum Systems*, Springer Tracts in Modern Physics; v.161 (Springer, Berlin, 2000).

[135] K. Richter and M. Sieber, "Semiclassical Theory of Chaotic Quantum Transport", Physical Review Letters **89**, 206801 (2002).

[136] M. Rigol, V. Dunjko, and M. Olshanii, "Thermalization and its mechanism for generic isolated quantum systems", Nature **452**, 854–858 (2008).

[137] D. J. Luitz, N. Laflorencie, and F. Alet, "Many-body localization edge in the random-field Heisenberg chain", Physical Review B **91**, 081103 (2015).

[138] H. Kim and D. A. Huse, "Ballistic Spreading of Entanglement in a Diffusive Nonintegrable System", Physical Review Letters **111**, 127205 (2013).

[139] I. Bloch, J. Dalibard, and W. Zwerger, "Many-body physics with ultracold gases", Reviews of Modern Physics **80**, 885–964 (2008).

[140] M. Lewenstein, A. Sanpera, and V. Ahufinger, *Ultracold Atoms in Optical Lattices: Simulating Quantum Many-Body Systems* (Oxford University Press, Oxford, 2012).

[141] A. M. Kaufman, M. E. Tai, A. Lukin, M. Rispoli, R. Schittko, P. M. Preiss, and M. Greiner, "Quantum thermalization through entanglement in an isolated many-body system", Science **353**, 794–800 (2016).

[142] J. von Neumann, *Mathematical Foundation of Quantum Theory* (Princeton University Press, Princeton, NJ, 1938).

[143] M. Žnidarič, T. Prosen, and P. Prelovšek, "Many-body localization in the Heisenberg X X Z magnet in a random field", Physical Review B **77**, 064426 (2008).

[144] B. Bauer and C. Nayak, "Area laws in a many-body localized state and its implications for topological order", Journal of Statistical Mechanics: Theory and Experiment **2013**, P09005 (2013).

[145] J. A. Kjäll, J. H. Bardarson, and F. Pollmann, "Many-Body Localization in a Disordered Quantum Ising Chain", Physical Review Letters **113**, 107204 (2014).

[146] J. Eisert, M. Cramer, and M. B. Plenio, "Colloquium: Area laws for the entanglement entropy", Reviews of Modern Physics **82**, 277–306 (2010).

[147] M. Szyniszewski, A. Romito, and H. Schomerus, "Entanglement transition from variable-strength weak measurements", Physical Review B **100**, 064204 (2019).

[148] S. Goto and I. Danshita, "Measurement-induced transitions of the entanglement scaling law in ultracold gases with controllable dissipation", Physical Review A **102**, 033316 (2020).

[149] A. Rényi, "On measures of entropy and information", in Proceedings of the Fourth Berkeley Symposium on Mathematical Statistics and Probability, Volume 1: Contributions to the Theory of Statistics, Vol. 4 (University of California Press, 1961), pp. 547–562.

[150] C. von Keyserlingk, T. Rakovszky, F. Pollmann, and S. Sondhi, "Operator Hydrodynamics, OTOCs, and Entanglement Growth in Systems without Conservation Laws", Physical Review X **8**, 021013 (2018).

[151] A. Nahum, S. Vijay, and J. Haah, "Operator Spreading in Random Unitary Circuits", Physical Review X **8**, 021014 (2018).

[152] D. N. Page, "Average entropy of a subsystem", Physical Review Letters **71**, 1291–1294 (1993).

[153] D. M. Basko, I. L. Aleiner, and B. L. Altshuler, "Metal-insulator transition in a weakly interacting many-electron system with localized single-particle states", Annals of Physics **321**, 1126–1205 (2006).

[154] I. V. Gornyi, A. D. Mirlin, and D. G. Polyakov, "Interacting Electrons in Disordered Wires: Anderson Localization and Low-T Transport", Physical Review Letters **95**, 206603 (2005).

[155] A. Pal and D. A. Huse, "Many-body localization phase transition", Physical Review B **82**, 174411 (2010).

[156] E. Altman and R. Vosk, "Universal dynamics and renormalization in many-body-localized systems", Annual Review of Condensed Matter Physics **6**, 383–409 (2015).

[157] D. J. Luitz and Y. B. Lev, "The ergodic side of the many-body localization transition", Annalen der Physik **529**, 1600350 (2017).

[158] C. E. Shannon, "A Mathematical Theory of Communication", Bell System Technical Journal **27**, 379–423 (1948).

[159] M. Srednicki, "Entropy and area", Physical Review Letters **71**, 666–669 (1993).

[160] E. H. Lieb and D. W. Robinson, "The finite group velocity of quantum spin systems", Communications in Mathematical Physics **28**, 251–257 (1972).

[161] D. A. Roberts and B. Swingle, "Lieb-Robinson Bound and the Butterfly Effect in Quantum Field Theories", Physical Review Letters **117**, 091602 (2016).

[162] A. I. Larkin and Y. N. Ovchinnikov, "Quasiclassical Method in the Theory of Superconductivity", Soviet Journal of Experimental and Theoretical Physics **28**, 1200 (1969).

[163] D. A. Roberts and B. Yoshida, "Chaos and complexity by design", Journal of High Energy Physics **2017**, 121 (2017).

[164] V. Khemani, A. Vishwanath, and D. A. Huse, "Operator Spreading and the Emergence of Dissipative Hydrodynamics under Unitary Evolution with Conservation Laws", Physical Review X **8**, 031057 (2018).

[165] T. Rakovszky, F. Pollmann, and C. W. Von Keyserlingk, "Diffusive Hydrodynamics of Out-of-Time-Ordered Correlators with Charge Conservation", Physical Review X **8**, 031058 (2018).

[166] X. Mi, P. Roushan, C. Quintana, S. Mandrà, J. Marshall, C. Neill, F. Arute, K. Arya, J. Atalaya, R. Babbush, J. C. Bardin, R. Barends, J. Basso, A. Bengtsson, S. Boixo, A. Bourassa, M. Broughton, B. B. Buckley, D. A. Buell, B. Burkett, N. Bushnell, Z. Chen, B. Chiaro, R. Collins, W. Courtney, S. Demura, A. R. Derk, A. Dunsworth, D. Eppens, C. Erickson, E. Farhi, A. G. Fowler, B. Foxen, C. Gidney, M. Giustina, J. A. Gross, M. P. Harrigan, S. D. Harrington, J. Hilton, A. Ho, S. Hong, T. Huang, W. J. Huggins, L. B. Ioffe, S. V. Isakov, E. Jeffrey, Z. Jiang, C. Jones, D. Kafri, J. Kelly, S. Kim, A. Kitaev, P. V. Klimov, A. N. Korotkov, F. Kostritsa, D. Landhuis, P. Laptev, E. Lucero, O. Martin, J. R. McClean, T. McCourt, M. McEwen, A. Megrant, K. C. Miao, M. Mohseni, S. Montazeri, W. Mruczkiewicz, J. Mutus, O. Naaman, M. Neeley, M. Newman, M. Y. Niu, T. E. O'Brien, A. Opremcak, E. Ostby, B. Pato, A. Petukhov, N. Redd, N. C. Rubin, D. Sank, K. J. Satzinger, V. Shvarts, D. Strain, M. Szalay, M. D. Trevithick, B. Villalonga, T. White, Z. J. Yao, P. Yeh, A. Zalcman, H. Neven, I. Aleiner, K. Kechedzhi, V. Smelyanskiy, and Y. Chen, "Information scrambling in quantum circuits", Science **374**, 1479–1483 (2021).

[167] S. H. Shenker and D. Stanford, "Multiple shocks", Journal of High Energy Physics **2014**, 46 (2014).

[168] D. A. Roberts, D. Stanford, and L. Susskind, "Localized shocks", Journal of High Energy Physics **2015**, 51 (2015).

[169] D. Stanford, "Many-body chaos at weak coupling", Journal of High Energy Physics **2016**, 9 (2016).

[170] Y. Gu, X.-L. Qi, and D. Stanford, "Local criticality, diffusion and chaos in generalized Sachdev-Ye-Kitaev models", Journal of High Energy Physics **2017**, 125 (2017).

[171] D. A. Roberts, D. Stanford, and A. Streicher, "Operator growth in the SYK model", Journal of High Energy Physics **2018**, 122 (2018).

[172] J. Maldacena, "The Large-N Limit of Superconformal Field Theories and Supergravity", International Journal of Theoretical Physics **38**, 1113–1133 (1999).

[173] I. Kukuljan, S. Grozdanov, and T. Prosen, "Weak quantum chaos", Physical Review B **96**, 060301 (2017).

[174] B. Dóra and R. Moessner, "Out-of-Time-Ordered Density Correlators in Luttinger Liquids", Physical Review Letters **119**, 026802 (2017).

[175] E. M. Fortes, I. García-Mata, R. A. Jalabert, and D. A. Wisniacki, "Gauging classical and quantum integrability through out-of-time-ordered correlators", Physical Review E **100**, 042201 (2019).

[176] P. Shukla, "Many body density of states in the edge of the spectrum: non-interacting limit", Journal of Physics A: Mathematical and Theoretical **55**, 224018 (2022).

[177] F. M. Izrailev, "Simple models of quantum chaos: Spectrum and eigenfunctions", Physics Reports **196**, 299–392 (1990).

[178] M. Suzuki, "General theory of fractal path integrals with applications to many-body theories and statistical physics", Journal of Mathematical Physics **32**, 400–407 (1991).

[179] B. Misra and E. C. G. Sudarshan, "The Zeno's paradox in quantum theory", Journal of Mathematical Physics **18**, 756–763 (1977).

[180] A. Peres, "Zeno paradox in quantum theory", American Journal of Physics **48**, 931–932 (1980).

[181] C. Noel, P. Niroula, D. Zhu, A. Risinger, L. Egan, D. Biswas, M. Cetina, A. V. Gorshkov, M. J. Gullans, D. A. Huse, et al., "Measurement-induced quantum phases realized in a trapped-ion quantum computer", Nature Physics **18**, 760–764 (2022).

[182] J. M. Koh, S.-N. Sun, M. Motta, and A. J. Minnich, "Measurement-induced entanglement phase transition on a superconducting quantum processor with mid-circuit readout", Nature Physics **19**, 1314–1319 (2023).

[183] J. C. Hoke, M. Ippoliti, E. Rosenberg, D. Abanin, R. Acharya, T. I. Andersen, M. Ansmann, F. Arute, K. Arya, A. Asfaw, J. Atalaya, J. C. Bardin, A. Bengtsson, G. Bortoli, A. Bourassa, J. Bovaird, L. Brill, M. Broughton, B. B. Buckley, D. A. Buell, T. Burger, B. Burkett, N. Bushnell, Z. Chen, B. Chiaro, D. Chik, J. Cogan, R. Collins, P. Conner, W. Courtney, A. L. Crook, B. Curtin, A. G. Dau, D. M. Debroy, A. Del Toro Barba, S. Demura, A. Di Paolo, I. K. Drozdov, A. Dunsworth, D. Eppens, C. Erickson, E. Farhi, R. Fatemi, V. S. Ferreira, L. F. Burgos, E. Forati, A. G. Fowler, B. Foxen, W. Giang, C. Gidney, D. Gilboa, M. Giustina, R. Gosula, J. A. Gross, S. Habegger, M. C. Hamilton, M. Hansen, M. P. Harrigan, S. D. Harrington, P. Heu, M. R. Hoffmann, S. Hong, T. Huang, A. Huff, W. J. Huggins, S. V. Isakov, J. Iveland, E. Jeffrey, Z. Jiang, C. Jones, P. Juhas, D. Kafri, K. Kechedzhi, T. Khattar, M. Khezri, M. Kieferová, S. Kim, A. Kitaev, P. V. Klimov, A. R. Klots, A. N. Korotkov, F. Kostritsa, J. M. Kreikebaum, D. Landhuis, P. Laptev, K.-M. Lau, L. Laws, J. Lee, K. W. Lee, Y. D. Lensky, B. J. Lester, A. T. Lill, W. Liu, A. Locharla, O. Martin, J. R. McClean, M. McEwen, K. C. Miao, A. Mieszala, S. Montazeri, A. Morvan, R. Movassagh, W. Mruczkiewicz, M. Neeley, C. Neill, A. Nersisyan, M. Newman, J. H. Ng, A. Nguyen, M. Nguyen, M. Y. Niu, T. E. O'Brien, S. Omonije, A. Opremcak, A. Petukhov, R. Potter, L. P. Pryadko, C. Quintana, C. Rocque, N. C. Rubin, N. Saei, D. Sank, K. Sankaragomathi, K. J. Satzinger, H. F. Schurkus, C. Schuster, M. J. Shearn, A. Shorter, N. Shutty, V. Shvarts, J. Skruzny, W. C. Smith, R. Somma, G. Sterling, D. Strain, M. Szalay, A. Torres, G. Vidal, B. Villalonga, C. V. Heidweiller, T. White, B. W. K. Woo, C. Xing, Z. J. Yao, P. Yeh, J. Yoo, G. Young, A. Zalcman, Y. Zhang, N. Zhu, N. Zobrist, H. Neven, R. Babbush, D. Bacon, S. Boixo, J. Hilton, E. Lucero, A. Megrant, J. Kelly, Y. Chen, V. Smelyanskiy, X. Mi, V. Khemani, and P. Roushan, "Measurement-induced entanglement and teleportation on a noisy quantum processor", Nature **622**, 481–486 (2023).

[184] A. Zabalo, M. J. Gullans, J. H. Wilson, S. Gopalakrishnan, D. A. Huse, and J. H. Pixley, "Critical properties of the measurement-induced transition in random quantum circuits", Physical Review B **101**, 060301 (2020).

[185] O. Lunt, M. Szyniszewski, and A. Pal, "Measurement-induced criticality and entanglement clusters: A study of one-dimensional and two-dimensional Clifford circuits", Physical Review B **104**, 155111 (2021).

[186] A. Lavasani, Y. Alavirad, and M. Barkeshli, "Topological Order and Criticality in $(2+1)$D Monitored Random Quantum Circuits", Physical Review Letters **127**, 235701 (2021).

[187] X. Turkeshi, R. Fazio, and M. Dalmonte, "Measurement-induced criticality in $(2+1)$-dimensional hybrid quantum circuits", Physical Review B **102**, 014315 (2020).

[188] M. J. Gullans and D. A. Huse, "Dynamical Purification Phase Transition Induced by Quantum Measurements", Physical Review X **10**, 041020 (2020).

[189] M. J. Gullans and D. A. Huse, "Scalable Probes of Measurement-Induced Criticality", Physical Review Letters **125**, 070606 (2020).

[190] A. Zabalo, M. Gullans, J. Wilson, R. Vasseur, A. Ludwig, S. Gopalakrishnan, D. A. Huse, and J. Pixley, "Operator Scaling Dimensions and Multifractality at Measurement-Induced Transitions", Physical Review Letters **128**, 050602 (2022).

[191] Y. Li, X. Chen, A. W. W. Ludwig, and M. P. A. Fisher, "Conformal invariance and quantum nonlocality in critical hybrid circuits", Physical Review B **104**, 104305 (2021).

[192] Y. Bao, S. Choi, and E. Altman, "Theory of the phase transition in random unitary circuits with measurements", Physical Review B **101**, 104301 (2020).

[193] S. Choi, Y. Bao, X.-L. Qi, and E. Altman, "Quantum Error Correction in Scrambling Dynamics and Measurement-Induced Phase Transition", Physical Review Letters **125**, 030505 (2020).

[194] X. Cao, A. Tilloy, and A. De Luca, "Entanglement in a fermion chain under continuous monitoring", SciPost Physics **7**, 024 (2019).

[195] X. Chen, Y. Li, M. P. A. Fisher, and A. Lucas, "Emergent conformal symmetry in nonunitary random dynamics of free fermions", Physical Review Research **2**, 033017 (2020).

[196] C.-M. Jian, B. Bauer, A. Keselman, and A. W. W. Ludwig, "Criticality and entanglement in nonunitary quantum circuits and tensor networks of noninteracting fermions", Physical Review B **106**, 134206 (2022).

[197] O. Alberton, M. Buchhold, and S. Diehl, "Entanglement Transition in a Monitored Free-Fermion Chain: From Extended Criticality to Area Law", Physical Review Letters **126**, 170602 (2021).

[198] M. Buchhold, Y. Minoguchi, A. Altland, and S. Diehl, "Effective Theory for the Measurement-Induced Phase Transition of Dirac Fermions", Physical Review X **11**, 041004 (2021).

[199] Q. Tang, X. Chen, and W. Zhu, "Quantum criticality in the nonunitary dynamics of $(2+1)$-dimensional free fermions", Physical Review B **103**, 174303 (2021).

[200] P. Zhang, C. Liu, S.-K. Jian, and X. Chen, "Universal Entanglement Transitions of Free Fermions with Long-range Non-unitary Dynamics", Quantum **6**, 723 (2022).

[201] G. Kells, D. Meidan, and A. Romito, "Topological transitions in weakly monitored free fermions", SciPost Physics **14**, 031 (2023).

[202] A. Altland, M. Buchhold, S. Diehl, and T. Micklitz, "Dynamics of measured many-body quantum chaotic systems", Physical Review Research **4**, L022066 (2022).

[203] B. Bertini, P. Kos, and T. Prosen, "Exact Correlation Functions for Dual-Unitary Lattice Models in 1+1 Dimensions", Physical Review Letters **123**, 210601 (2019).

[204] L. Piroli, B. Bertini, J. I. Cirac, and T. Prosen, "Exact dynamics in dual-unitary quantum circuits", Physical Review B **101**, 094304 (2020).

[205] T. Prosen, "Many-body quantum chaos and dual-unitarity round-a-face", Chaos: An Interdisciplinary Journal of Nonlinear Science **31**, 093101 (2021).

[206] P. Y. Chang, X. Chen, S. Gopalakrishnan, and J. H. Pixley, "Evolution of Entanglement Spectra under Generic Quantum Dynamics", Physical Review Letters **123**, 190602 (2019).

[207] M. Szyniszewski, A. Romito, and H. Schomerus, "Universality of Entanglement Transitions from Stroboscopic to Continuous Measurements", Physical Review Letters **125**, 210602–210602 (2020).

[208] I. Karatzas and S. E. Shreve, *Brownian Motion and Stochastic Calculus*, 2nd ed., Graduate Texts in Mathematics; v. 113 (Springer, New York, 1991).

[209] J. F. Le Gall, *Brownian Motion, Martingales, and Stochastic calculus*, Graduate Texts in Mathematics; v. 274 (Springer International Publishing, Cham, 2016).

[210] X. Chen and T. Zhou, "Quantum chaos dynamics in long-range power law interaction systems", Physical Review B **100**, 064305 (2019).

[211] T. Zhou and X. Chen, "Operator dynamics in a Brownian quantum circuit", Physical Review E **99**, 052212 (2019).

[212] S. Xu and B. Swingle, "Locality, Quantum Fluctuations, and Scrambling", Physical Review X **9**, 031048 (2019).

[213] T. Zhou, S. Xu, X. Chen, A. Guo, and B. Swingle, "Operator Lévy Flight: Light Cones in Chaotic Long-Range Interacting Systems", Physical Review Letters **124**, 180601 (2020).

[214] T. Tao and V. Vu, "Random matrices: Universality of local eigenvalue statistics", Acta Mathematica **206**, 127–204 (2011).

[215] P. W. Brouwer, "Generalized circular ensemble of scattering matrices for a chaotic cavity with nonideal leads", Physical Review B **51**, 16878–16884 (1995).

[216] P. Forrester and T. Nagao, "Correlations for the circular Dyson brownian motion model with Poisson initial conditions", Nuclear Physics B **532**, 733–752 (1998).

[217] G. Dyson, "Freeman John Dyson. 15 December 1923—28 February 2020", Biographical Memoirs of Fellows of the Royal Society **73**, 197–226 (2022).

[218] K. Itô, "Brownian motions in a Lie group", Proceedings of the Japan Academy **26**, 4–10 (1950).

[219] K. Yosida, "On Brownian motion in a homogeneous Riemannian space", Pacific Journal of Mathematics **2**, 263–270 (1952).

[220] G. A. Hunt, "Semi-groups of measures on Lie groups", Transactions of the American Mathematical Society **81**, 264–293 (1956).

[221] M. Katori, *Bessel Processes, Schramm-Loewner Evolution, and the Dyson Model*, SpringerBriefs in Mathematical Physics; v. 11 (Springer Singapore, Singapore, 2016).

[222] L. Erdős and H.-T. Yau, *A Dynamical Approach to Random Matrix Theory*, Courant Lecture Notes in Mathematics; v. 28 (American Mathematical Society, Providence, RI; Courant Institute of Mathematical Sciences, New York, NY, 2017).

[223] P. J. Forrester, "Differential Identities for the Structure Function of Some Random Matrix Ensembles", Journal of Statistical Physics **183**, 33 (2021).

[224] P. J. Forrester, "High–low temperature dualities for the classical β-ensembles", Random Matrices: Theory and Applications **11**, 2250035 (2022).

[225] H. Schomerus, "Noisy monitored quantum dynamics of ergodic multi-qubit systems", Journal of Physics A: Mathematical and Theoretical **55**, 214001 (2022).

[226] C. Sünderhauf, L. Piroli, X.-L. Qi, N. Schuch, and J. I. Cirac, "Quantum chaos in the Brownian SYK model with large finite N: OTOCs and tripartite information", Journal of High Energy Physics **2019**, 38 (2019).

[227] L. Agarwal and S. Xu, "Emergent symmetry in Brownian SYK models and charge dependent scrambling", Journal of High Energy Physics **2022**, 45 (2022).

[228] S. Xu, "Dynamics of operator size distribution in q-local quantum Brownian SYK and spin models", Journal of Physics A: Mathematical and Theoretical **58**, 045301 (2025).

[229] S. Xu, L. Susskind, Y. Su, and B. Swingle, "A Sparse Model of Quantum Holography", arXiv:2008.02303 [cond-mat.str-el] (2020).

[230] A. M. García-García, Y. Jia, D. Rosa, and J. J. M. Verbaarschot, "Sparse Sachdev-Ye-Kitaev model, quantum chaos, and gravity duals", Physical Review D **103**, 106002 (2021).

[231] E. Cáceres, A. Misobuchi, and A. Raz, "Spectral form factor in sparse SYK models", Journal of High Energy Physics **2022**, 236 (2022).

[232] P. Orman, H. Gharibyan, and J. Preskill, "Quantum chaos in the sparse SYK model", arXiv:2403.13884 [hep-th] (2024).

[233] W. Fu and S. Sachdev, "Numerical study of fermion and boson models with infinite-range random interactions", Physical Review B **94**, 035135 (2016).

[234] L. Fidkowski and A. Kitaev, "Topological phases of fermions in one dimension", Physical Review B **83**, 075103 (2011).

[235] D. Meidan, A. Romito, and P. W. Brouwer, "Scattering Matrix Formulation of the Topological Index of Interacting Fermions in One-Dimensional Superconductors", Physical Review Letters **113**, 057003 (2014).

[236] J. Behrends, J. H. Bardarson, and B. Béri, "Tenfold way and many-body zero modes in the Sachdev-Ye-Kitaev model", Physical Review B **99**, 195123 (2019).

[237] R. R. Tucci, "An Introduction to Cartan's KAK Decomposition for QC Programmers", arXiv:quant-ph/0507171 (2005).

[238] P. Zanardi, C. Zalka, and L. Faoro, "Entangling power of quantum evolutions", Physical Review A **62**, 030301 (2000).

[239] B. Kraus and J. I. Cirac, "Optimal creation of entanglement using a two-qubit gate", Physical Review A **63**, 062309 (2001).

[240] M. Musz, M. Kuś, and K. Życzkowski, "Unitary quantum gates, perfect entanglers, and unistochastic maps", Physical Review A **87**, 022111 (2013).

[241] D. Morachis Galindo and J. A. Maytorena, "Entangling power of symmetric two-qubit quantum gates and three-level operations", Physical Review A **105**, 012601 (2022).

[242] J. H. Bardarson, "A proof of the Kramers degeneracy of transmission eigenvalues from antisymmetry of the scattering matrix", Journal of Physics A: Mathematical and Theoretical **41**, 405203 (2008).

[243] G. W. Anderson, A. Guionnet, and O. Zeitouni, *An Introduction to Random Matrices* (Cambridge University Press, Cambridge, 2009).

[244] A. Kitaev and J. Preskill, "Topological Entanglement Entropy", Physical Review Letters **96**, 110404 (2006).

[245] M. Levin and X. G. Wen, "Detecting Topological Order in a Ground State Wave Function", Physical Review Letters **96**, 110405 (2006).

[246] N. Dowling, P. Kos, and K. Modi, "Scrambling Is Necessary but Not Sufficient for Chaos", Physical Review Letters **131**, 180403 (2023).

[247] A. Touil and S. Deffner, "Information scrambling versus decoherence—two competing sinks for entropy", PRX Quantum **2**, 010306 (2021).

[248] A. Touil and S. Deffner, "Quantum scrambling and the growth of mutual information", Quantum Science and Technology **5**, 035005 (2020).

[249] M V Berry and J P Keating, "A rule for quantizing chaos?", Journal of Physics A: Mathematical and General **23**, 4839 (1990).

[250] M. V. Berry and J. P. Keating, "A New Asymptotic Representation for ζ (1/2+it) and Quantum Spectral Determinants", Proceedings: Mathematical and Physical Sciences **437**, 151–173 (1992).

[251] E B Bogomolny, "Semiclassical quantization of multidimensional systems", Nonlinearity **5**, 805 (1992).

[252] J. P. Keating, "Periodic Orbit Resummation and the Quantization of Chaos", Proceedings: Mathematical and Physical Sciences **436**, 99–108 (1992).

[253] M. Winer and B. Swingle, "Hydrodynamic Theory of the Connected Spectral form Factor", Physical Review X **12**, 021009 (2022).

[254] M. Winer and B. Swingle, "Reappearance of Thermalization Dynamics in the Late-Time Spectral Form Factor", arXiv:2307.14415 [nlin.CD] (2023).

[255] E. Abrahams, P. W. Anderson, D. C. Licciardello, and T. V. Ramakrishnan, "Scaling Theory of Localization: Absence of Quantum Diffusion in Two Dimensions", Physical Review Letters **42**, 673 (1979).

[256] L.-k. Hua, *Harmonic analysis of functions of several complex variables in the classical domains*, Translations of Mathematical Monographs; v. 6 (American Mathematical Society, Providence, 1963).

[257] P. A. Mello, P. Pereyra, and T. H. Seligman, "Information theory and statistical nuclear reactions. I. General theory and applications to few-channel problems", Annals of Physics **161**, 254–275 (1985).

[258] E. B. Rozenbaum, S. Ganeshan, and V. Galitski, "Lyapunov Exponent and Out-of-Time-Ordered Correlator's Growth Rate in a Chaotic System", Physical Review Letters **118**, 086801 (2017).

[259] R. A. Jalabert, I. García-Mata, and D. A. Wisniacki, "Semiclassical theory of out-of-time-order correlators for low-dimensional classically chaotic systems", Physical Review E **98**, 062218 (2018).

[260] A. Lakshminarayan, "Out-of-time-ordered correlator in the quantum bakers map and truncated unitary matrices", Physical Review E **99**, 012201 (2019).

[261] J. Li, R. Fan, H. Wang, B. Ye, B. Zeng, H. Zhai, X. Peng, and J. Du, "Measuring Out-of-Time-Order Correlators on a Nuclear Magnetic Resonance Quantum Simulator", Physical Review X **7**, 031011 (2017).

[262] Q. Hummel, B. Geiger, J. D. Urbina, and K. Richter, "Reversible Quantum Information Spreading in Many-Body Systems near Criticality", Physical Review Letters **123**, 160401 (2019).

[263] E. M. Fortes, I. García-Mata, R. A. Jalabert, and D. A. Wisniacki, "Signatures of quantum chaos transition in short spin chains", Europhysics Letters **130**, 60001 (2020).

[264] T. Ali, A. Bhattacharyya, S. S. Haque, E. H. Kim, N. Moynihan, and J. Murugan, "Chaos and complexity in quantum mechanics", Physical Review D **101**, 026021 (2020).

[265] T. Xu, T. Scaffidi, and X. Cao, "Does Scrambling Equal Chaos?", Physical Review Letters **124**, 140602 (2020).

[266] K. Hashimoto, K.-B. Huh, K.-Y. Kim, and R. Watanabe, "Exponential growth of out-of-time-order correlator without chaos: inverted harmonic oscillator", Journal of High Energy Physics **2020**, 68 (2020).

[267] T. Morita, "Extracting classical Lyapunov exponent from one-dimensional quantum mechanics", Physical Review D **106**, 106001 (2022).

[268] Y. Huang, Y.-L. Zhang, and X. Chen, "Out-of-time-ordered correlators in many-body localized systems", Annalen der Physik **529**, 1600318 (2017).

[269] R. Fan, P. Zhang, H. Shen, and H. Zhai, "Out-of-time-order correlation for many-body localization", Science Bulletin **62**, 707–711 (2017).

[270] B. Swingle and D. Chowdhury, "Slow scrambling in disordered quantum systems", Physical Review B **95**, 060201 (2017).

[271] A. Chan, S. Shivam, D. A. Huse, and A. De Luca, "Many-body quantum chaos and space-time translational invariance", Nature Communications **13**, 7484 (2022).

[272] M. V. Berry, "Semiclassical theory of spectral rigidity", Proceedings of the Royal Society of London. A. Mathematical and Physical Sciences **400**, 229–251 (1985).

[273] M. Szyniszewski and H. Schomerus, "Random-matrix perspective on many-body entanglement with a finite localization length", Physical Review Research **2**, 032010 (2020).

[274] E. Onofri, "$SU(N)$ lattice gauge theory with villain's action", Il Nuovo Cimento A **66**, 293–318 (1981).

[275] G. E. Andrews and E. Onofri, "Lattice Gauge Theory, Orthogonal Polynomials and q-Hypergeometric Functions", in *Special Functions: Group Theoretical Aspects and Applications* (Springer Netherlands, Dordrecht, 1984), pp. 163–188.

[276] B. Collins and P. Śniady, "Integration with Respect to the Haar Measure on Unitary, Orthogonal and Symplectic Group", Communications in Mathematical Physics **264**, 773–795 (2006).

[277] D. Weingarten, "Asymptotic behavior of group integrals in the limit of infinite rank", Journal of Mathematical Physics **19**, 999–1001 (1978).

[278] T. Lévy and M. Maïda, "Central limit theorem for the heat kernel measure on the unitary group", Journal of Functional Analysis **259**, 3163–3204 (2010).

[279] A. R. Brown, D. A. Roberts, L. Susskind, B. Swingle, and Y. Zhao, "Holographic Complexity Equals Bulk Action?", Physical Review Letters **116**, 191301 (2016).

[280] T. Prosen, "Lower bounds on high-temperature diffusion constants from quadratically extensive almost-conserved operators", Physical Review E **89**, 012142 (2014).

[281] M. Blake, "Universal Charge Diffusion and the Butterfly Effect in Holographic Theories", Physical Review Letters **117**, 091601 (2016).

[282] E. Altman, K. R. Brown, G. Carleo, L. D. Carr, E. Demler, C. Chin, B. DeMarco, S. E. Economou, M. A. Eriksson, K.-M. C. Fu, M. Greiner, K. R. Hazzard, R. G. Hulet, A. J. Kollár, B. L. Lev, M. D. Lukin, R. Ma, X. Mi, S. Misra, C. Monroe, K. Murch, Z. Nazario, K.-K. Ni, A. C. Potter, P. Roushan, M. Saffman, M. Schleier-Smith, I. Siddiqi, R. Simmonds, M. Singh, I. Spielman, K. Temme, D. S. Weiss, J. Vučković, V. Vuletić, J. Ye, and M. Zwierlein, "Quantum Simulators: Architectures and Opportunities", PRX Quantum **2**, 017003 (2021).

[283] J. Verbaarschot, "Spectrum of the QCD Dirac operator and chiral random matrix theory", Physical Review Letters **72**, 2531–2533 (1994).

[284] D. V. Savin, Y. V. Fyodorov, and H.-J. Sommers, "Reducing nonideal to ideal coupling in random matrix description of chaotic scattering: Application to the time-delay problem", Physical Review E **63**, 035202 (2001).

[285] P. Diaconis and S. N. Evans, "Linear Functionals of Eigenvalues of Random Matrices", Transactions of the American Mathematical Society **353**, 2615–2633 (2001).

[286] P. Diaconis and A. Gamburd, "Random Matrices, Magic Squares and Matching Polynomials", The Electronic Journal of Combinatorics **11**, 2 (2004).